Westerduinweg 3
1755 LE Petten
P.O. Box 15
1755 ZG Petten
The Netherlands

www.tno.nl

T +31 88 866 50 65

TNO report

TNO 2018 S11661

Inflow conditions resulting in atypical wind turbine fatigue loading

Master of Science Thesis

For obtaining the degree of Master of Science in Aerospace Engineering at Delft University of Technology

Date	4 January 2019
Author(s)	S.F.M. Harmsen
Copy no	
No. of copies	
Number of pages	115 (incl. appendices)
Number of appendices	3
Sponsor	
Project name	Master of Science Thesis
Project number	
Supervisor TNO	Dr. W.P. Engels
Supervisor TUDelft	Prof. Dr. S.J. Watson
In collaboration with	Wind Energy Research Group, Faculty of Aerospace Engineering, Delft University of Technology

Contents

List of tables and figures

Tables

Figures

List of symbols and abbreviations

Abbreviations

ANN	artificial neural networks
BladeOut	out-of-plane bending moment
BladeIn	in-plane bending moment
BladeFlap	flapwise bending moment
BladeEdge	edgewise bending moment
EM	Expectation-Maximisation
EWTW	ECN Wind turbine test site Wieringermeer
GMM	Gaussian mixture models
GPR	Gaussian process regression
PCA	principal component analysis
PDF	probability distribution function
ShaftTilt	tilt bending moment
ShaftYaw	yaw bending moment
TowerFore	fore-aft bending moment
TowerSide	side-to-side bending moment

Symbols

α	wind shear exponent	$-$
θ	wind direction	$^\circ$
λ	tip speed ratio	$-$
ρ	air density	kgm^{-3}
DEL	damage equivalent load	Nm
DRE	decrease in relative error	$-$
GE	generalised error	$-$
k	number of clusters	$-$
LR	load residual	$-$
m	Wöhler exponent	$-$
R	radius of rotor swept area	m
SD	sector dependency	$-$
TI	Turbulence Intensity	$-$
U	mean wind speed	ms^{-1}
V	lateral wind speed component	ms^{-1}
w	soft clustering assignment	$-$
W	vertical wind speed component	ms^{-1}
$wdci$	wind direction change intensity	$^\circ$
z	height	m

Preface

This report regards a master's thesis in wind energy. The research for this thesis is done at ECN part of TNO. The thesis itself is part of a master Aerospace Engineering at Delft University of Technology. Prior to this thesis, a literature study has been done, resulting in a literature report on the same topic.

The research topic regards the relationship between inflow conditions and wind turbine fatigue loading. Basic knowledge of wind turbines and of the atmospheric boundary layer is considered pre-knowledge for this report. Knowledge in machine learning and unsupervised machine learning in particular is not required to read this report. However, as it regards the most important parts of the research method, it can be of use.

This report is divided into two parts. The first part can be used to determine a methodology for other projects with a similar research problem. In this case it can also be advised to read through the third and fourth section of Chapter 9. For readers specifically interested in wind turbine fatigue loading, the second part is most important. However, in order to properly understand the used research methods especially Section 3.2 is required reading. The second part can also be of interest for atmospheric scientists. In this case, Chapter 5 is of most relevance.

I am thankful for the opportunity offered by ECN part of TNO. In particular, I would like to thank Wouter Engels for his supervision of the research project. I am also grateful to Simon Watson for being my responsible supervisor at the university.

Summary

A proper prediction of the fatigue loads on a wind turbine is relevant for control purposes, maintenance and end-of-life predictions. The general aim of this project is to increase the knowledge on the relation between inflow conditions and wind turbine fatigue loading. More specifically, the inflow conditions that result in atypical fatigue loading are of interest. I.e., fatigue loading that does not comply with widely accepted theory. The main research question is formulated as follows:

What inflow conditions result in atypical wind turbine fatigue loading?

The research objective is achieved by using experimental data obtained from a 2.5 MW wind turbine. The damage equivalent load of several bending moments are investigated. Depending on the wind direction, the inflow of the meteorological mast and the wind turbine differ from each other. Based on the site layout, three undisturbed wind sectors and one disturbed wind sector are defined.

Firstly, differences between wind sectors are investigated in terms of inflow conditions. In addition, an expected fatigue loading is defined based on the mean wind speed and a linear relationship with turbulence intensity. This is done using regression with the experimental data.

Afterwards, two research methods are used to find an explanation for the differences between measured and expected fatigue loading. Continuous correlations are investigated using stepwise regression and discrete correlations are investigated using Gaussian mixture models (clustering). In both cases, a selection on variables representing the inflow conditions is made.

Lastly, data points with a very large deviation from the expected fatigue loading are considered. Both highly underestimated and highly overestimated data is plotted in the clustering space and in the space that is defined by the stepwise regression.

It is found that the correlation between turbulence intensity and fatigue is strongest for the flapwise and side-to-side bending moment. For the in-plane and edgewise bending moment (dominated by gravitational forces) and for the fore-aft bending moment, the correlation is weak.

The correlation between mean wind speed and turbulence intensity with fatigue loading differs between inflow from land and inflow from a nearby lake. The differences are largest for the flapwise bending moment measured at the blade root and the side-to-side bending moment measured at the tower bottom. They increase with the mean wind speed. In case of the fore-aft bending moment, no differences between wind directions were found.

The stepwise regression is by itself useful for determining the most relevant variables. Wind shear is found to be relevant for the out-of-plane bending moment, but less for the other bending moments. Wind veer negatively correlates with the side-to-side bending moment. This correlation however, is partly related to differences in wind sectors and is likely not a causal relationship.

In general, the decrease in estimation error is found to be small. Considering the bending moments measured at the blade root, the stepwise regression is still more useful than the Gaussian mixture models. I.e., the relationship between inflow conditions and atypical fatigue is mostly continuous.

Also the yaw and tilt bending moments were investigated. However, no solid conclusions could be drawn, because the size of the corresponding dataset was too limited. The dataset sizes of the other bending moments were larger. Also in these cases, however, a larger dataset would considerably increase the certainty on the results and conclusions.

1 Introduction

A proper prediction of fatigue loads is relevant for the maintenance and end-of-life predictions of wind turbines. In addition, a good prediction can be useful for the design of the control system. It can improve the decision making on the conflict between maximising power output and minimising fatigue loading.

Wide support exist for the relevance of mean wind speed and turbulence intensity for wind turbine loads. In addition to these variables, wind shear can also affect the fatigue loading. A study based on simulation (Dimitrov et al., 2015), showed a difference in the importance of turbulence intensity and wind shear between different wind turbine components. Also studies combining simulation with atmospheric data show differences in the effect of atmospheric stability on different parts of wind turbines (e.g. Sathe et al. (2013); Holtslag et al. (2014a, 2016)). Effects of wind veer on the yawing moment in specific, were found by Park et al. (2015) and Gutierrez et al. (2016).

The research discussed in this report aims to improve the knowledge on wind turbine fatigue loads by analysing experimental data. The obtained knowledge can be used to make a better fatigue prediction. In view of this aim, the research question is defined as follows:

What inflow conditions result in atypical wind turbine fatigue loading?

In order to make sure the objective is not open for interpretation, two parts are in need of clarification. The word ”atypical” refers to wind turbine fatigue loads that do not support theory that is widely accepted by engineers and scientists. What theory is considered widely accepted is discussed in Chapter 3. Furthermore, the ”inflow conditions” can be defined inside or outside a wind farm. Depending on the definition, the answer to the research question will be different for wake situations. In this research project, the inflow conditions are defined inside the wake/wind farm.

As stated, the research question will be answered using experimental data. This data was retrieved from the ECN Wind Turbine Test site Wieringermeer (EWTW) in another project. Data from a meteorological mast (metmast) is used and data from a 2.5 MW wind turbine. The fatigue loading (damage equivalent load) is determined at several locations on the turbine. The bending moments investigated in this research regard blade root bending moments, rotor bending moments, main shaft bending moments and tower bottom bending moments. Only 10-minute averaged data is used.

The first part of this project regards the removal of meaningless and not useful data. Several datasets are made such that the availability of measurement signals are used efficiently.

After the proper data is selected, various variables are defined that can be used to represent the inflow conditions. In this report, these variables will be referred to as ”inflow variables”. They are fully based on data from the metmast.

Based on, what is considered widely accepted theory, the mean wind speed and the turbulence intensity are used to define an expected fatigue loading. This expected fatigue loading is a regression model based on data from undisturbed wind directions.

The inflow variables are tested on whether they can explain the differences between expected and measured fatigue loading. The continuous correlations are investigated using stepwise linear regression and the discrete correlations using Gaussian mixture models. The research focuses on the latter, because this method is new in the field of research. An extensive analyses is done on the clustering results.

During both the continuous and discrete analysis, a selection is made on the most

relevant inflow variables. It is this selection of inflow variables that will be referred to as the relevant ”inflow conditions”. The usefulness of the different methods to predict the fatigue loading is evaluated with the decrease in relative standard error of the estimate. I.e., the error in estimating the fatigue loading relative to the average fatigue loading.

Before analysing the fatigue loading, however, the inflow conditions at the test site are investigated in more detail. In order to draw proper conclusions on fatigue loading, differences in inflow variables between the wind directions are investigated. Moreover, the different clusters used to analyse discrete correlations with fatigue are defined using solely inflow variables. They can therefore also include valuable information on inflow conditions in general.

Figure 1 shows how the different parts of the project and the report are related to each other. The report is set out into two parts. In the first part, the methodology is discussed in more detail. The second part regards the results and the discussion of the results.

More information on the test setup can be found in Chapter 2. This chapter also regards the use of different datasets and the data filtering. In Chapter 3 the inflow variables and the expected fatigue loading are discussed. This chapter is followed by a chapter on the two used research methods (regression method and clustering method) (Ch. 4). It concludes the part on methodology.

The second part, considering the results and discussion, is split into five chapters. Firstly, the results of the data analysis on solely the inflow variables are shown and discussed in Chapter 5. The chapter includes a discussion on differences between wind sectors and an analysis on several clustering results with different combinations of variables. This chapter is followed by a chapter on the discrete and continuous effects on fatigue loading (Ch. 6). Eight bending moments are discussed. The results of the different bending moments are compared in Chapter 7. Chapter 8 states the most important conclusions and the last chapter in this report gives recommendations for future work (not included in Figure 1).

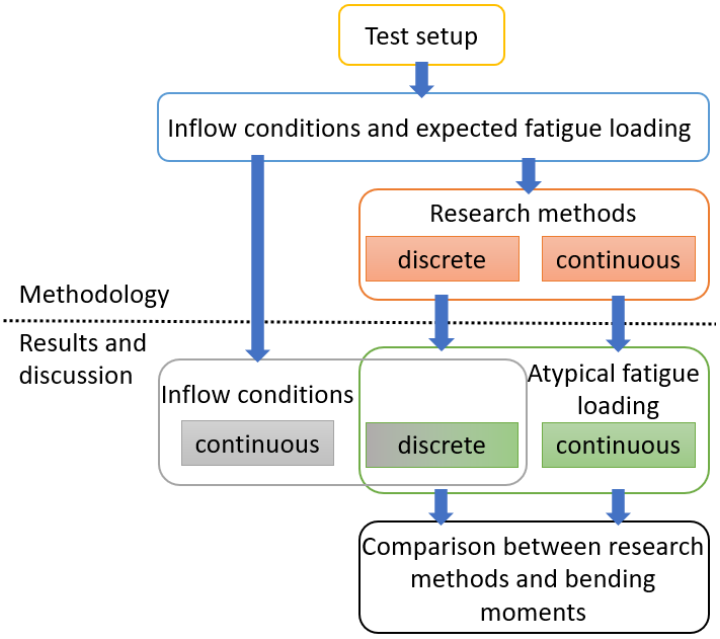

Figure 1: Project and report structure

Part I Methodology

2 Test setup

In this chapter, the test setup is discussed. The first section gives information on the test site. Based on the site layout, four different wind sectors are considered useful for this project. The second section gives specific information on the atmospheric measurements, fatigue load measurements and turbine signals. Not all signals are available at all times and not all available data is useful. With the use of several constraints, the data is filtered from bad and not useful data (Section 2.3). In order to make a proper selection of the data, several datasets are made. These datasets are discussed in Section 2.4.

As stated in the introduction, this research project is based on experimental data. The used data is not retrieved for this project in specific, but was already available from the Lawine project (a collaboration with TUDelft and ECN part of TNO). It regards data from the ECN Wind Turbine Test Site Wieringermeer (EWTW). The first data point in time is measured at 1 June 2013 and the last data point at 31 December 2014.

The fatigue loading of the considered wind turbine components were computed from sensor signals beforehand. This is also the case for the other pseudo signals. Details of these computations are not discussed in this report. The data used, regards variables from 10 minute measurement periods.

The same fatigue load measurements were used for a report focusing on wind shear (Poodt and Wouters, 2017). In the corresponding project, the wind shear was determined by LiDAR measurements. This report, however, is more elaborate and does not make use of these LiDAR measurements.

2.1 Test site

As stated, the data is retrieved from EWTW. This is an onshore test site in the Netherlands. There are multiple wind turbines and metmasts at EWTW. For this research project, only one of the turbines and one of the metmasts are used. The considered wind turbine is a Nordex N80. The turbine has a hub height of 80 m and diameter of 80 m. It is pitch controlled and has a rated power of 2.5 MW.

Not all wind directions are useful in this project. In some cases, the inflow of the metmast is different from the inflow of the turbine. It is therefore decided to define several wind sectors. These wind sectors are based on the site layout.

2.1.1 Site layout

The layout of the test site EWTW is shown in Figures 2 and 3. A larger version of Figure 2 can be found in Appendix A. The site has two lines of wind turbines and a single turbine in between. The latter is not shown on the figures because it does not regard a test turbine from EWTW. The turbines of the Northern row are identical. The second turbine from the left is used in this project. The Southern row contains different sizes of test turbines.

Figure 3 shows the distances between the most Northern five turbines of the first figure together with the used metmast. In the figure, the used turbine is called N6 and the metmast MM3. The distance between the considered wind turbine and the metmast is 201 m (2.5 rotor diameters).

The inflow conditions differ between wind directions. As can be seen from the two figures, the five northern turbines (including N6) can cause the metmast to be in a wake. This is also the case for the turbines in the South. A second aspect that is relevant for this site is a nearby lake called IJsselmeer. This lake is 2 km East from the metmast. When the wind is coming from this wind direction some aspects are

similar to an offshore environment. A third relevant aspect is a row of trees West of the turbine and metmast. Also this affects the inflow condition.

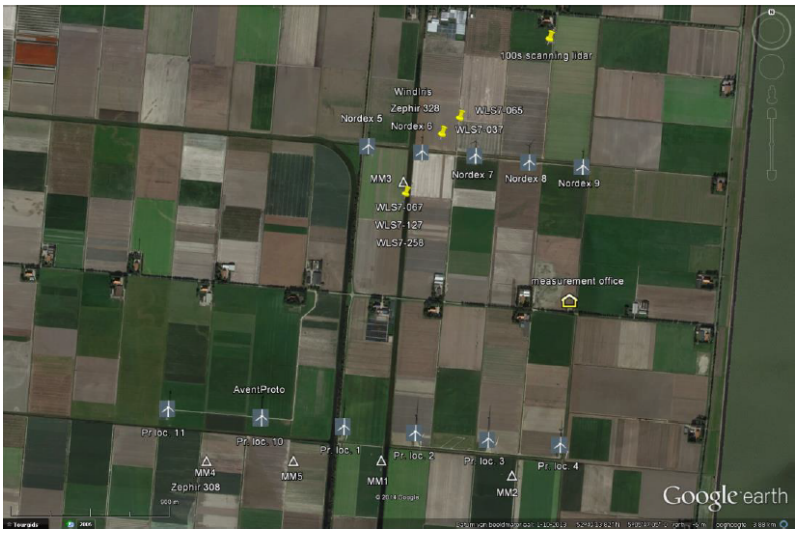

Figure 2: Layout EWTW

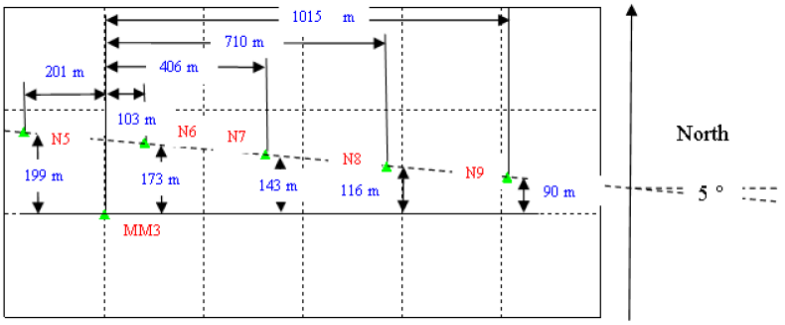

Figure 3: Detailed layout EWTW(from internal document)

2.1.2 Wind sectors

The wind directions can be divided into 12 different sectors. Each wind sector is defined by having two neighbouring sectors with different terrain in front of the metmast and or turbine. The disturbed and undisturbed wind sectors for the metmast and turbine were determined separately for the Lawine project. Combining the two, gives Table 1.

Three sectors have an undisturbed metmast and undisturbed turbine (sectors starting with UMUT, Undisturbed Metmast Undisturbed Turbine). Apart from these three sectors, there is a fourth sector where the metmast and turbine have comparable inflow conditions. This is sector DMDT-S, which is directed to the South. The inflow conditions are in this case comparable because the disturbing factors (the Southern wind turbines) are relatively far away. The distance between the Southern turbines and the metmast/turbine varies between 12.5 and 17.1 rotor diameters (rotor diameter of the considered turbine in the South). Only data points from these four sectors are used in this research project. In Figure 4 the sectors are shown with respect to the metmast. The colours and names representing the wind sectors are used throughout the report.

Table 1: Wind sectors

sector name	wind direction range (deg)
Undisturbed Metmast and Undisturbed Turbine	
UMUT-N	345.92 - 353.75
UMUT-SE	125.76 - 132.52
UMUT-SW	241.84 - 244.63
Disturbed Metmast and Undisturbed Turbine	
DMUT-N	353.75 - 32.67
DMUT-SE	132.52 - 138.40
DMUT-SW	239.85 - 241.84
DMUT-NW	305.14 - 345.92
Undisturbed Metmast and Disturbed Turbine	
UMDT-E	102.35 - 125.76
UMDT-W	244.63 - 283.22
Disturbed Metmast and Disturbed Turbine	
DMDT-NE	32.67 - 102.35
DMDT-S	138.40 - 239.85
DMDT-NW	283.22 - 305.14

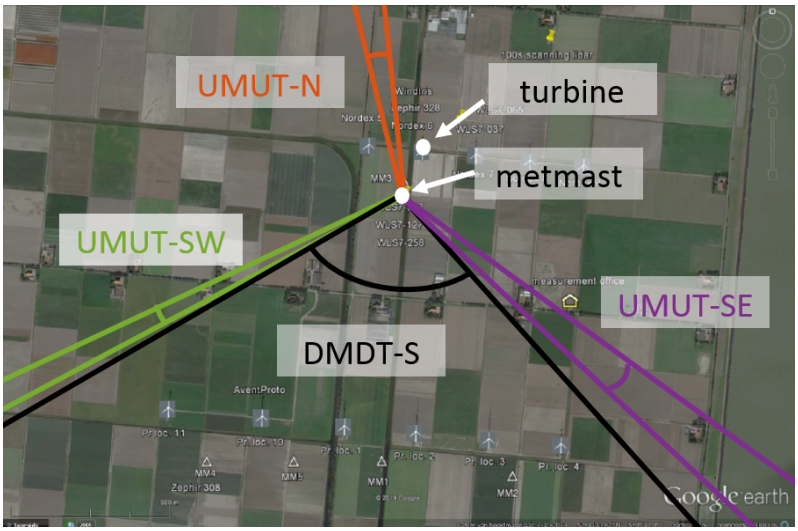

Figure 4: Wind sectors with respect to metmast

2.2 Measurement systems

Three types of measurements are used in this project: Atmospheric measurements, turbine signals and fatigue load measurements. The atmospheric measurements all come from the metmast. The other measurement systems were placed on the wind turbine.

2.2.1 Atmospheric measurements

The used atmospheric measurements include wind speeds, wind directions and the air density. The latter is not discussed in detail. It is derived from the temperature and pressure measured at hub height (80 m).

The wind direction is measured from wind vanes at two different heights (52 and 80 m). These heights correspond to 0.7 R (rotor radius) below hub height and hub height itself. Both cup and sonic anemometers are used for wind speed measurements. Cup anemometers are also situated at 52 m and 80 m. The sonic anemometers are situated at three heights: At 52 m, 80 m and at 108 m (0.7 R above hub height). The three sonic anemometers also provide wind directions.

The sonic anemometers at 52 and 80 m are situated on a boom directed to the North. Being disturbed by the metmast itself, they are not useful for the wind sector in the South (DMDT-S). The sonic anemometer at 108 m is free from disturbance as it is situated on top of the metmast.

The wind vanes and the cup anemometers at both heights have replicates at two booms. Booms directed to the Southeast at 120° (North = 0°) and booms directed to the Southwest at 240°. Depending on the wind direction, the wind vane and cup anemometer on one of the booms are used (at both heights):

UMUT-SE	cup anemometer at 120°, wind vane at 240°
UMUT-SW	cup anemometer at 240°, wind vane at 120°
UMUT-N	average of two cup anemometers, wind vane at 240°
UMUT-S	partly cup anemometer at 120°, partly cup anemometer at 240°, partly an average of the two (depending on wind direction), for most part wind vane at 120°, for a small part wind vane at 240°

Because of the size of the Southern wind sector and the direction of the booms, the use of sensors differ within this sector.

The availability of the sonic anemometer at 52 m is limited. Moreover it cannot be said with certainty that, in case of wind sectors UMUT-SE and UMUT-SW, the sonic anemometer at 80 m is in undisturbed flow. Fast changes in wind direction can occur within the 10-minute averaging period. It is therefore possible that the sonic anemometer is disturbed by beams or by a cup anemometer of the same metmast. The relationship between sonic anemometer and the relevant cup anemometer is investigated in more detail.

It is found that the ratio (sonic/cup) and difference (sonic-cup) of the two mean wind speeds depends on the wind sectors. The highest ratio is found in sector UMUT-SE and the lowest in UMUT-N. Apart from the natural spread within a wind sector, additional outliers are found for all three undisturbed sectors (outliers that cannot be explained by natural spread). It is assumed that this additional variation is caused by a disturbed sonic anemometer.

These findings regard the mean wind speed. For the sonic anemometer however, the standard deviation of the wind speed is more important. Because no other measure of standard deviation is available at 80 m, it is not possible to check whether

this signal is influenced by the metmast. The sonic anemometer can therefore not be used for sector DMDT-S (always disturbed by metmast) and for sectors UMUT-SE and UMUT-SW.

2.2.2 Turbine signals

The turbine signals used in this report are mostly used for the removal of meaningless or not useful data (Section 2.3). It regards 10-minute averages of the pitch angles, power output and the rotational speed. In addition, the signals containing operational mode, maximum pitch angles and minimum rotational speeds are used.

Signals of the pitch angle of all three blades exist. However, the availability of these signals and the availability of the load measurements on the blades differ per blade. In Section 2.3, only the maximums and minimums of two of the three pitch angles are used. Moreover, only one of the average pitch angle is used to set other limitations. This regard the pitch angle of the blade also used for the fatigue loading.

2.2.3 Fatigue load measurements

Three sets of strain gauges were placed on different places on the turbine. All sets are discussed below, together with the used pseudo signals. For each bending moment, 10-minute fatigue data is used.

Fatigue loads are generally determined using the concept of damage equivalent load/equivalent fatigue load (DEL) as in Equation 2.1 (notation of Sathe et al. (2013)). Using this equation, the damage from different load ranges are linearly added to a total fatigue damage (Palmgren-Miner linear damage rule). In this case the total fatigue damage regards damage over the 10-minute periods.

$$DEL = \left[\frac{\sum_i (D_i)^m N_i}{N_{EQ}} \right]^{\frac{1}{m}} \tag{2.1}$$

where D_i are the fatigue load ranges and N_i the fatigue cycles. m is the Wöhler exponent.

Holtslag et al. (2016) and Sathe et al. (2013) both used a number of equivalent cycles, N_{EQ}, of 10^7. However, because the absolute values are in this case not of interest (Section 3.2), this also regards this equivalent number of cycles. In the research considered in this report, rainflow counting is used to estimate the fatigue load ranges and fatigue cycles. The appropriate Wöhler exponent differs between materials and structures. The fatigue loads used in this report are computed using a Wöhler exponent of either 4 or 10 (see Table 2).

Table 2: Wöhler exponents used for bending moments

bending moment	Wöhler exponent
Rotor loading	
out-of-plane	4
in-plane	4
Blade root loading	
flapwise	10
edgewise	10
Tower bottom loading	
fore-aft	4
side-to-side	4
Main shaft loading	
yaw	4
tilt	4

Two strain gauge bridges located at one of the blade roots are used for the blade root and rotor loading. These strain gauges give together with the pitch angle, four pseudo-signals: the flapwise, edgewise, out-of-plane and in-plane moments. Use of the data of all 3 blades is not considered useful. The used blade is selected based on the availability of the fatigue data.

In terms of blade loading, the flapwise and edgewise moment are the most relevant, because they are defined in the blade axis system. For fatigue loading on the pitch bearing/on the hub (rotor loading), on the other hand, the out-of-plane and in-plane moments are useful. The Wöhler exponent is selected based on the material of the turbine components they affect (see Table 2).

The tower bottom loads (fore-aft and side-to-side bending moments) are measured at a height of 8.41 m above ground level. Four strain gauges are located exactly at the Northern, Eastern, Southern and Western side of the tower. Apart from the signals of the strain gauges, also the yaw position signal is used for the pseudo-signals.

The tilt and yaw bending moments are derived from signals of strain gauges at the main shaft. The azimuthal position is used to account for the rotation of the strain gauges and therewith compute the two bending moments.

2.3 Data filtering

Several constraints are set to filter the data. The goal of this filtering is to remove meaningless data and remove inflow conditions and operating conditions that do not significantly contribute to fatigue loading. In addition, filter steps are included when they are required for later analysis. Each step is discussed below. The steps are sorted by differences in reasoning.

Section 2.4 discusses the use of several datasets. With the exception of one dataset, all filtering steps are used. The exception considers a dataset solely including atmospheric variables. In this case, only steps 1 (excluding requirement on fatigue data), 2, 4 and 7 are used.

2.3.1 Removal of data points with unavailable and incorrect signals

First of all, data points are removed that contain unavailable or incorrect signals. The status signal of the sonic anemometer is used to check if it is working correctly. Data points with a status signal referring to an error are removed. Data points for which not all required variables are available are removed as well.

An additional constraint is required regarding incorrect fatigue load data. Next to fatigue data, statistic data of the bending moments (min,max,average,standard deviation) is also available. The availability of fatigue data and statistic data can differ from each other. These differences are caused by not updating the database after post-processing. Differences in availability therefore refer to incorrect measurements. All data points for which either the fatigue data or the statistic data is not available are removed.

1. all the required signals are available
2. the status signals of the sonic anemometers give the expected value
3. both fatigue data and load statistics are available of the considered bending moment

2.3.2 Removal of data points with different inflow conditions for metmast and wind turbine

Secondly, measurements from the metmast and turbine are not meaningful when the inflow conditions differ (see Section 2.1). As previously discussed, only four wind sectors are used. Based on the average wind direction measured by the wind vane, data points in other wind sectors are removed.

4. the average wind direction is inside one of the used wind sectors

2.3.3 Removal of undesired operating conditions

Thirdly, several operating conditions are not useful for analysis. It regards the use of very low rotational speeds, parked situations, start-up situations, idling and pitch control.

In normal operating conditions, the maximum 10-minute loading corresponds to a specified azimuthal position. It is therefore problematic when the blades do not complete a single round. This is the case when the average rotor speed is less than 0.1 rpm. Below or close to this number, the fatigue loading will be affected by differences in the contribution of azimuthal positions to the 10-minute data. This is mainly relevant for the edgewise and in-plane moment because at very low wind speeds, gravitational forces dominate.

Additionally, idling situations and data points where the turbine is in parked position are not useful for analysis. Apart from the bending moments dominated by gravitational forces, these situations have a limited effect on fatigue loading.

In addition to parked and idling situations, start-up conditions are removed. It is not useful to analyse these data points because large differences in rotational speed exist within the 10-minutes.

Operating conditions that rarely occur after the other filtering steps have to be removed as well. This is necessary because the fatigue loading cannot be properly compared with other data points. After investigation, it is found that this problem relates to situations with an active pitch controller.

In order to remove the above stated situations, the 10-minute minimum of the rotational speed is given a minimum of 11.4 rpm. In addition, a requirement of a maximum 10-minute maximum pitch angle of 0.2° is set in order to remove the parked, idling and pitch control situations. These filtering steps are verified using a signal containing

the operational mode. The resulting datasets only include data points during optimal power tracking.

One should note that the thresholds in these filtering steps are turbine specific. The most limiting factor for the threshold on the rotational speed is the removal of start-up conditions. For the threshold on the pitch angle, the most limiting factor is the removal of situations with an active pitch controller.

5. the 10-minute minimum rotational speed is larger than 11.4 rpm
6. the 10-minute maximum pitch angles are smaller than 0.20°

2.3.4 Removal of too low and too high wind speeds

A wind speed range is set from 4 to 11 m/s. Data points with a mean wind speed outside this range are removed. The goal of this filtering step is not to remove meaningless data or data that does not significantly contribute to wind turbine fatigue loading. This step, however, is required for later analysis (see Section 3.2). The specified wind speed range is not specific to a wind turbine, but it depends on differences between the mean wind speed probability distributions of the used wind sectors.

7. the mean wind speed is larger than 4 m/s and smaller than 11 m/s

2.4 Datasets

Not at every instant in time, all variables used in this project are available. However, not all variables are needed for the same calculations. In order to use the available data efficiently, different datasets are made.

Because each time, only one bending moment is used, it is possible to give each a separate dataset. In addition, a dataset is made containing only parameters defining the inflow conditions. This dataset contains the data points in the other datasets and more. It is used for the analysis discussed in Section 5.1.

Not all bending moments, need a separate dataset because some are derived from the same variables. This is the case for the tower bottom bending moments and the main shaft bending moments. The situation for the rotor and blade loading is also similar.

When only considering the availability of the bending moments, differences between blade flap-wise/edgewise moments and blade out-of-plane/in-plane moments can exist. This is the case because, unlike the blade loads, the rotor loads also depend on the pitch angle. However, because the pitch angle is used in the analysis, the availability of pitch data is always relevant. Blade and rotor loads can therefore be included in the same dataset.

The sizes of the different datasets are stated in Table 3. It states the number of data points after all filtering steps. In addition to the total number of data points in undisturbed wind sectors, the number of data points in each of the four wind sectors is given. The amount of data points in the Southern sector (DMDT-S) is larger than the others because it includes a larger range of wind directions.

Table 3: Number of data points from different wind sectors in the datasets

dataset	UMUT-N	UMUT-SE	UMUT-SW	total	DMDT-S
inflow conditions	1063	592	896	2551	23318
blade root & rotor loading	785	458	442	1685	14224
tower bottom loading	848	461	484	1793	15010
main shaft loading	283	22	162	467	4430

3 Inflow variables and expected fatigue loading

The research question and the used research methods did not allow for a direct use of the data discussed in the previous chapter. Instead, several inflow variables and an expected fatigue loading are defined. Both are discussed in this chapter.

The first section discusses the inflow variables that are used to represent the inflow conditions. These inflow variables are solely based on the data from the metmast discussed in the previous chapter. Section 3.2 discusses the expected fatigue loading. The expected fatigue relates to theory that is considered widely accepted by engineers and scientists. It is based on both fatigue data and data from the metmast. The third and last section of this chapter regards the regression models used in the first two sections and the regression models used in Chapter 5.

3.1 Variables representing inflow conditions

This section regards inflow variables that are considered relevant for regression or clustering. Relevant variables are potentially able to affect the fatigue loading directly. This is not the case for, for example, the wind direction and the atmospheric stability. These variables are expected to affect the fatigue loading indirectly via the turbulence intensity and the wind shear.

Use of the wind direction or the atmospheric stability will partly take away the importance of variables that directly affect the fatigue loading. Because this will make it impossible to analyse the true effects of the variables directly affecting the loading, variables like the wind direction and the atmospheric stability are not used for regression or clustering.

The variables considered useful for representing the inflow conditions are stated below. All variables are measured in the rotor swept area. Variables defined above or below the rotor swept area cannot directly affect the fatigue loading. Moreover, only 10-minute averages and 10-minute standard deviations are used when defining the variables.

- mean wind speed $U = U_{80}$
- turbulence intensity $TI = \frac{f(U_{80},U_{108},\sigma_{108})}{U_{80}} \approx \frac{\sigma_{U,80}}{U_{80}}$
- wind direction change intensity $wdci = \frac{\sigma_{\theta,108}}{TI_{108}}$
- wind shear exponent $\alpha = f(U_{52}, U_{80}, U_{108})$

  $\alpha_2 = \log\left(\frac{U_{80}}{U_{52}}\right) / \log\left(\frac{80}{52}\right)$
- wind shear change $\Delta\alpha = \log\left(\frac{U_{108}}{U_{80}}\right) / \log\left(\frac{108}{80}\right) - \alpha_2$
- wind veer $\Delta\theta/\Delta z = \frac{\theta_{80}-\theta_{52}}{80-52}$

  $(\Delta\theta/\Delta z)_2 = \frac{\theta_{108}-\theta_{52}}{108-52}$
- air density ρ

To the right of the variables, their definition is shown. In these definitions, U is the mean wind speed, z is the height from ground level and θ the wind direction. The symbol σ refers to the use of a standard deviation. The numbers 52, 80 and 108 refer to the heights in metres at which the variables are measured. 80 m is equal to the hub height. 52 and 108 m are 0.7 R below and above hub height.

With exception of the air density, the considerations for all variables are discussed below. The air density signal in the Lawine database is used as it is.

3.1.1 Mean wind speed

The mean wind speed strongly affects the other variables considered. Together with the wind direction (effects of terrain) and atmospheric stability, the mean wind speed largely determines the inflow conditions. Other variables determining the inflow conditions such as turbulence intensity, wind shear and wind veer are largely dependent on these three variables. From these three variables, only the mean wind speed is considered to be useful for clustering and regression because it affects the fatigue loading directly.

The mean wind speed is measured at three heights (see Ch. 2). At 52 m and 80 m, the signal of the cup anemometers are used and at 108 m, the signal of the sonic anemometer. The sonic anemometer at 52 m is not used because of its limited availability. The sonic anemometer at 80 m is not used either, because both sonic anemometers are always disturbed by the metmast in the Southern sectors. Moreover, they can also be disturbed in two of the undisturbed sectors (see Ch. 2).

The mean of the wind speed aligned with the mean wind direction is approximated by the mean wind speed (small angle approximation). In other words: The mean wind speed is an average value of a wind speed that differs in wind direction within the 10 minute periods.

The use of an equivalent wind speed (e.g. taking into account wind shear) can also be considered in the future (see Ch. 9). However, at this moment, the IEC standards (International Electrotechnical Commission, (IEC, 2009)) and most research projects related to fatigue (e.g. Holtslag et al. (2014b); Veldkamp (2006)) still make use of the mean wind speed at hub height.

3.1.2 Turbulence intensity

Turbulence (σ_U) is strongly correlated with the mean wind speed. When both parameters are used in a clustering problem, this correlation is problematic (see Section 4.2). In case only the turbulence is used, the effects on fatigue loading and the correlation with other parameters might actually be caused by the mean wind speed. In order to avoid this problem, the turbulence intensity (TI) is used. The correlation of turbulence intensity with mean wind speed is lower, with exception of very low wind speeds (Bot, 2014).

The turbulence intensity uses the standard deviation of the wind speed. Just like the mean wind speed, the deviation of the mean is not aligned with the 10-minute mean wind direction. Instead it is based on the wind direction at each time instance within the 10-minute averaging periods. I.e., the direction used for σ_U can slightly differ within the 10 minute periods.

The most appropriate location of measuring turbulence intensity is at hub height. However, the sonic anemometer at 80 m can be disturbed by the metmast. It can only be said with certainty for the Northern sector (UMUT-N) that the anemometer is not disturbed. Alternatively using a turbulence intensity measured at a different height would be problematic. It will be dependent on other differences in inflow conditions such as wind shear and the difference in turbulence with height.

The turbulence intensity used in this report is an estimate of the turbulence intensity at hub height. It is estimated using a function (f) based on the mean wind speed at 80 m (U_{80}), the mean wind speed at 108 m (U_{108}) and the turbulence at 108 m (σ_{108}) (see Eq. 3.1). Following this approach, differences in wind shear are accounted for. Differences in turbulence with height ($\Delta\sigma/\Delta z$) however, will affect the estimation of TI. In previous research at EWTW, a higher turbulence intensity was found at 80 m

with respect to 52 m (Bot, 2014). $\frac{\Delta TI}{\Delta z}$ is therefore mostly positive.

$$TI = \frac{f(U_{80}, U_{108}, \sigma_{108})}{U_{80}} \tag{3.1}$$

The function is defined by regression of the data of the Northern sector (UMUT-N). The data is only filtered using filtering steps 1, 2 and 7: Availability of required signals, the status signal of the sonic anemometers, the correct wind direction and the wind speed range. The selection of the used regression method is discussed in Sector 3.3.

3.1.3 Wind direction change intensity

The wind direction change intensity ($wdci$) can be used as a variable to represent a change in wind direction. Firstly, a wind direction change can be defined as the standard deviation of the wind direction (σ_θ). This variable is strongly related to the turbulence intensity. It can therefore not be used directly. The relationship is approximately linear. In order to solve this problem, the standard deviation of the wind direction is divided by the turbulence intensity. The unit of the resulting parameter, the wind direction change intensity, is still in degrees.

The standard deviation of the wind direction being almost linear with the turbulence intensity can be explained by a small angle approximation. If expressed in radians, a deviation from the mean wind direction is equal to V/U with V being the horizontal lateral wind speed component. With a small angle approximation, $wdci$ is therefore proportional to the ratio of σ_V and σ_U. Because in this report, $wdci$ is expressed in degrees instead of radians, it is in a small angle approximation, proportional but not equal to the ratio.

The wind direction change intensity does not only include information of a change in wind direction, but also includes differences in the contribution of the different wind speed components to the turbulence kinetic energy ($\frac{1}{2}(\sigma_U^2 + \sigma_V^2 + \sigma_W^2)$ with W being the vertical wind speed component).

Using the standard deviation, only the absolute value of the change in wind direction is included. It is therewith assumed that the effect on the fatigue loading is independent on the direction of the change in wind direction (i.e. negative or positive change in wind direction are considered equal). Because of the asymmetry of the rotor, the potential effects on fatigue are expected to be different. Depending on how much the differences are, the assumption can be a valid one.

The assumption is made because from the 10-minute values, the direction of the change could not be retrieved for each point. Combining measurements of different data points could solve this problem but will lead to a small loss of available data points.

In this project, $wdci$ is only measured with signals of the sonic anemometer at 108 m. This is done because, the turbulence intensity should be measured at the same height as the wind direction change. The use of a TI estimation based on a sonic anemometer at a different height is not considered useful. The property of $wdci$ being equal to $\frac{\sigma_V}{\sigma_U}$ in small angle approximation, would largely depend on differences in turbulence with height.

3.1.4 Wind shear exponent

As previously stated, the wind speed is measured at 52 m, 80 m and 108 m. At 52 m and 80 m, the cup anemometers are used and at 108 m the sonic anemometer. Differences in mean wind speed with height can be measured using the ratio of wind speeds (wind shear). This can be done using 3 combinations of wind speed measurements. Alternatively, an estimate of the wind shear exponent (α) can be made. This can be done using the same combinations, or using all three measurements. The power law stated in Equation 3.2 can be used to directly estimate α with two wind

speeds. When the same combinations are used, the variables are directly dependent on each other. However, stepwise linear regression or clustering with wind shear exponent instead of wind shear (i.e. dependent parameters) can lead to different results.

$$\frac{U_x}{U_{ref}} = \left(\frac{z_x}{z_{ref}}\right)^{\alpha} \tag{3.2}$$

with U_x and U_{ref} being two wind speeds measured at heights z_x and z_{ref} respectively.

After clustering solely variables defining inflow conditions, it is decided to use the different estimates of the wind shear exponent. The ratios of the mean wind speeds are not used. This decision is made by weighing the final clustering results with the computational effort. Testing both shear and shear exponent estimates would double the computational effort. The final result on the other hand, is not expected to change.

Which of the three combinations of two measurement heights is best cannot be said with certainty. A decreasing wind shear with height would favor the combination of 52 - 80 m above the combination 80 - 108 m. The expected difference between the two wind speed is larger and therefore less affected by measurement errors. In the same view, the combination of 52 - 108 m would be better. The latter would also represent a better average wind shear across the rotor swept area. On the other hand, two types of sensors are used (cup anemometer and sonic anemometer). Moreover, a wind shear exponent based on all three signals could give an even better representation of the wind shear across the rotor swept area. This is done by using Eq. 3.2 and taking the mean wind speed at 80 m as U_{ref}. The value of α is optimised by minimising the squared error on $U_x = U_{52}$ and $U_x = U_{108}$.

It is decided to test two estimates of the wind shear exponent to represent the wind shear in the rotor swept area. The wind shear exponent based on measurements of the cup anemometers at 52 and 80 m (α_2) and the wind shear exponent based on all three measurements (α).

3.1.5 Wind shear change

The power law might not be a good representation for all wind conditions. It is therefore decided to define a measure of how good the wind profile is represented by the power law. Only differences from the power law within the rotor swept area could affect the fatigue loading. For this reason, the difference in wind shear exponent between 52 - 80 m and 80 - 108 m is used to define the wind shear change ($\Delta\alpha$).

3.1.6 Wind veer

The wind direction is measured at 52 m and 80 m using wind vanes and at 108 m using a sonic anemometer. The wind veer (the difference in wind direction with height) can be estimated using these measurements.

Wind veer is not expected to differ between heights. Park et al. (2015) found that the wind veer profile is by approximation linear up to 160 m. Naturally, the best combination of wind direction measurements should be far away from each other ($(\Delta\theta/\Delta z)_2$). However, this would require the use of two different sensors (wind vane and sonic anemometer). The use of two wind vanes ($\Delta\theta/\Delta z$) could give more accurate results. Both combinations are therefore tested. The relative error introduced by using different types of sensors would be largest between the wind vane at 80 m and the sonic anemometer at 108 m. This combination is therefore not tested.

Use of both $\Delta\theta/\Delta z$ and $(\Delta\theta/\Delta z)_2$ in the same clustering problem will result in an unnecessary high dimensionality. The same holds for the use of α and α_2. This is not desired (see Section 4.2). Moreover, the variables correlate too strongly. These

combination of variables are therefore not used in the clustering. For the stepwise regression discussed in Section 4.1 these combinations can be used.

3.2 Expected fatigue loading

In the introduction (Ch. 1), ”atypical fatigue loading” was defined as fatigue loads that do not support widely accepted theory. In order to define atypical fatigue loading as a quantitative measure, one can first define ”typical fatigue loading” or ”expected fatigue loading”. This is done in the first part of this section. The expected fatigue loading is defined by two regression models. Because the regression models differ from each other, they are not made at once, but optimised in an iteration. This iteration is discussed in Subsection 3.2.2. The third subsection regards an issue on probability distributions and the last subsection regards a measure for atypical fatigue loading.

Both the measured and expected fatigue are normalised with the average fatigue load measured in the three undisturbed wind sectors ($\overline{DEL}$ with DEL being the damage equivalent load). This is done for each bending moment separately. In this way, the estimation errors of the bending moments can be compared with each other.

3.2.1 Defining expected fatigue loading

The expected fatigue loading is defined using the mean wind speed and the turbulence intensity. The effects of these variables on fatigue loading can be considered well known. They are part of widely accepted theory.

The expected loading should not include other differences in inflow conditions besides the mean wind speed and turbulence intensity. These differences could unintentionally be included in the model when the probability distributions of different inflow conditions depend on the mean wind speed and/or the turbulence intensity. This issue is discussed in more detail in Subsection 3.2.3.

The mean wind speed increases the forces on the blade (lift and drag), and therewith also the fatigue loading on a wind turbine. The relationship between mean wind speed and fatigue loading largely depends on the type of turbine. A single model estimating the fatigue based on the mean wind speed does therefore not exist. Instead, the expected fatigue is based on measured fatigue loading at the same wind turbine. The appropriate regression model is selected using cross-validation (Section 3.3).

The research question (see Ch. 1) does not refer to turbine conditions. However, the mean wind speed, affects the power output, the controller and therewith the rotational speed. Because also the rotational speed affects the loading, the mean wind speed directly and indirectly affects fatigue. In ”normal” operating conditions the rotational speed only depends on the power output. However, given a mean wind speed, the rotational speed does have a certain variation. This variation can have an effect on the fatigue loading.

Part of this variation can be explained by the turbulence intensity. However, the rotational speed could also be affected by other differences in inflow conditions. Not only directly, but also indirectly. Differences in inflow conditions could have a small effect on the power output, and therefore indirectly affect the torque and rotational speed. Because of the potential effect of different inflow conditions on the rotational speed (direct or indirect), the rotational speed is not included in the expected fatigue loading.

In case of an active pitch controller, the pitch angle changes with the mean wind speed (via the rotational speed). In addition, it could also be affected by other differences in inflow conditions. However, all situations with an active pitch controller are removed from the data (see Section 2.3). The pitch angle is therefore not of major concern in this project.

Based on literature (e.g. Veldkamp (2006)), one can expect a linear relation between turbulence intensity and fatigue. This linear relationship is related with the aerodynamic forces, F_A being proportional with the relative wind speed squared, (see Eq. 3.3).

$$F_A \propto V_{rel}^2 = \overline{(V_{rel} + v'_{rel})^2} \approx \overline{V_{rel}}^2 \left(1 + 2\frac{\overline{v'_{rel}}}{\overline{V_{rel}}}\right) \tag{3.3}$$

with V_{rel} being the relative wind speed and v'_{rel} the deviation of the mean of this relative wind speed. The term $\frac{\overline{v'_{rel}}}{\overline{V_{rel}}}$ relates to the turbulence intensity and the deviations in the speed of the blade.

When making an expectation for the fatigue loading, this linear relationship should be used. Nonlinear models would not relate to widely accepted theory. However, considering experimental data, this linear relationship is only valid if other variables are not related to turbulence or do not affect the loading. This is not expected to be the case. Wind shear for example might also affect fatigue loading (Dimitrov et al., 2015), and it is connected to turbulence. Preferably, a model should be made using a linear relationship with turbulence while accounting for other variables like wind shear.

In short, the relation with the mean wind speed is unknown and the relation with the turbulence intensity is expected to be linear. In order to use the proper regression models, an iteration is required between a mean wind speed model and a turbulence intensity model. This iteration is discussed in the next subsection. Both the regression models minimise the least squares error.

3.2.2 Iteration

Because the mean wind speed and the turbulence intensity require different regression models (model based on cross-validation and a linear fit), the regression is done by iteration. In the first step of the iteration, the effect of the mean wind speed ($E(U)$) is estimated (Eq. 3.4 with $E(TI)$ moved to the right hand side). In the second step of the iteration, the effect of turbulence intensity ($E(TI)$) is estimated using a linear fit and using the same equation. In this case $E(U)$ is moved to the right hand side and is given by the first step in the iteration.

The initial value of $E(TI)$ is set to zero. Afterwards, $E(TI)$ is equal to the slope of the turbulence intensity fit multiplied by the turbulence intensity ($E(TI) = TI\frac{dDEL}{dTI}$). The resulting mean wind speed model can be considered a zero turbulence model. The linear fit with turbulence intensity goes through the origin.

$$E(U) + E(TI) \approx \frac{DEL}{\overline{DEL}} \tag{3.4}$$

with $E(U)$ and $E(TI)$ being an estimate of $\frac{DEL}{\overline{DEL}}$ based on the mean wind speed and turbulence intensity respectively.

The iteration is finished after the change in slope of the linear fit with turbulence intensity is small. At least 5 iterations are performed. In the fourth iteration, the model of the mean wind speed is optimised by cross-validation (see Section 3.3). In the first three iterations, an artificial neural network with 3 nodes is used.

3.2.3 Equalising contributions

As previously stated in Subsection 3.2.1, differences in probability distributions between inflow conditions are problematic when they regard the mean wind speed and/or turbulence intensity. Differences are problematic because they affect the regression models.

In Figure 5 a sketch is shown for clarification. It shows what the meaning of the expected fatigue loading would look like if two inflow conditions giving different fatigue loading, have a different probability distribution. To simplify the situation, the probability distributions are assumed to be the same till half way the independent variable (mean wind speed or turbulence intensity). The distribution of only one of the two inflow conditions is assumed to continue afterwards.

In the first half, the expected fatigue loading (regression model) is an average of the two inflow conditions. In the second half however, the expected fatigue is equal to the fatigue of the upper inflow condition. As a result, the meaning of the expected fatigue differs between the first half and the second half. This problem always exist with differences in probability distributions. I.e., in order for the expected loading to have the same meaning across the space defined by U and TI, the probability distributions of the different inflow conditions should be the same.

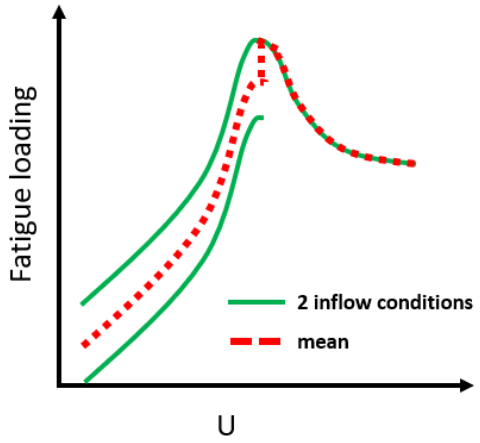

Figure 5: Fatigue loading of inflow conditions with different probability distributions

The objective of this project is to define inflow conditions based on differences in atypical fatigue loading. The inflow conditions are not defined beforehand. In order to be able to account for differences in probability distributions of unknown inflow conditions, the following assumption is made:

Probability distributions of inflow conditions are directly related to probability distributions of wind sectors

The inflow conditions are expected to relate to the wind sectors because of differences in terrain (see Ch. 2). Using this assumption, the issue changes to a difference in probability distributions of wind sectors. These differences are known, and can be eliminated. Firstly, the mean wind speed is considered and afterwards the turbulence intensity.

The mean wind speed probability distributions of the three undisturbed wind sectors are shown in Figure 6.

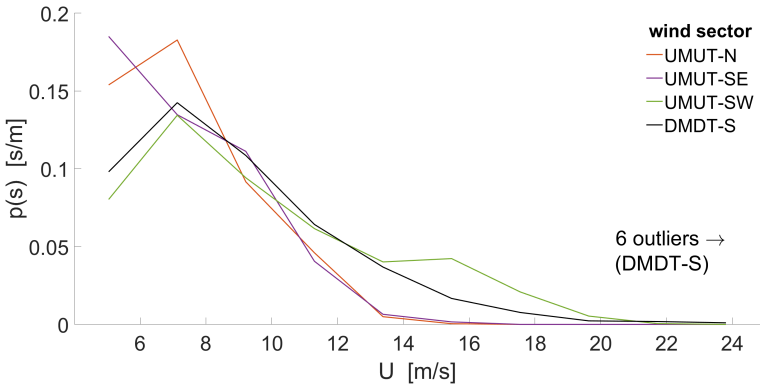

Figure 6: Probability distributions of U

As can be seen from the figure, the probability distributions of the mean wind speed are indeed different. The main difference concerns the higher wind speeds. These are only measured in the Southwestern sector (UMUT-SW). From 11 m/s onwards, the contribution of the Northern sector decreases and from 12 m/s this is also the case for the Eastern sector. The results slightly differ for each bending moment because of differences in data availability.

In order to confirm that these differences are problematic, three separate zero-turbulence mean wind speed models are made for the undisturbed wind sectors. The method used to select these regression models is stated in the next section (Section 3.3). The removed effect of turbulence intensity (E(TI)) is determined by the linear fit based on all undisturbed wind sectors.

The result for the out-of-plane bending moment is shown in Figure 7. Results of this and other bending moments can be seen in Chapter 6. Clearly, the regression models differ from each other. The differences between the probability distributions (PDFs) are therefore problematic and should be eliminated.

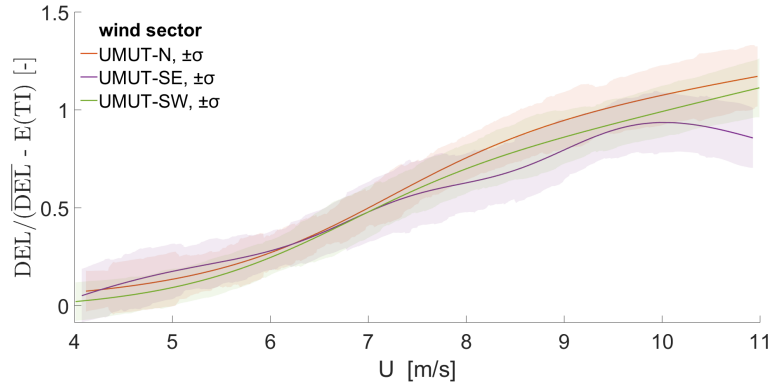

Figure 7: Regression with U

Also for the turbulence intensity, the differences in probability distribution are problematic. Figures 8 and 9 give prove of this for the out-of-plane bending moment. Again, Figure 9 of this and other bending moments are shown in Chapter 6. The first figure is based on a single regression model estimating turbulence intensity based on the mean wind speed (method of Section 3.3). The second figure shows the three linear fits with turbulence intensity. In this case, the mean wind speed contribution (E(U)) is determined by the model based on all undisturbed wind sectors.

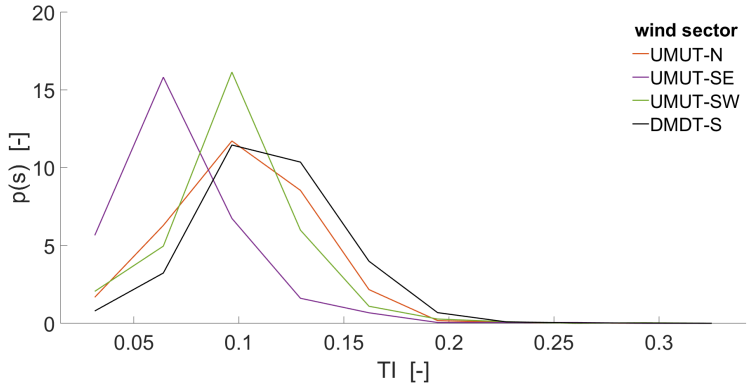

Figure 8: Probability distributions of TI

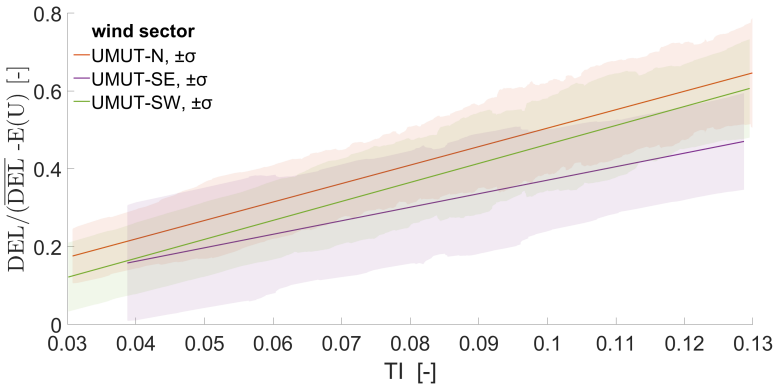

Figure 9: Linear regression with TI

The differences between PDFs are eliminated using the iterative algorithm stated below. The threshold to stop the iteration is set to 0.8. The bin width for the mean wind speed is set to 0.7 m/s and the bin width for the turbulence intensity is 0.025. Both the bin widths and the threshold are determined by weighing the accuracy of the algorithm and the resulting number of data points.

The bin widths resulted in ten bins for the mean wind speed and four bins for the turbulence intensity. Because a linear fit is used for the turbulence intensity, the regression is less sensitive to differences in probability distributions. The required number of bins is therefore smaller.

Iterative algorithm equalising sector contributions:

1. The number of data points of the different wind sectors are counted in each bin.
2. The counts are normalised with the total number of data points in the bins (all undisturbed wind sectors).
3. The resulting contributions are normalised by the contributions of the wind sector across all bins. The result is a relative contribution for each bin and sector.
4. In the bin and wind sector corresponding to the highest normalised contribution, a randomly chosen data point is removed.
   $\rightarrow$ iteration between steps 1-4
5. The iteration is stopped with a threshold for the ratio of smallest and largest normalised contribution ($\frac{\min(\text{contributions})}{\max(\text{contributions})} > thr$).

At the end, the contribution of each wind sector to the dataset is largely independent on wind speed or turbulence intensity bin. In other words, the major differences between the probability distributions are removed. The overall contribution of wind sectors are different than before the situation. It is possible that in one wind sector, all points are removed. Although, a high amount of data points are preferred for regression, this is in itself not problematic. The removal of the data points only regards the training set of the regression model. The data points can still be used to evaluate the dataset. One should keep in mind that the result is partly dependent on the definition of the wind speed bins.

The overall algorithm computing the expected fatigue and load residuals is used for every bending moment separately. Because at step four a point is removed at random, small differences exist between identical datasets. This regards the blade root and rotor bending moments, the tower bottom moments and the main shaft loading.

Using this method, a problem arises for the higher wind speeds. Because only the Western sector gives higher wind speeds, the algorithm will remove all the points in the other sectors. In essence, this is not problematic. However, it does decrease the amount of data points, and therewith the accuracy on the lower wind speed bins.

Moreover, it is known from previous research that the higher wind speeds can be considered as a different class of inflow conditions. They have a particularly neutrally stable atmospheric conditions (Holtslag et al., 2014a). Considering that these higher wind speeds can likely be considered a single inflow condition, it is decided not to use them in this project. Based on Figure 6, only data points with wind speeds lower than 11 m/s are used.

At the very low wind speed bins, a similar problem arises. It is therefore also decided to only use data points above 4 m/s. The resulting wind speed range of 4-11 m/s regard all data. In the case of the mean wind speed it does not make sense to evaluate the regression model with a data point out of this range.

In the first dataset with wind speeds below 11 m/s, only a few data points (amount depending on bending moment) have a pitch angle pointing towards an active pitch controller. For all the other points, the pitch angle is approximately the same. It makes sense to remove the few points with a different pitch angle, because the lack of more data will give poor results on the effect of pitch angle on fatigue. The remaining dataset only contains data points during optimal power tracking.

For the same reason as using a wind speed range of 4-11 m/s, a turbulence intensity range of 0.03-0.13 is set. In this case however, it only regards the dataset used for regression and not for evaluation. Because it regards a linear fit, it still makes sense to evaluate data points out of this turbulence intensity range.

3.2.4 Defining atypical fatigue loading

The atypical fatigue loading is defined in a quantitative way using a load residual (LR). This load residual is the difference between the expected fatigue and the measured fatigue (Eq. 3.5). The load residual is positive for a measured load higher than expected and negative for a measured load lower than expected. Because of the normalisation with the mean fatigue load ($\overline{DEL}$), the load residual is a dimensionless quantity.

$$LR = \frac{\text{measured fatigue - expected fatigue}}{\text{mean fatigue}} = \frac{DEL}{\overline{DEL}} - E(U) - E(TI) \qquad (3.5)$$

The use of residuals instead of the actual fatigue loading is beneficial for the clustering method. The strong relations between turbulence intensity and mean wind speed with the fatigue data are removed. As a result, the influence of other variables are retrieved more easily. An approach using residuals of a model based on the mean wind speed and the turbulence is also used by Nelson et al. (2003). They, however,

used a single regression model with both the mean wind speed and the turbulence intensity. Moreover, the analysis on the residuals is different from the research methods used in this project (Ch. 4).

The residuals of the combined mean wind speed and turbulence intensity model are used for further analysis. Data points in the disturbed wind sector are also evaluated using the model.

3.3 Regression models

Regression models are used in several parts of this project. This section regards the regression models used to estimate the expected fatigue loading with the mean wind speed. In addition, it is used for estimation of TI at hub height (Section 3.1) and for regression of solely inflow variables (Section 5.1).

3.3.1 Choice of regression method

Regression models can be made with several methods. It is not evident which method is best. Multiple methods are therefore tested. Considered regression methods are Gaussian process regression (GPR) and regression with artificial neural networks (ANN).

The results of the two different methods depend on different settings defining the model. In case of Gaussian process regression this is the form of the covariance function (kernel) and in case of neural networks, this is the number of hidden layers and number of nodes in these layers. Proper settings make sure the model is accurate enough, but also assures that no over-fitting occurs. The effect of these different settings should therefore also be tested.

The two tested regression methods are stated below, along with their tested settings. The best model with optimal settings is selected using 2 layer cross-validation. After testing the required number of nodes for a neural network with 1 hidden layer, it was not considered useful to add more layers.

Gaussian process regression (kernels)	exponential, squared exponential, matern with parameter 3/2, matern with parameter 5/2
neural network	1 hidden layer with 1-8 nodes

3.3.2 Cross-validation

In order to compare the performance of different models, 2-layer cross-validation is used. The nested layer regards a 20-fold cross-validation and contains 80% of the data. The remaining 20% is used as a test set. The best model gives the lowest average Generalised Error (GE) in the nested layer.

The data points in the nested layer are selected randomly from the dataset. The dataset in the nested layer is split into the 20 parts (folds). Each time, one part is used as validation set and the other parts together as training set (cross-validation). The validation set, is used to estimate the GE for the different models. The final estimate of the GE is the average error of the 20 folds.

The resulting estimate of the GE is biased as one selects a maximum of several models. The test set is used to evaluate the best model and get an unbiased estimate of the GE. In this case, the best model is trained with a new and randomly selected dataset containing 95% of the data previously used in the nested layer. In case the unbiased estimate of the GE is close to the biased estimate, the model selection is accepted.

However, in general it is found that the GE is not close to the biased GE. Moreover, the GE is strongly dependent on what data is in the test set. The main source of this problem is considered the size of the test set and the datasets in general. The GE dependents on whether none, one or a few outliers are included. In order for the model selection to be independent of which data points are in the validation set and training set, the same data sets are used for testing each model.

3.3.3 Model evaluation

The best method based on the cross-validation is used to evaluate the data and obtain the residuals. The fastest way to obtain residuals is to train a regression model using all points. However, the result will be biased, because the model is based on the data points considered. The actual residuals are a little larger than this biased residuals.

An unbiased residual can be obtained by using a model based on data excluding the data point that is to be evaluated. Ideally, all residuals should be estimated with a training dataset containing all the other points. However, this was found computationally too expensive. Alternatively, the dataset is separated into 50 subsets. Just like in k-fold cross-validation, each subset is evaluated using a model based on all the other subsets. With enough subsets, the expected loading is still accurate for each data point.

Residuals are also computed for data points from the disturbed sector, and data points removed by the algorithm equalising the PDFs. This is done with a model based on all data points used in the cross-validation. All residuals are therewith unbiased.

4 Research methods

In the previous chapter, the differences between measured and expected fatigue loading (the load residuals) were set as the quantitative measure for atypical fatigue. Moreover, variables were defined that can potentially be used to represent inflow conditions.

The two research methods used to select the most relevant variables for each bending moment in specific are discussed in this chapter. The related inflow conditions are based on these inflow variables. One of the research methods defines inflow conditions based on continuous correlations and the other research method defines inflow conditions based on discrete correlations. As stated in the introduction, this report focuses on the latter, because it regards a new method in the field of research.

The first section of this chapter regards the continuous correlations. These are analysed by creating a linear model with stepwise regression. The second section regards the research method used for analysing discrete correlations (clustering). It discusses the properties of the clustering problem, the choice of the clustering method and the used clustering algorithm. The third, fourth, fifth and sixth section all state the methods used to analyse the clustering results in more detail. Section 4.3 regards the analysis on a single clustering result and Section 4.4 a comparison of two clustering results. The fifth section discusses the appropriate number of clusters and the sixth section discusses the best combination of variables used for the clustering space.

The optimal number of clusters depends on the clustering space. Several approaches can be used to combine the best combination of variables with the optimum number of clusters. However, because of difficulties in selecting the optimal number of clusters (Section 4.5), it is decided not to combine this selection with the selection of variables. Recommendations for combining the two, in case a proper selection on the number of clusters is possible, are stated in Chapter 9. There are two important limitations introduced here:

- The selected combination of variables and number of clusters is not guaranteed to be a local optimum.
- The number of clusters is not guaranteed to be optimal for the selected combination of variables.

4.1 Regression method

The continuous correlations between the inflow variables and the load residuals are investigated using stepwise regression. The stepwise regression itself is useful to select the most relevant variables for each bending moment. The linear model resulting from the stepwise regression can be used to compute a new estimation error. This estimation error is relevant when comparing the two research methods (continuous and discrete) in Chapter 7.

In order to include a verification on the strong correlation between turbulence and fatigue loading it is decided to use the load residuals (LR) from solely the zero-turbulence mean wind speed model. I.e., the load residual is, in case of the stepwise regression, derived from an expected fatigue that is only based on the mean wind speed (not the turbulence intensity). In case the correlation between turbulence and the load residual is indeed the strongest of the tested variables, this is confirmed by the stepwise regression.

All the parameters defining the inflow conditions as stated in Section 3.1 can be used for stepwise regression. In addition, it is decided to include the pitch angle (β), tip

speed ratio (λ) and yaw misalignment (γ). These variables include information on the turbine. They affect the fatigue loading, but are not useful for clustering. For the stepwise regression however, they can improve the model and explain a certain amount of uncertainty in fatigue loading.

The pitch angle is based on a single turbine signal. The tip speed ratio is computed with the radius of the rotor swept area, the rotational speed (Ω) and the mean wind speed measured at 80 m ($\lambda = \frac{R\Omega}{U}$). The yaw misalignment is derived from the wind vanes at 80 m and the yaw position of the turbine.

4.1.1 Linear regression model

As stated, the stepwise regression results in a linear model. The maximum polynomial degree of this model is set at 4 and the distribution is assumed to be Gaussian. Moreover, it is decided not to allow multiplication of different variables within the model. I.e., X_1^2 is allowed, but $X_1 X_2$ is not. This constraint is set in order to improve the interpretation of the results and to limit the computational effort. Terms combining two or more variables make an interpretation increasingly difficult. The interpretation is most problematic when the range of a variable includes positive and negative values. Increasing the other variable(s) will either give a negative or positive effect, depending on the first value being positive or negative.

An example of what the regression models can look like is shown in Equation 4.1. The terms are ordered from left to right in order of importance (see stepwise regression). The model does not necessarily contain terms of the maximum degree that is set. Moreover, higher order terms are only included in the model if the lower terms of the same variable are also included.

$$LR \approx c_0 + c_1 X_3 + c_2 X_1 - c_3 X_3^2 + c_4 X_2 \tag{4.1}$$

with c_x being the positive coefficients of the model and X_x the used variables.

Similar to the load residuals based on a combined mean wind speed and turbulence intensity model, load residuals can be computed from the linear regression model. Again, PDFs of the load residuals are plotted for the different wind sectors.

The meaning of the residuals of the resulting model are not obvious. The same problem as the mean wind speed and turbulence models applies here. Different probability distributions of different inflow conditions will affect the regression model. In this case however, this is not problematic. The goal of the regression method used in this chapter is to remove all continuous correlation between variables defining the inflow conditions and fatigue loading. If the PDFs of the residuals are different for different inflow conditions/wind sectors, the research problem is at least partly discrete. Discrete changes in correlation with variables defining inflow conditions and fatigue loading cannot fully be accounted for in the linear regression model.

As with all regression models, the model regards correlation and not causality. The correlation between the inflow variables and the fatigue loading is not necessarily the direct relation between them. Potential hidden factors influencing the loading directly, can also influence inflow variables. The correlation between the inflow variables and fatigue are not investigated in more detail.

Because the regression model is based on least-squares, the relative estimation error is lower with respect to the relative error after using the combined mean wind speed and turbulence model. The decrease in relative error is shown in Chapter 7.

4.1.2 Stepwise regression

There is wide spread consensus on the fact that there are several issues with stepwise regression. The use of hypothesis tests one after the other, for example, increases

the Type 1 errors (terms are included when they should not be included) (Whittingham et al., 2006). This problem also regards other stepwise techniques. However, in this project, the selected variables are analysed in a second way as well (see Ch. 6). Moreover, the issues are recognised as such and the results are not considered to represent the indisputable truth. Considerable improvements on the regression method can be made (see Ch. 9), but the used approach is still useful for the scope of this project.

There exist two approaches for using stepwise regression. One can start with a constant (c_0) and add terms one by one, or one can start with all terms and remove terms one by one. The two approaches often give different results. Moreover, they both result in a local optimum.

Terms are added or removed based on the p-value of the chi-squared test. This p-value is estimated for each possible model with a term added or removed. In case of the approach adding terms, the first term is added based on the p-value of the F-test. The second approach, starting with all the terms, is found to be problematic because of the number of allowed terms.

It is possible that terms depend on each other. In this case one term will only be added/removed if the other is also added/removed. These terms are less likely to be to added/removed from the model than terms that are not dependent on others. This property, is the main source of the two approaches being different from each other (Whittingham et al., 2006).

The used approach combines the two approaches. Firstly thirty terms are added. No threshold value is used while doing so. The model with 30 terms is likely to contain terms that do not significantly improve the model. In the second step, terms are therefore removed using the desired threshold. This results in a model containing between 0 and 30 terms. Depending on the threshold, all thirty terms are included. This would make the approach questionable. Taking this issue into account, the threshold (maximum p-value) was set to 10^{-13} (dimensionless quantity). This is a relatively low value. Terms giving only a small improvement to the linear model are therefore also included.

As with all regression techniques, over-fitting can occur. However, given the low amount of terms with respect to the number of data points, over-fitting is not likely. In addition, the threshold for adding or removing a term, contains a correction on the degrees of freedom. The threshold therewith prevents over-fitting. The model is therefore evaluated without cross-validation.

4.2 Clustering method

In this project, clustering is used to find discrete changes in fatigue loading. First, some statements about clustering problems in general and this clustering problem in specific are made. Afterwards, the choice for Gaussian Mixtures as clustering method is explained. The clustering algorithm itself is discussed in the last subsection.

4.2.1 Properties of clustering problems

The choice of using this research method is based on two assumptions that are strongly related to the research question. The conclusions stated in Chapter 8 show whether these assumptions hold or if they need to be reconsidered.

Clustering algorithms define groups of data points that belong to each other (clusters). Between the groups, discrete differences exist. They can therefore not be represented by a single (multivariate) probability distribution. The existence of multiple probability distributions (PDFs) can lead to multiple peaks in the (multidimensional) frequency distribution. In addition, there can a discontinuity in the relationship be-

tween two variables or a discontinuity in the variance of a variable.

In this project, clustering is useful if it can be assumed that all inflow conditions together cannot be represented by a single probability distribution. In other words:

Assumption 1

There is a need of multiple probability distributions in order to represent all inflow conditions.

The clustering problem in this project meets this requirement as follows: Variables or relations between variables differ between wind directions (Section 3.2). Because the undisturbed wind sectors are not located next to each other (disturbed wind sectors are in between undisturbed sectors), these differences appear as a discontinuity/discrete step in the data. Although the research problem as a whole is not strictly discontinuous or discrete, the data cannot be represented by a single multivariate distribution.

The effect of the inflow variables used in this report, can also be found by the linear models discussed in Section 4.1. However, these variables are not the main reason for using a clustering method. The main reason regards differences in variables that are not directly measured. This includes, for example, the turbulence time and length scales.

The turbulence length scale is known to be smaller in the wake of a turbine than in undisturbed flow (Højstrup, 1999; Jimenez et al., 2008). Some research (e.g. (Dimitrov et al., 2017)) suggest that these factors can have an influence on fatigue. Other research (Rinker, 2016), however, point towards a negligible effect. The clustering method does not specifically investigate these turbulence characteristics, but searches for discrete differences in general.

Clusters are defined based on the location of the data points in the clustering space. However, the first assumption does not state whether the PDFs can be defined by the variables used to define the inflow conditions (see Section 3.1) or used in the clustering algorithm in general. In order for the research method to be useful, the following assumption should also be valid:

Assumption 2

The relevant probability distributions exist in the space defined by the variables used for the clustering algorithm.

For this assumption to be true, it is essential to select the proper variables used in the clustering algorithm. However, because of the ”curse of high dimensionality”, the performance of all clustering algorithms is limited for a high number of input variables. This ”curse of high dimensionality” relates to the distances between data points. Beyer et al. (1999) proved that the distances between data points all approach to the same value when the dimensionality is increased. It is therefore not possible to cluster with all variables defined in Section 3.1 at the same time. The used variable selection method is stated in Section 4.6.

4.2.2 Choice of clustering method

The expected shape of clusters is crucial for selecting the best clustering method. Different clustering methods either assume spherical clusters, ellipsoidal clusters or arbitrarily shaped clusters.

In arbitrarily shaped clusters, the correlations between different variables can be non-linear within a cluster. Discrete steps in the relationships between variables are al-

lowed within clusters. The appropriate clustering methods are in this case based on different densities in the data. In the case of this project, no clear transition in density is expected. Variation in inflow variables can be relatively large within the desired clusters compared to differences between clusters. I.e., the probability distributions of the desired clusters are expected to largely overlap with each other. If this is indeed the case, density based clustering algorithms will result in a single arbitrarily shaped cluster (Wang and Huang, 2009). These methods are therefore not useful for this project.

Because the desired clusters should allow for different correlations between variables, the clusters cannot solely be spherical. This rules out the use of k-means, one of the best known clustering algorithms.

The relationships between variables in these sub-clusters are not expected to be exactly linear. However, when considering them as arbitrary shaped clusters instead, density based clustering algorithms are expected to solely find the single large cluster. In short, the ellipsoidal cluster, is the most useful clustering shape. It will, however, introduce restrictions to the relationships within clusters.

In this project, a Gaussian Mixture Model (GMM) using the Expectation-Maximisation (EM) algorithm is used as clustering algorithm. Gaussian mixture models are based on the assumption that the clusters can be represented by a multivariate *normal* distribution. They result in ellipsoidal shaped clusters.

4.2.3 GMM algorithm

The proximity measure/distance measure of a GMM is the Mahalanobis distance. In a 1-D space, the Mahalanobis distance is equal to the distance to the cluster centroid (mean μ) divided by the standard deviation of the considered cluster. In a multidimensional space, the Mahalanobis distance is defined as in Eq. 4.2, using the inverse of the covariance matrix Σ.

$$d(x,\mu)^2 = (x-\mu)\Sigma^{-1}(x-\mu)^T \tag{4.2}$$

with $d(x,\mu)$ being the Mahalanobis distance from point x to cluster centroid μ.

The covariance matrix is directly related to the shape of the clusters. In case the covariance matrix is a diagonal matrix, no correlations between variables exist. In this case, the clusters can still be ellipsoidal. When all the diagonal elements (variances) are also all equal to each other, the clusters are spherical. In this case, the size of the spherical clusters can still differ from each other. The clusters are of equal size if the all covariance matrices are the same.

Because correlations between variables within clusters are expected, the covariance matrices are allowed to be full matrices. The size of the clusters can also differ from each other.

The number of clusters is an input parameter for the clustering algorithm. At the start of the algorithm, the initial centroid locations and covariance matrices are set (initialisation). Afterwards, an iteration is used to optimise those centroid locations and covariance matrices. The goal of the optimisation is to maximise the likelihood of all points belonging to their cluster. The iteration consists of an Expectation step and a Maximisation step (EM-algorithm). It is stopped using a threshold on the increase in likelihood.

A schematic diagram of the GMM with the Expectation-Maximisation algorithm is shown in Figure 10. The three main parts (initialisation, expectation and maximisation) are discussed below in more detail.

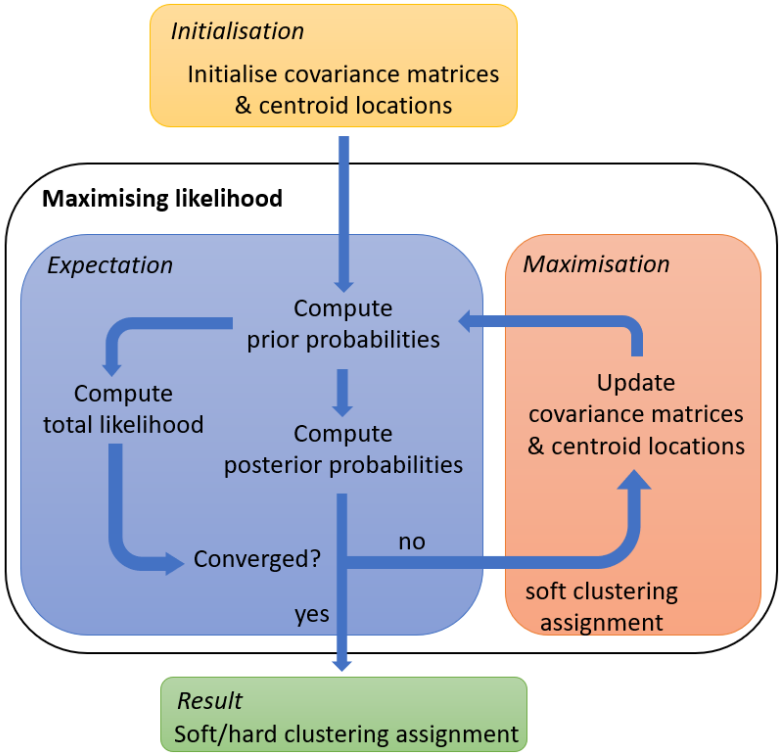

Figure 10: GMM algorithm

A known property of GMM is that it might assign a cluster to the outliers (data points with low probability belonging to any of the clusters) (Fraley and Raftery, 2002). In this case, the ellipsoid of the cluster is large, as it includes outliers in the entire domain.

4.2.4 Initialisation

There are multiple algorithms that can be used for initialisation. In this case, the initialisation of the k-means++ algorithm is used. This algorithm is often used for initialising the centroids of a GMM (Blömer and Bujna, 2013).

K-means++ initialisation chooses the first cluster centroid randomly from all the data points with uniform probability. The other centroids are defined one after the other. Using the Mahalanobis distance, the probability of points being selected as the next centroid (p_j) is computed by Equation 4.3. Using this equation, new centroids are chosen away from the already defined centroids.

$$p_j = \frac{\min_{\forall \mu}(d^2(x_j, \mu))}{\sum_{i=1}^{N} \min_{\forall \mu}(d^2(x_i, \mu))} \tag{4.3}$$

The initial covariance matrices of all clusters are defined as the diagonal matrix with the variances of the whole dataset on the diagonal.

The clustering result depends on the initial centroid locations. It regards a local optimum. Because the initial centroids are chosen at random, the result will differ when the algorithm is repeated. Because of this sensitivity to the initial centroid locations, it is common to generate multiple replicates (Blömer and Bujna, 2013). The replicate giving the highest likelihood is taken as final result. This replicate however, is still not guaranteed to be the global optimum because it depends on the initial centroid locations set in the different replicates.

In this project, this sensitivity can be problematic. The sensitivity on the initial centroids is therefore investigated in more detail. A short analysis and a method to

deal with the problems are discussed in Subection 4.3.1. In the same subsection, the used number of replicates is discussed.

4.2.5 Expectation

In the expectation step of GMM, the probabilities of points belonging to the different clusters are computed. This is done by first multiplying the probability of the multivariate normal distribution at the location of the data point with the probability of a random point belonging to that cluster (Eq. 4.4). I.e., the prior is weighted with the cluster probability. This intermediate result is the likelihood ($\mathcal{L}$) or prior probability. The sum of all the likelihoods or log-likelihoods (Eq. 4.5) is maximised in GMM by the iteration.

$$p_(x_i, c) = \frac{P(c)}{\sqrt{(2\pi)^D \det(\Sigma_c)}} \exp(-\frac{1}{2}(x_i - \mu_c)\Sigma_c^{-1}(x_i - \mu_c)^T) \tag{4.4}$$

$$\log \mathcal{L}_(x_i, c) = \ln P(c) - \frac{1}{2}\left(D \ln(2\pi) + \ln\det(\Sigma_c) + (x_i - \mu_c)\Sigma_c^{-1}(x_i - \mu_c)^T\right) \tag{4.5}$$

where $P(c)$ is the probability of a random point belonging to cluster c. In this case Σ_c refers to the covariance matrix of that considered cluster computed in the maximisation step. In the first iteration, $P(c)$ is equal for all clusters ($P(c) = 1/k$) and the covariance matrix is the diagonal covariance matrix used during initialisation (see previous section). D is the dimensionality of the clustering problem.

After computing the prior probabilities, the probabilities are standardised such that the probability of each point belonging to the individual clusters sums up to 1 ($\sum_{c=1}^{k} p(x_i, c) = 1$). The result is called the posterior probabilities.

The probability of a random point belonging to cluster c, $P(c)$, can be computed by adding the individual posterior probabilities of points belonging to this cluster.

During the expectation step, an estimate of the inverse covariance matrix is computed. However, in order to do so, the covariance matrix should not be ill-conditioned. An ill-conditioned covariance matrix would make a proper estimation impossible and will therefore break the algorithm.

Amongst other factors, the probability of ending up with an ill-conditioned covariance matrix depends on the initial centroid locations and on the clustering space (Fraley and Raftery, 1998). Using multiple replicates could solve the first problem. Increasing the number of replicates, it is more likely that at least a few replicates can finish the iteration.

Regarding the clustering space, it is useful to look at the combinations of variables that are used. Variables with too high correlation (within a cluster) will result in an ill-conditioned covariance matrix. They are therefore avoided (see Chapter 3).

4.2.6 Maximisation

In the maximisation step, the new cluster centroids and covariance matrices are computed. Both the centroids and covariance matrices are computed using the posterior probabilities as weights. The centroid location of a cluster is the weighted mean in each dimension. The covariance matrix consist of the weighted variances and weighted covariances.

4.3 Analysis of a single clustering result

Not all clustering results are analysed in detail. The first subsection on sensitivity, however, does relate to all clustering results.

The clustering results of the best combinations of variables (Section 4.6) are analysed in more detail. Firstly, it is checked which wind sectors contribute most to which

clusters. Afterwards, the multivariate distributions defining each cluster are investigated. This analysis includes the fatigue loading.

Both the PDFs in the clustering space and the dependence on wind sectors solely dependent on the inflow variables. They are therefore not discussed in the chapter regarding the atypical fatigue loading but in the chapter on inflow conditions (Ch. 5).

4.3.1 Sensitivity

The used clustering method finds a local optimum. Which local optimum is found depends on the initial location of the centroids. It is therefore necessary to investigate their sensitivity.

There are four relevant factors that affect the sensitivity of the clustering results:

- clustering space
- number of clusters
- convergence tolerance
- number of replicates

Firstly, the clustering space affects the number of local optimums. A clustering space with clusters that largely overlap each other will be more sensitive to the initial conditions than a clustering space with clusters that do not overlap each other. Secondly, the sensitivity depends on the number of clusters that are used and the appropriate number of clusters. Both the clustering space and the number of clusters are optimised in Subsections 4.6 and 4.5. Although these factors do affect the sensitivity, they are less relevant for tackling the sensitivity problem.

Thirdly, the sensitivity of the initialisation depend on the convergence tolerance. I.e., the threshold on the increase in total likelihood. However, this sensitivity can be assumed negligible if the tolerance is set small enough.

Lastly, the sensitivity of the results depend on the number of replicates. In order to explain, one can make a difference between the sensitivity of the initialisation algorithm (results based on 1 replicate) and the sensitivity of the actual results (based on multiple replicates). The latter is the most relevant one in this study. The sensitivity of the initialisation algorithm will mostly be higher than the sensitivity of the actual results. With more replicates, it is more likely to find the global optimum.

However, when the probability of finding the global optimum is low but the probability of finding e.g. the second global optimum is high, the situation is different. This can happen with relatively small clusters near the borders of the clustering space. In this case, the probability of a point in this cluster being selected as initial position of a centroid is small. Also the probability of a centroid ending up in this cluster after convergence is small. As a result, it becomes unlikely that the global optimum will be found. A clustering with less replicates will often find the second global optimum while with more replicates, the differences between the results will increase as the probabilities of finding the global or the second global optimum are more in balance.

In order to check whether sensitivity could be an issue, the GMM algorithm is used multiple times with the same inputs and number of replicates, but with different initial centroid locations in these replicates. For multiple combinations of variables and different numbers of clusters, it is found that sensitivity is indeed an issue.

In order to limit the effects of this sensitivity, 10 results each based on 10 replicates are generated. The results are compared using the average F_1 score stated in Section 4.4. The result with the highest similarity to the other results (average of average F_1 scores) is used for further analysis. This result can be considered similar to a median

result. It is the result, which is closest related to the other results. Other results could have a higher likelihood. However, eliminating the sensitivity of the initial centroid locations is considered more important when comparing results based on different inputs (different combination of variables or different number of clusters).

4.3.2 Wind sectors

In order to visualise what the main wind directions are in the different clusters, weighted and normalised bar plots are made. Each bar represents a wind sector and each group of bars a cluster. The counts in the bar plots are based on a soft clustering assignment referring to the ”weighted” part.

The overall wind rose (including all clusters) is not of direct interest when analysing the results. The bar plots of the individual clusters are therefore normalised with the wind rose. In this way, only the relative portion of points within a cluster are visualised in the bar plots.

In addition to the bar plot, a parameter called the sector dependence (SD) is defined. It is a measure of how many data points in the clusters are part of a single wind sector. Soft clustering assignment is used (Eq. 4.6). The maximum value of the sector dependence is 1. In this case each cluster only contains data points from a single wind sector. The minimum value is equal to $1/N_s$ with N_s being the number of wind sectors. In this report, the minimum value is always 1/3.

$$SD = \frac{1}{N} \sum_{c=1}^{k} \max \left(\sum_{i \in s}^{s} w_{i,c} \right) \tag{4.6}$$

with $w_{i,c}$ being the soft clustering assignment of data point i and cluster c. The maximisation considers the wind sector s. I.e., the wind sector with the maximum value is used.

4.3.3 Probability distributions

Firstly, the PDFs of the inflow variables used in the clustering space are investigated on their Gaussianity. In case of more than two dimensions, the probability distributions cannot be visualised. Multivariate variants of the kurtosis and the skewness are therefore not used. However, both the univariate kurtosis and univariate skewness are also relevant.

Recall that the data points can be assigned to a cluster using hard and soft assignment (Section 4.2). Considering Gaussianity, it is not useful to look at a hard assignment. If two clusters are close enough to each other, the tails on sides between the clusters will be cut off. As a result, both clusters would have a high skewness. Instead, a soft assignment is used. Points being only partly assigned to a cluster, weighted versions of the kurtosis and skewness are needed.

The weighted skewness or weighted Fisher-Pearson coefficient is stated in Eq. 4.7 and the weighted excess kurtosis in Eq. 4.8. For clarity reasons, n_w is defined as follows: $n_w = \sum_{i=1}^{N} w_i$. With w_i being the soft clustering assignment of data point i to the considered cluster.

$$skewness = \frac{\sum_{i=1}^{N} w_i (x_i - X)^3}{n_w \sigma^3} \tag{4.7}$$

$$kurtosis = \frac{\sum_{i=1}^{N} w_i (x_i - X)^4}{n_w \sigma^4} - 3 \tag{4.8}$$

Both the skewness and excess kurtosis regard sampled forms. These forms are biased estimators of the true skewness and excess kurtosis. That is, they are dependent on the number of data points. Several corrections exist to account for this bias.

In this case, the correction of Dubnov et al. (1996) is used for the weighted skewness and the correction of Moors (1988) is used for the weighted kurtosis. Both corrections are also approved by Zar et al. (1999) and Sheskin (2003). The latter, describing the kurtosis form as the ”most precise method of estimating kurtosis” (Sheskin, 2003).

$$skewness_{corr} = \frac{\sqrt{n_w(n_w-1)}}{n_w-2} skewness \tag{4.9}$$

$$kurtosis_{corr} = \frac{n_w-1}{(n_w-2)(n_w-3)}(n_w(n_w+1)(kurtosis+3)-3(n_w-1)) \tag{4.10}$$

The probability distributions of the clusters are investigated using histograms. On top of the histograms, a fit of a normal distribution is shown, based on the same data. Moreover, arrows are used to visualise the skewness and kurtosis. An arrow to the left represents a positive skewness and to the right a negative skewness. Two arrows pointing away from each other represents a negative kurtosis (heavy tails) and arrows pointing towards each other a positive kurtosis (light tails). It is chosen to only show histograms of the distributions having an absolute value of either skewness or kurtosis larger than 0.25.

In addition to the variables used for clustering, also the probability distributions of the load residuals are relevant. They are shown for each cluster in the chapter concerning the results with fatigue loading (Ch. 6). Because the clusters could represent different types of probability distributions (e.g. Gaussian or Weibull distribution), it is decided not to use a fit to visualise the distributions. Instead, the distributions are based on a histogram. Lines are drawn based on the height of the histogram bars (y-axis) and the middle of the bins (x-axis). The counts used for the histogram are based on a soft-clustering assignment. The different clusters are plotted together in the same figure. To improve the interpretation, the distributions are normalised with the number of data points in the different clusters.

4.4 Comparison of two clustering results

This section regards a measure of how similar two clustering results are to each other. This measure is used in both the previous and next section of this chapter. Two clustering results can be considered similar/comparable if data points that belong to the same cluster in the first result, also belong to the same cluster in the second result.

For this purpose, the F_1 score is used (Eq. 4.11). There are two properties that make especially the F_1 score useful. Firstly, with normalising by the cluster size, each cluster is equally important. Secondly, the measure is symmetric in the sense that the similarity of A and B is the same as the similarity of B and A.

$$\begin{aligned} F_1 &= 2\frac{\text{precision} * \text{recall}}{\text{precision} + \text{recall}} \\ &= \frac{2 * \text{true positives}}{2 * \text{true positives} + \text{false positives} + \text{false negatives}} \\ &= 2\frac{\sum_{i\in A\cap B}^{N}}{\sum_{i\in A}^{N} + \sum_{i\in B}^{N}} \end{aligned} \tag{4.11}$$

with A and B being clusters from different clustering results and N again the number of data points.

Before one is able to compare the clusters, one should assign each cluster of result A with a cluster of result B. When the comparison of two clustering results is part of a comparison of more than two clustering results, this can be done in two ways: One can compare two clustering results at the time or one can compare all the clustering results at the same time. If the latter option is used the following statement holds:

if cluster "a" from result A is coupled with cluster "b" from result B
and cluster "a" from result A is coupled with cluster "c" from result C,
than cluster "b" from result B is also coupled with cluster "c" from result C

This statement does not necessarily hold when cluster results are compared one at the time.

Because of the way the similarity between results is used and because of the nature of the clustering problem, the statement should not always hold. A cluster not found in result A should not affect how similar results B and C are. The cluster results will therefore be compared one to one when coupling the clusters of multiple results.

For each comparison of different results, $k!$ options exist for coupling the clusters (with k being the number of clusters). Selection of the best option will be based on maximising the average F_1 score of the different clusters (Eq. 4.12). Using the average F_1 score of all clusters and not the F_1 score based on all results ($F_1 = \sum_{q=1}^{k} \sum_{i \in A_q \cap B_q}^{N} /N$), the clusters are equally important. They are not weighted based on the number of points in the clusters.

$$\max\left\{\frac{1}{k}\sum_{c=1}^{k} F_1(A_c, B_c)\right\} = \max\left\{\frac{2}{k}\sum_{c=1}^{k} \frac{\sum_{i \in A_c \cap B_c}^{N}}{\sum_{i \in A_c}^{N} + \sum_{i \in B_c}^{N}}\right\} \tag{4.12}$$

When comparing two clustering results, four cases can be considered. These cases are important for interpreting the average of the average F_1 score used in Section 4.6. The cases relate to what information about the true/appropriate clusters is included in the clustering and how this information relates to the information in the second clustering result. The four cases that can be considered are:

1. both results contain no information
2. both results contain the same information
3. the results contain different information
4. one of the two results contains information

In case of the sensitivity analysis, only the first and second case are relevant. When results based on a different combination of variables are compared, all four cases are relevant. In practice, all pairs of results are a combination of the four cases. However, it makes sense to discuss them separately.

It is clear that results with the same information will have a higher average F_1 score than results with different information. In addition, the F_1 score will also be higher than when only one of the results contains information on the true clusters or when both results contain no information.

However, it is not clear whether the first case will result in a higher average F_1 score than the third or fourth case. This is most relevant, when considering that the actual situation is a combination of the four cases. It is worth reasoning what happens to the average F_1 score when part of the information is the same and the other part relates to case 1,3 or 4. This is the case when for example three variables are the same, but the fourth variable is different.

Different or more information in the fourth variable would have a real effect on how the clusters are defined. It will therefore lower the average F_1 score. This is not the case when the second part (fourth variables) contains no information in both results. In this case, both the fourth variables will only increase the scatter in the clustering. This will also lower the F_1 scores. However, it will give a higher average F_1 score than when the fourth variable is really different.

4.5 Optimal number of clusters

As previously stated, the number of clusters is an input for the clustering algorithm. In order to select the most optimal number of clusters, the results should be compared to each other. When clusters are clearly separated, evaluation indices exist to select the best clustering result. Most indices, however, have difficulty selecting the best result in case results with a different amount of clusters are compared. An example of such a measure is the average Silhouette value (Wang et al., 2017). Another index, the S_Dbw index (Halkidi and Vazirgiannis, 2001), was defined to solve this issue. However, it was found that when clusters are not clearly enough separated, also this index is not useful.

Alternatively, weighted digraphs are made in order to visualise differences in cluster results with a different number of clusters. An example of a weighted digraph is shown in Figure 11. The weighted digraph is based on a hard clustering assignment.

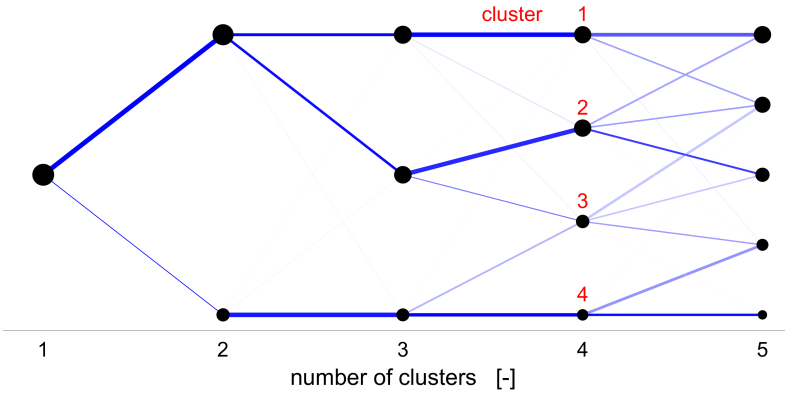

Figure 11: Weighted digraph (example)

The weighted digraph has the following four properties:

- nodes above each other correspond to different clusters from the same clustering result
- the size of the nodes (area) are related to the number of points in the different clusters
- the width of the lines are related to the number of points belonging to both the left and the right node, normalised with the number of points in the left node
- the colours of the lines connecting the nodes are related to the number of points belonging to both the left and the right node, normalised with the number of points in the right node
- the numbers in red are the cluster numbers of the used clustering result

In order to ease the interpretation of the digraph, the nodes are arranged based on the width of the lines. Clusters that are strongly connected, lie closer to each other than those that are not. It is not obvious from each digraph which number of clusters

is most appropriate. They can however be useful to relate clusters to each other and therewith derive the most likely amount of truly different inflow conditions.

It is decided to test 2, 3, 4 and 5 numbers of clusters. A higher amount of clusters increase the likelihood for an ill-conditioned covariance matrix. Moreover, it makes it difficult to interpret the results.

In addition to the digraph, the Gaussianity of the PDFs of the clusters (see Subsection 4.3.1) can give information on the appropriate number of clusters. However, also this will not give a solid answer to the problem. It is therewith decided to only use the results with four clusters. The number of clusters are therefore not necessarily optimal for the given clustering space.

4.6 Optimal combination of variables

Because of high dimensionality problems it is not possible to cluster with all available variables (see Section 4.2). A combination of inflow variables has to be selected that contributes most to answering the research question. This is discussed first. In case of this report, the optimal combination of variables contains the most information about the bending moment. It can be selected based on the relative estimation error of the fatigue loading. In order to analyse the variable selection in more detail, evaluation tables are made that include the decrease in estimation error, the sector dependence (SD) and a measure on variable dissimilarity.

4.6.1 Relevant clusters

Before defining a utility for the optimal combination of variables, one should recall the second assumption made for using clustering as a research method:

> Assumption 2
>
> *The relevant probability distributions exist in the space defined by the variables used for the clustering algorithm.*

Both assumptions are essential to interpret the clustering results. However, this second assumption could give a major limitation to the results. Considering that the research focus is on atypical fatigue loading, mainly probability distributions with different fatigue are important. Next to the use of inflow variables, the load residuals themselves can be used in the clustering space. This can result in different, but also relevant clusters. Two expectations are made on this regard:

1. Most clusters can be solely defined by inflow variables.
2. Not all clusters can be solely defined by inflow variables. I.e., they need the load residuals.

Both types of clusters are equally important to answer the research question. However, depending on the input space, the first or second type of clusters, will be found more easily. Especially, if the difference in residuals is small compared to differences in inflow parameters, it is difficult to find the second type.

More variables defining inflow conditions will make sure more clusters can be found with solely these variables. I.e., less clusters need the load residuals. High dimensionality, however, will give problems for too many variables.

In this case the load residuals become less important for assigning points to clusters. As a result, it becomes less likely that the clustering algorithm will find clusters not already determined by the variables defining the inflow conditions (the clusters of expectation 2).

It is decided to focus on the first type of clusters. Only by using solely inflow variables, a proper estimation error can be determined.

4.6.2 Dimensionality

As stated, not all variables can be used at the same time. The high dimensionality problem depends on the clustering problem. It is therefore not clear what the optimal dimensionality is. It can differ between bending moments. It is decided to cluster with 2, 3 and 4 inflow variables. In addition, all combination of variables are also clustered together with the load residual.

The utilities discussed below are independent on the number of variables. Combinations of 2 variables can therefore be compared with combinations of 3 or 4 variables.

In case three variables are better than two variables, one can check which of the three variables contribute the most to the high utility. The three best variables are also clustered in three pairs of two variables. Using the utilities of below, one can compare which combination gives the best result and therefore which variable of the three is least important.

4.6.3 Utilities

Two utilities are considered to define how good a combination of inflow variables is. Firstly, the clusters resulting from parameters defining inflow conditions should have different load residuals. If there is a large difference in fatigue between clusters of one result, this means that the variables contain a lot of information about the bending moment. In this case, the variance of the load residual within the clusters is small with respect to the overall variance of the load residual. The utility DRE (Decrease in Relative Error) is defined as in Equation 4.13. It is equal to the decrease in the relative estimation error which is minimised in this project.

$$DRE = 1 - \frac{\sqrt{\frac{1}{N-1}\sum_{c=1}^{k}\sum_{i=1}^{n_c}(LR_{i,c} - \mu_c)^2}}{\sigma(LR)} \tag{4.13}$$

with LR being the load residuals, k the number of clusters and N the total number of data points. LR_i, c are the load residuals of data points i in cluster c (hard clustering assignment) and μ_c is the mean load residual in the considered cluster. n_c represents the number of data points in cluster c.

This parameter has a range between 0 and 1. In case all points in the clusters have equal load residual (zero variance), the value of the parameter is 1 (provided that the total variance of the load residual is nonzero). In case no differences exist between the clusters, the variance within the clusters are equal to the overall variance. This gives a value of 0. In practice, the value is always larger than 0 because the size of the dataset is limited. Uncertainty in the mean load residual within the clusters depend on the number of data points in the cluster. The expected minimum value is therefore dependent on the ratio of the total number of data points and the number of clusters (N/k).

Using this parameter, the importance of the clusters is equal to their size. I.e., the variance of clusters with a large number of data points are more important than the variance of small clusters.

Secondly, cluster results are compared with cluster results based on the same variables and the load residual. In case the load residual does not add any information, the results are similar. This means that the information of the load residual is already included in the other variables. In order to check how similar the two results are, the method of Section 4.4 is used. Also the average F_1 score ranges from 0 to 1, with 1 being the most optimal case.

The four cases of comparing two clustering results (see Section 4.4) make this utility less useful. Comparing a large number of cluster results based on solely this

utility, would make the interpretation difficult. Moreover, this utility does not directly minimise the relative estimation error. It is therefore not used in this report.

4.6.4 Evaluation tables

In Chapter 6, the comparison between different combinations of variables is shown with ”evaluation tables”. An example is shown in Figure 4. In the table, the rows represent different combinations of variables. The used variables are determined by the black circle. To the right, the value of three parameters are shown for each combination in percentages.

Table 4: Evaluation table with three variables

α_2	Δα	wdci	α	Δθ/Δz	DRE %	SD %	VD %
●	●	●			4.1	48.8	42.6
	●	●	●		4	48.9	41.6
		●	●	●	3.9	49.2	41.4

Tables are made with the best 3 combinations of 2 variables and 3 variables. Moreover, tables are made with the best combination with 3 variables comparing the 3 combinations based on 2 of the 3 best variables. A fourth type of table shows the best combination of variables in comparison with clustering results adding a fourth variable. Depending on the most appropriate number of variables, different tables are shown in this report.

In addition to the used utility DRE, two other utilities are shown in the tables. These regard the sector dependence of the clusters (SD) and the similarity between the used variables (VD).

The third measure represents the dissimilarity between the used variables (VD = Variable Dissimilarity). It is computed by comparing results of different combinations of variables. The minimum and maximum values of VD are 0 and 1. A high variable dissimilarity means that the information included in the variables are different from each other.

All different combinations of variables are compared to each other one-to-one when a variable is exchanged for another variable (e.g. two variables in common and 1 variable different). This can be done multiple times for each combination of two exchanged variables. The wind shear exponent and the wind veer can for example be exchanged with clustering results having different combinations of variables in common.

The third measure considers an average of the average F_1 scores of all these combinations exchanging two variables. In case more than two variables are used for the considered clustering result, all combinations of two variables are tested. Afterwards, the average of the average of the average F_1 scores is computed (Eq. 4.14).

$$VD = 1 - \frac{1}{N_{comb}} \sum_{k=1}^{N_{comb}} \frac{1}{N_{exc,k}} \sum_{j=1}^{N_exc,k} \frac{1}{N} \sum_{i=1}^{N} F_1(x_i) \tag{4.14}$$

with N_{comb} the number of combinations with two variables (k) that can be made with the variables used. $N_{exc,k}$ is the number of pairs of clustering results that exchange the variable combination k. N is again the number of data points (x_i) in the dataset.

Recap

This concludes the part on methodology. Firstly, the origin of the used data was discussed. The site layout resulted in three undisturbed and one disturbed wind sector. Afterwards, variables were defined that can be used to represent inflow conditions. In addition, combined mean wind speed and turbulence regression models defined the expected fatigue loading. The load residuals from these models were used as the quantitative measure for atypical fatigue.

In the last chapter on methodology, two research methods were discussed that can relate inflow variables to the load residuals. Stepwise regression was selected as research method for continuous correlations and Gaussian mixtures as the clustering method for discrete correlations.

The next part of the report regards the results and the discussion of the results. Firstly, the four wind sectors defined in Chapter 2 are compared in terms of the inflow variables. The relevant methodology are the regression models discussed in Section 3.3. In the same chapter, the part of the clustering results related to inflow conditions are shown and discussed.

Chapter 6 shows all the results related to fatigue. It includes regression models for each undisturbed wind sector and each bending moment, the results of the stepwise regression and the part of the clustering results related to fatigue.

The two research methods (stepwise regression and Gaussian mixtures) discussed in the fourth chapter both result in a selection of inflow variables for each bending moment. These variables will be used to plot the extreme load residuals and therewith get to the core of this project. Moreover, the estimation error resulting from the two methods can point towards either a largely continuous problem or a largely discrete problem.

At the end of the second part, results are compared with each other and the most important conclusions are stated. The last chapter of the report regards recommendations for future work.

Part II Results and discussion

5 Inflow conditions

This chapter regards solely the inflow conditions. Before analysing fatigue loading, a proper analysis on the inflow conditions is required. This is done by analysing the relationships between inflow variables in relation to the different wind sectors (Section 5.1). The second section states the clustering results of the different combinations of variables used for each bending moment. Also this section solely regards inflow variables. The atypical fatigue (load residuals) corresponding to these clustering results are not discussed in this chapter, but in Chapter 6. The third and last section of this chapter compares the inflow conditions of the disturbed wind sector with those of the undisturbed wind sectors.

In figure captions of figures that refer to a specific bending moment, abbreviations of the bending moments are used. The first part of the abbreviations refer to the location on the turbine at which the bending moment is measured. The second part refers to the bending moment itself. The out-of-plane bending moment measured at the blade root is, for example, referred to as ”BladeOut”. All abbreviations are stated in the list of symbols and abbreviations. They are used in this chapter and in Chapter 6.

5.1 Differences between wind sectors

The dependencies of inflow variables on wind sectors are explored using regression. The variables can be directly or indirectly related to the wind direction. An example of a direct relation can be terrain effects like a row of trees in front of the turbine/metmast. Indirect dependencies can be dependencies on a certain wind condition (e.g. a low-level jet) which occurs more frequently in one of the wind sectors. Because the terrain in the three undisturbed wind sectors are different from each other (see Ch. 2), at least direct dependencies are expected.

Regression models are made for different inflow variables based on other inflow variables. Separate probability distributions (PDFs) of the residuals are made for each of the four used wind sectors. This gives an idea how much the inflow variables differ per sector. The y-axis of the figures with the PDFs, gives the probability given that a data point comes from a certain sector, $p(s)$.

Following the approach of the fatigue load regression models, the mean wind speed and turbulence intensity are used as independent variables. However, first the mean wind speed and the turbulence intensity are investigated themselves.

5.1.1 Mean wind speed and turbulence intensity

The probability distributions of the mean wind speed are shown in Figure 12. High wind speeds mainly come from the Southwestern wind sector (UMUT-SW). Because the PDFs of the different sectors, mainly differ for wind speeds larger than 11 m/s, higher wind speeds are not used for analysis (see Section 3.2).

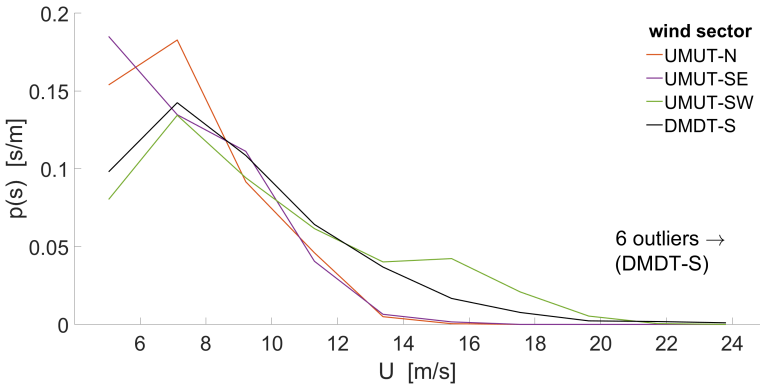

Figure 12: Probability distributions of mean wind speed

The PDFs of the turbulence intensity are shown in Figure 13. The disturbed sector gives the highest TI and the Southeastern sector gives the lowest TI.

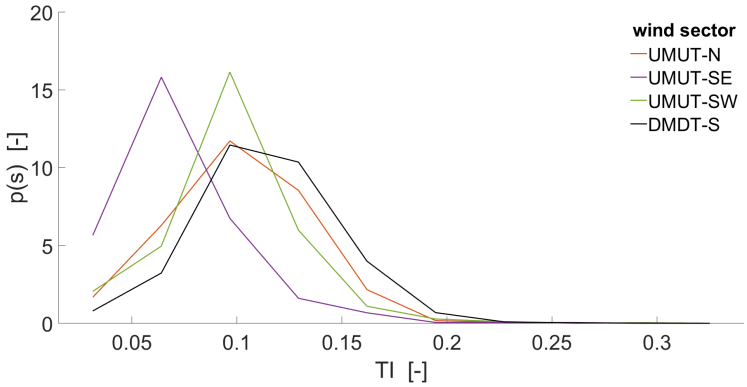

Figure 13: Probability distributions of turbulence intensity

It is known that for low wind speeds, TI decreases with U and for higher wind speeds, TI is about constant with U (Bot, 2014). When looking for differences in turbulence between wind sectors it makes sense to estimate the turbulence intensity given the mean wind speed. This is done using a regression model.

Doing so it is again important to keep the contribution of data points coming from each sector constant with mean wind speed. If this is not the case, the expected turbulence intensity will be biased towards a wind sector occurring relatively frequently in that wind speed range. More details on this problem is previously stated in Section 3.2. The problem is solved in the same way.

The PDFs of the residuals of the turbulence intensity fit are shown in Figure 14. In the label of the x-axis, E(U) represents the expected turbulence intensity based on the mean wind speed.

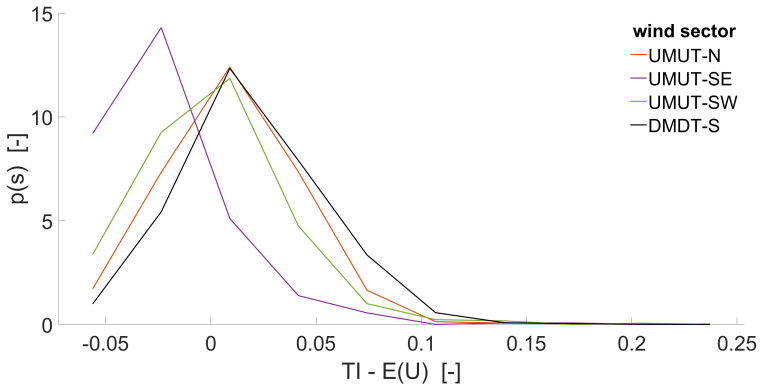

Figure 14: Probability distributions of turbulence intensity

While the distributions of the Southwestern, Northern (UMUT-N) and Southern (DMDT-S) sector are similar to each other, the distribution of the Southeastern sector (UMUT-SE) is quite different. Directed from the nearby lake, the sector generally gives a lower turbulence intensity for a given mean wind speed.

The inflow being disturbed by the turbines in the South, the Southern sector gives a higher turbulence intensity than expected compared to UMUT-SE and UMUT-N. However, compared to the differences in PDF with the Southeastern sector, the increased turbulence intensity is limited. Before drawing conclusions, it should be noted that the wake situations differ between data points in the disturbed wind sector. The shown PDF can be seen as a combination of PDFs of these different wake situations. It gives an overall view of the situation in the sector. In case only full wake situations are used, the PDF is expected to shift to the right having a higher average turbulence intensity.

5.1.2 Regression based on U and TI

As stated, the regression models estimating the other variables are based on the mean wind speed and turbulence intensity. It regards models for the two wind shear exponents, the wind shear change, the two wind veer variables, the wind direction change intensity and the air density.

In this case, the multivariate probability distribution of mean wind speed and turbulence should be the same for all wind sectors. If this is not the case, the resulting model will again be biased by the different wind sectors.

In this project, the use of the same method as done for the load residuals is favoured over the accuracy. Equal multivariate probability distributions are therefore approximated using the same approach as stated in Section 3.2. I.e., the uni-variate PDFs of the mean wind speed and the turbulence intensity are considered instead of the multivariate PDF.

5.1.3 Wind shear exponent

Figures 15 and 16 show the PDFs of the two wind shear exponents. In the figures, E(U,TI) is the expected value of the considered variable based on the mean wind speed and the turbulence intensity.

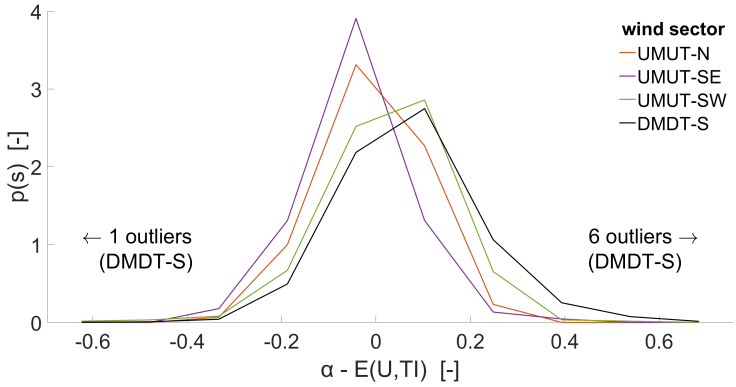

Figure 15: Probability distributions of wind shear exponent, given U and TI

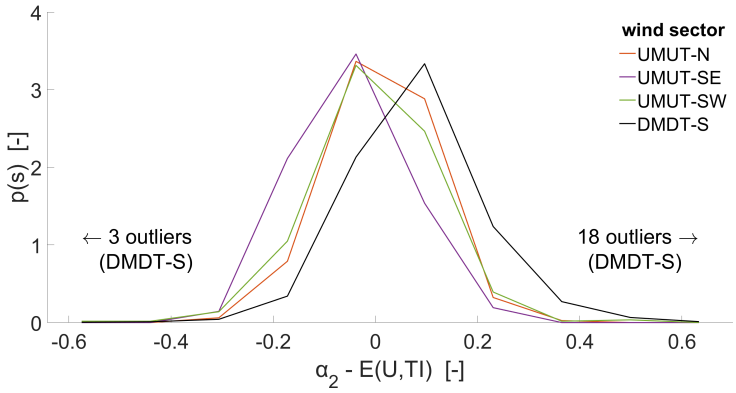

Figure 16: Probability distributions of second wind shear exponent, given U and TI

The two wind shear exponents give different results. However, both figures show that given U and TI, the wind shear in the Southeastern sector (coming from the lake) is lower than expected. In addition, the disturbed Southern sector gives higher wind shear. Bending moments that are affected by wind shear would therefore also differ between wind sectors.

The found differences in wind shear with a given turbulence intensity are not extensively discussed in existing literature. The sources of these differences are therefore investigated further.

In the wake of a wind turbine, the mean wind speed is lower than the free stream wind speed (i.e. the wind speed above the wake). The wind shear can therefore be relatively high. In addition, the contact with the upstream turbine increases the amount of turbulence. As a result, the wind shear in the Southern sector is higher for a given turbulence intensity.

The relatively low wind shear in the Southeastern wind sector can be caused by inflow conditions such as low-level jets. Although low-level jets generally occur above height of the metmast, they can influence the wind profile and turbulence intensity below. Gutierrez et al. (2016), for example, found a relatively small scale turbulence during a low-level jet.

5.1.4 Wind shear change

Only small differences in the PDFs of $\Delta\alpha$ are found between the undisturbed wind sectors (Fig. 17). Most notable is the large spread in the PDF of the Southern sector. This large spread could confirm that large differences exist within this sector. Moreover, differences within this wind sector affect the relationship between the wind profile and the turbulence intensity.

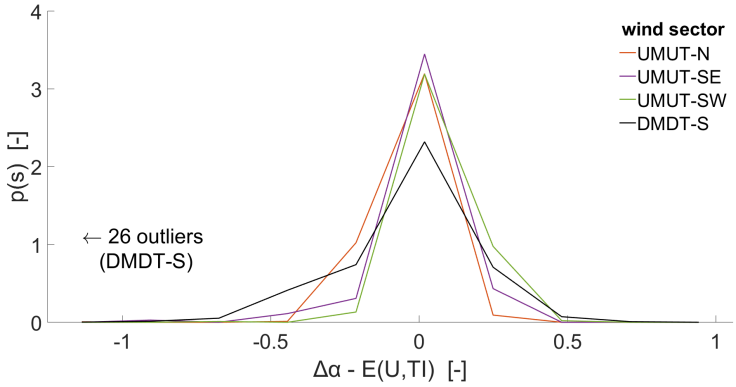

Figure 17: Probability distributions of wind shear change, given U and TI

5.1.5 Wind veer

The PDFs of the first wind veer variable (Fig. 18) show a difference between the wind sectors with an inflow from land with the wind sector with inflow from the lake (lower wind veer). Compared to the spread within the wind sectors, however, the difference is small.

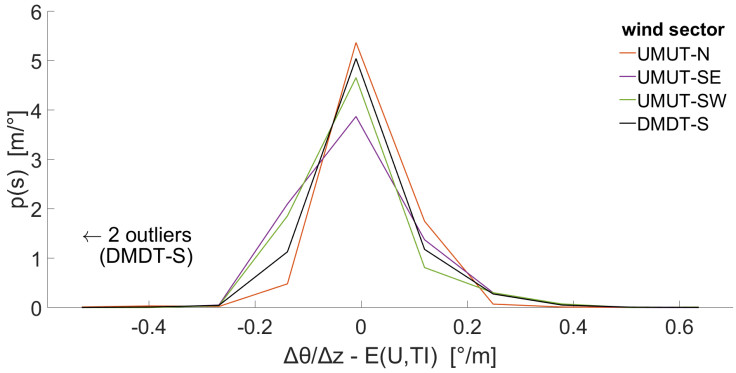

Figure 18: Probability distributions of wind veer, given U and TI

The PDFs of the second wind veer variable shows different results (Fig. 19). In this case, the Northern sector gives higher wind veer than the Southwestern sector. The PDFs of the disturbed wind sector is in approximation equal to that of the Southeastern sector. Both give higher wind veer than the other two sectors.

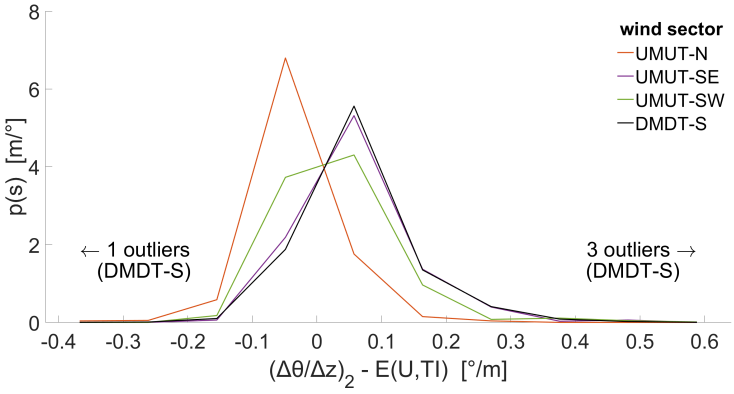

Figure 19: Probability distributions of the second wind veer, given U and TI

The differences in PDFs of the wind veer point towards differences in wind veer profiles. Because such strong differences between the two wind veer variables, are not expected. They should be investigated in more detail (see Ch. 9). The differences in wind veer do not seem to be related to the differences in wind shear. This suggests that clustering with one variable or the other would give different results. I.e., inflow conditions cannot be defined by just wind shear or just wind veer.

In case the Southeastern sector contains a significant amount of low-level jets, the wind veer results support the findings of Gutierrez et al. (2016). Gutierrez et al. (2016) found a wind veer in opposite direction below a low-level jet nose. Also in this project, differences with the other undisturbed wind sectors are found. Moreover, the existence of data points with low wind shear and high wind veer point towards the existence of low-level jets (see Section 6.1). However, with the current test setup, low-level jets cannot be recognised as such.

5.1.6 Wind direction change intensity

The PDFs of the wind direction change intensity do not result in large differences between wind sectors (Fig. 20). In case differences exist between sectors in terms of bending moments (see Ch. 6), these differences cannot be explained by $wdci$. This also holds for the other way around. Correlation with $wdci$ and the load residual cannot be related to the wind sectors.

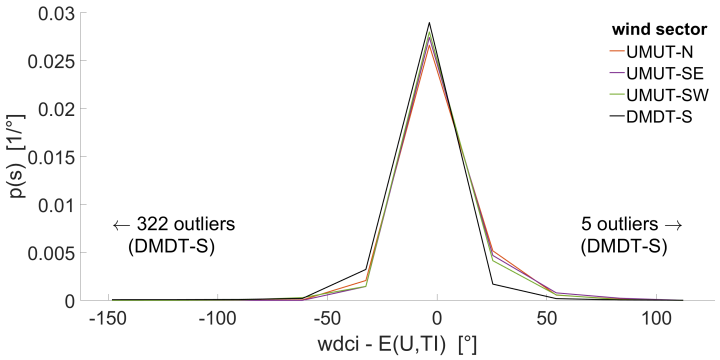

Figure 20: Probability distributions of wind direction change intensity, given U and TI

5.1.7 Air density

The use of a regression model estimating air density with U and TI could seem inappropriate. However, consistency in the research methods (compare with other inflow

variables and fatigue loading) is considered more important. Moreover, the differences between the PDFs are more clear and therewith worth discussing.

Figure 21 shows the PDFs of the air density. The PDFs of the undisturbed Southwestern and disturbed Southern sector are comparable. Moreover, the Northern sector gives a little higher air density. This is expected because the temperature is generally lower with the wind coming from the direction of the North Pole.

The PDF of the Southeastern sector has two maximums. This points towards a summation of two different PDFs with different mean and variance. I.e., the Southeastern wind sector contains at least two different types of inflow conditions. Moreover, inflow conditions with a higher air density occur more often than those with a lower air density.

The air density from this sector is investigated in more detail. It is found that the two maximums are caused by a seasonal variation. The variation is strongest in this wind sector because of the continental inflow. The lake in front of the wind sector does not have such a strong affect on the temperature and therewith the air density.

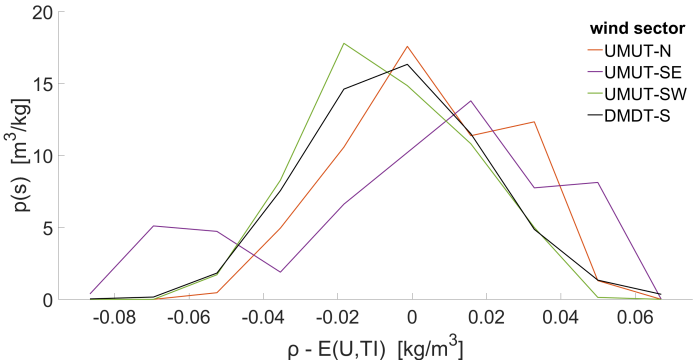

Figure 21: Probability distributions of wind direction change intensity, given U and TI

Because the differences in air density are relatively small compared to the average air density, no major differences in fatigue loads are expected. However, the differences can help to cluster the inflow conditions and therewith indirectly contribute to a better load expectation (see Section 6.2 and 6.7).

5.2 Clustering different combinations of inflow variables

In this section, the clustering of different combinations of variables is discussed. Each subsection indirectly regards a different bending moment. The selection of the variables used for the clustering results are based on the variation of the different load residuals. However, the clustering results themselves are not based on fatigue data.

The in-plane bending moment and the edgewise bending moment are discussed in the same subsection. The same variables are used and the results are based on the same dataset.

The variable combination of the fore-aft bending moment measured at the tower bottom is not discussed in this chapter. The reason not to discuss this bending moment is the low decrease in estimation error (see 6.4).

The results of different combinations of variables are compared in Chapter 7. Depending on the used variables, a different number of clusters seems appropriate. Moreover, the different combinations result in different relations between clusters and wind sectors.

The last section of this chapter discusses the clustering results based on all wind sectors (including the disturbed Southern sector).

In each subsection the Gaussianity of the clusters is discussed. Only variables of clusters having a skewness or kurtosis with an absolute value higher than 0.25 are shown. Moreover, they all have at least 200 data points (soft clustering assignment) such that the worst estimates of skewness and kurtosis are not included. A more detailed explanation on the shown figures with histograms is stated in Subsection 4.3.3 in Chapter 4.

Clusters based on the mean wind speed regularly have a rather low kurtosis. This is expected because the cut-offs at 4 and 11 m/s are not natural boundaries. They are therefore not shown in this report. The kurtosis of the mean wind speed is generally higher if the cluster does not regard the whole wind speed range.

The amount of data points in each cluster of each bending moment is stated in Table 5. The cluster numbers are related to the size of the cluster such that cluster 1 is largest and cluster 4 is smallest. The cluster names of different bending moments are not related to each other. I.e., cluster 1 of the out-of-plane bending moment is not necessarily related to cluster 1 of the flapwise bending moment.

Table 5: Number of data points in clusters of undisturbed wind sectors

bending moment	cluster 1	cluster 2	cluster 3	cluster 4	total
out-of-plane	612	587	316	169	1685
flapwise	909	285	282	210	1685
in-plane	536	469	388	291	1685
edgewise	534	464	392	296	1685
side-to-side	730	466	334	263	1793
yaw	255	141	51	21	467
tilt	204	185	73	5	467

5.2.1 Out-of-plane bending moment

The best combinations of variables for the out-of-plane bending moment is found to be the wind shear exponent (α_2) the wind shear change ($\Delta\alpha$) and the wind direction change intensity ($wdci$). The two largest clusters are about equal in size (see Table 5).

The wind shear exponent in cluster 3 has a rather low kurtosis of -0.33 (Fig. 22). The probability distribution seems to have two peaks resulting in a heavily tailed distribution. These peaks could correspond to stable atmospheric conditions (right peak) and unstable atmospheric conditions (left peak). Details on how this and similar figures are obtained can be found in Subsection 4.3.3 in Chapter 4.

Finding two peaks in a PDF, it seems better to add a fifth cluster to the algorithm. However, looking at the digraph (Fig. 23), the points in cluster 3 are moved to three separate clusters if 5 instead of 4 clusters are used. I.e., it will not result in a clean separation of the two peaks. Moreover, the connections between the clusters of the two clustering results are weak.

Following the digraph, it makes more sense to use three clusters. Going from three to four clusters, parts of two inflow conditions are used to make the new cluster (cluster 3). The two inflow conditions found in cluster 3 also have a separate cluster

for themselves (cluster 2 and 4). A part of cluster 3 is connected to cluster 2 and a part to cluster 4.

The two peaks do support the first assumption in Section 4.2.1. Multiple probability distributions are required to represent the inflow conditions.

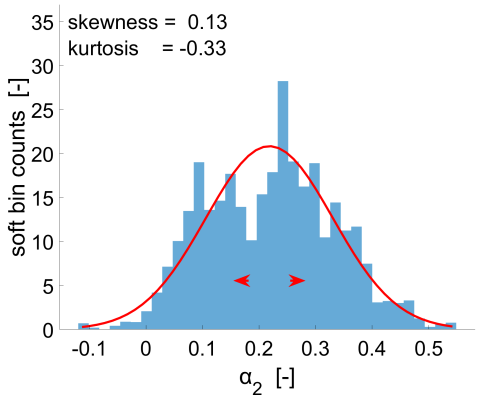

Figure 22: Gaussianity cluster 3 of Blade-Out

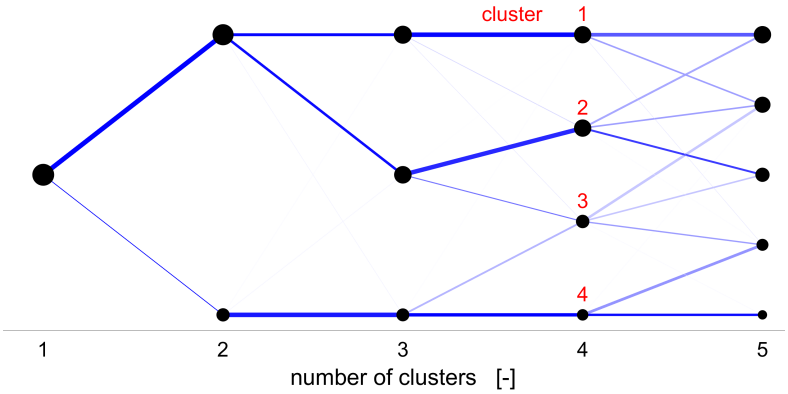

Figure 23: Digraph of BladeOut

The bar chart containing the contribution of different wind sectors to the four clusters is shown in Figure 24. Information on how this and the other bar charts in this chapter are made can be found in Chapter 4 Subsection 4.3.2. For the first cluster, the Southwestern sector is relatively important. Cluster 3 shows the opposite situation and cluster 2 shows a relatively large contribution of the Northern sector. Cluster 4 contains a relatively small amount of data points. A large proportion is measured with wind from the Southeast.

Based on the bar chart, it is indeed possible that a part of cluster 3 is connected to cluster 2 and a part to cluster 4. A summation of the wind sector contributions of cluster 2 and 4 could result in the relatively low contribution from the Southwestern sector in cluster 3.

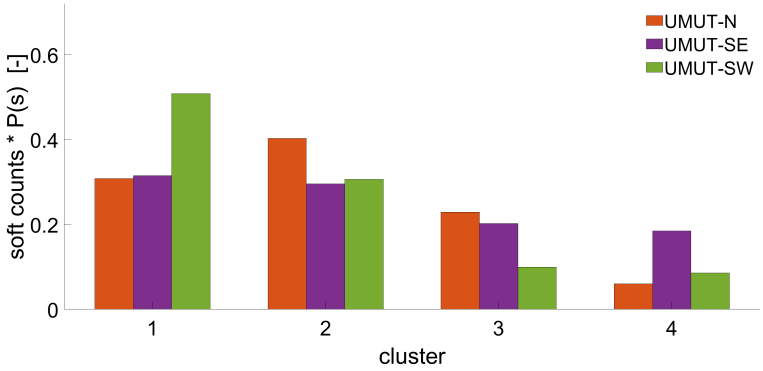

Figure 24: Wind sectors of clusters of BladeOut

5.2.2 *In-plane and edgewise bending moment*

This subsection regards the combination of variables used for the in-plane and edgewise bending moment. Results of the in-plane bending moment are shown. However, the same variables (α_2 and ρ) are used for the edgewise bending moment. Moreover, they are based on the same dataset. Equal values for SD and VD support the finding that the two clustering results are the same. This means that in this case the sensitivity is successfully eliminated (see Subsection 4.3.1 in Ch. 4).

The Gaussian approximation for the air density of cluster 1 is found to be poor (Fig. 25). Multiple peaks are visible. They result in a low kurtosis. An explanation of the large number of peaks is a direct dependency between consecutive data points. Air temperature and therewith air density can be stable for a longer period. I.e., the spectral gap at 10 minutes for the turbulence intensity, does not hold for the air density. Notable is that the air density is high in cluster 1 and that the range in air density is relatively small. The high air density relates to a low temperature and therewith mostly stable atmospheric conditions (night temperature lower than temperature during the day).

Alternatively, one could speak of four or five inflow conditions within this sector. Given the amount of data points however, this would result in inflow conditions that individually rarely occur. A division in more clusters is therefore not favourable.

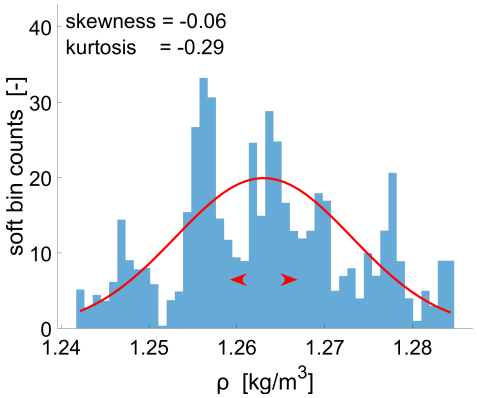

Figure 25: Gaussianity cluster 1 of BladeIn

The air density PDF of the fourth cluster has a relatively high kurtosis. In this case, only one large peak is visible. However, large differences between two neighbouring histogram bins, do point towards a direct dependency between consecutive data

points. The cluster contains less data points and considers a larger range of air densities.

The high kurtosis in the wind shear exponent of cluster 4 might relate to two inflow conditions with centroids near each other. However, the wind shear variation within these potentially different inflow conditions would be very large compared to the difference between the inflow conditions. Their existence is therefore far from certain.

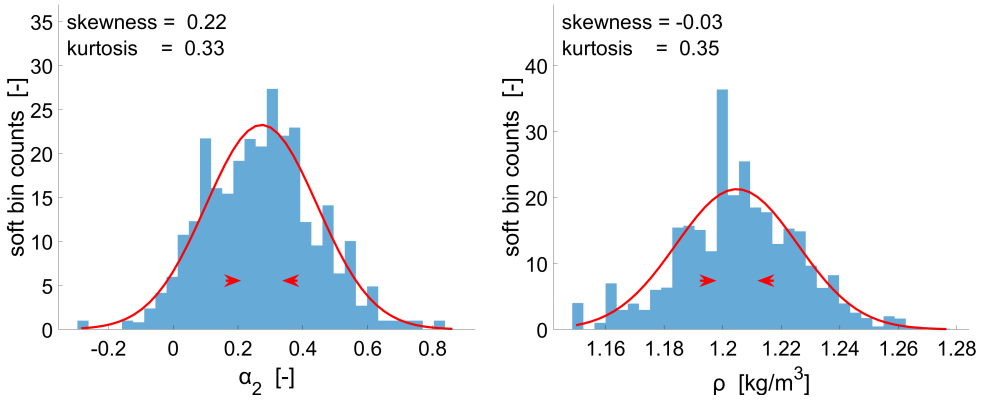

(a) Wind shear exponent (b) Air density

Figure 26: Gaussianity cluster 4 of BladeIn

The digraph of the in-plane bending moment is shown in Figure 27. Having a high air density, cluster 1 is the most constant cluster. It contains the same data points independently on the number of clusters used (2-5) in the algorithm. Representing about a third of all the data points, the clear difference between the first cluster and the other clusters confirms the need for multiple probability distributions.

Similar to the variable combination used for the out-of-plane bending moment, the use of three clusters seems more appropriate from the digraph. Part of cluster 4 could be connected to cluster 3 and the other part to cluster 2.

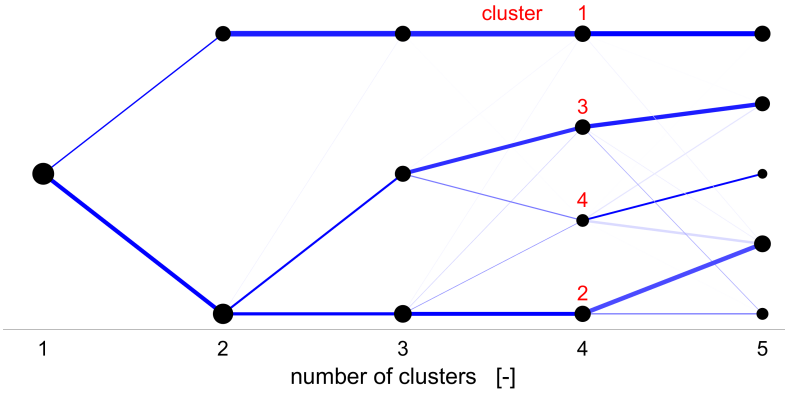

Figure 27: Digraph of BladeIn

The bar chart containing the contribution of different wind sectors to the four clusters is shown in Figure 28. The contributions of cluster 1 can be related to the expected temperature/air density in the different wind sectors. The Northern sector gives highest density, followed by the Southeastern sector. The lowest air density is found in the Southwestern sector.

The same explanation cannot be used for the other wind sectors. Moreover, a summation of the second an third cluster would not result in the contributions of the

fourth cluster. The bar chart does therefore not support the supposed existence of three inflow conditions.

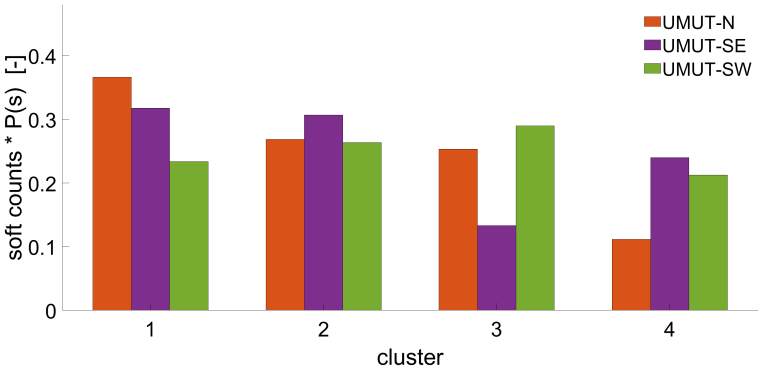

Figure 28: Wind sectors of clusters of BladeIn

5.2.3 *Side-to-side bending moment*

The combination of variables that give the based clusters for the side-to-side bending moment are the mean wind speed (U) and the second wind veer variable $(\Delta\theta/\Delta z)_2$. The data points are divided relatively equally amongst the clusters (Table 5).

Figures 29 and 30 show the PDFs of the second wind veer variable for clusters 1 and 3. The second figure shows a small skewness and includes a large range of wind veer values. The skewness is likely caused by the fact that the other three clusters only contain low wind veer.

More interestingly, the first cluster contains two peaks causing a low kurtosis. It could therefore include two inflow conditions. The digraph (not shown), showed that adding a cluster will not give strongly different results. The new cluster is rather small. Because the peaks are relatively close to each other, the clustering algorithm does not find it useful enough to split cluster 1 into two clusters. However, the existence of multiple peaks does again supports the need for multiple PDFs. Investigating the use of 6 or 7 clusters might give better results, but will make the analysis more complex. The same digraph showed that the fourth cluster is least related to the other clusters. Cluster 1 and 3 are most similar to each other.

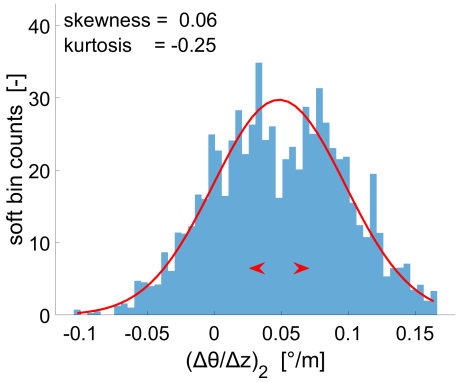

Figure 29: Gaussianity cluster 1 of TowerSide

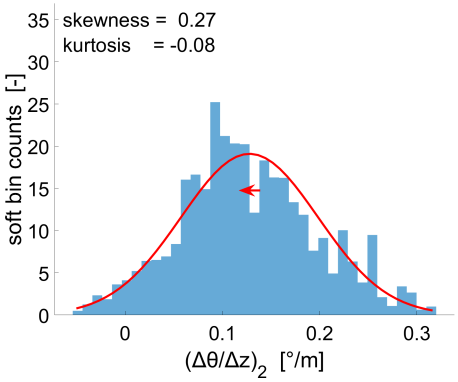

Figure 30: Gaussianity cluster 3 of TowerSide

Figure 31 shows the contribution of the wind sectors for each cluster. Large differences exist between the clusters. The sector dependence (SD) of 57.6% is a bit higher than the previously discussed load components, but far from 1.

Based on the bar graph, the relation between cluster 3 and 4 should be close. However, different conclusions could be drawn from the digraph. A direct relation between the two clusters is therewith not likely. Possibly, one cluster represents stable atmospheric conditions and one cluster unstable conditions.

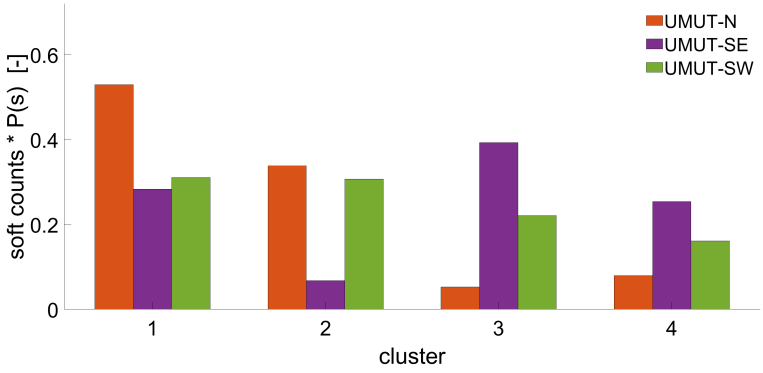

Figure 31: Wind sectors of clusters of TowerSide

Data points from the Southwestern sector are most equally distributed over the three sectors. Large differences exist between the contributions of the Northern and Southeastern sector.

The larger clusters 1 and 2 are dominated by points from UMUT-N and clusters 3 and 4 by points from UMUT-SE. The clear distinction between the two wind sectors was not found in the previously discussed combinations of variables and is therefore worth investigating in more detail.

The PDFs of the mean wind speed of the two wind sectors are by approximation equal (Fig. 12 in Section 5.1). The source of the clear difference in contributions is therefore likely the second wind veer variable. In this case, clear differences in PDF do exist between the wind sectors (Fig. 19 in Section 5.1). Moreover, the PDF of the Southwestern sector is situated in between the two.

As stated in Section 5.1, large differences between the two wind veer variables exist. Because these differences should be investigated further, no solid conclusions can be drawn on the importance of wind veer.

5.2.4 Yaw bending moment

Inflow variables used for the yaw bending moment are the wind shear exponent, the turbulence intensity and the second wind veer variable. Because the size of the considered dataset is limited, the clusters are small (Table 5). Moreover, the differences in cluster size are large.

The first cluster is found to have a high kurtosis for the wind shear exponent (Fig. 32). It takes a central position in the clustering space (no particularly low or high α). Other clusters have included data points with low or high α. They therewith took away the tails of the first cluster, resulting in the high kurtosis.

The Gaussianity of the other clusters are not considered because of their size. Having a limited amount of data points, no accurate representation of the PDFs can be made.

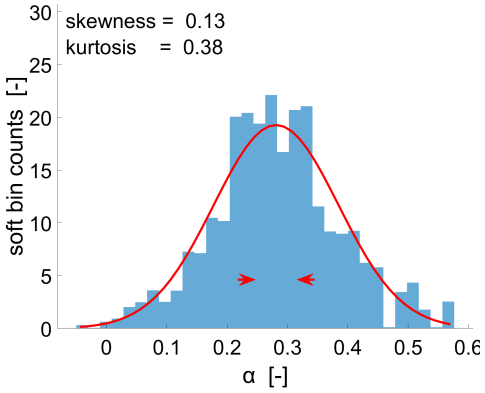

Figure 32: Gaussianity cluster 1 of ShaftYaw

The digraph (not shown) showed that cluster 4 is most different from the other clusters. However, being a cluster with only 21 data points, no solid conclusions can be drawn on this regard. When a fifth cluster is added, the other three clusters stay largely the same. The use of four clusters can therefore be considered appropriate.

The largest cluster contains data points of all three wind sectors (Fig. 24). This is not the case for the other clusters. The Southeastern wind sector does not contribute to cluster 2. Points of this sector can be found more often in the third and fourth cluster. The separation between the wind sectors is likely related to the second wind veer exponent. A similar separation was also found for the side-to-side bending moment (Subection 5.2.3). In this case, the sector dependence (SD) is found to be 63.3%.

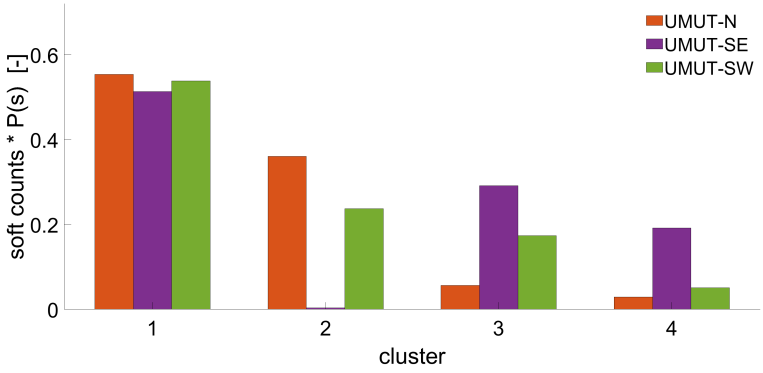

Figure 33: Wind sectors of clusters of ShaftYaw

5.2.5 *Tilt bending moment*

The best combination of variables for the tilt bending moment is TI, ρ and $\Delta\theta/\Delta z$. Being based on the same dataset as the yaw bending moment, the dataset is small. In this case the smallest cluster contains only 5 data points (Table 5).

The Gaussianity of solely the first cluster is considered. The other clusters contain too few data points to give a reliable probability distribution.

The PDF of the wind veer has a high skewness and kurtosis. The PDF has two peaks at each side and close to the main peak. However, with the limited amount of data points, it cannot be said with certainty if these peaks represent three different inflow conditions.

As found previously for clusters with high air density, the air density PDF for cluster 1 contains multiple peaks and has a low kurtosis. The peaks could represent multiple inflow conditions.

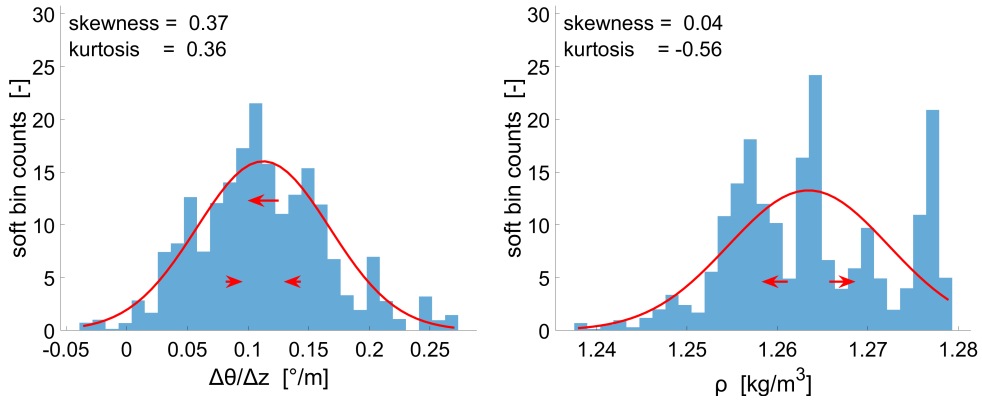

(a) Wind veer (b) Air density

Figure 34: Gaussianity cluster 1 of ShaftTilt

The digraph of the tilt bending moment is shown in Figure 35. One can derive from the digraph that cluster 1 and 2 are most closely related. Because of the limited amount of points, it is not possible to draw solid conclusions for cluster 4.

Going from three to four clusters, one of the clusters is removed, one new cluster (cluster 4) is added and a cluster is divided into cluster 1 and 2. The appearance and removal of a cluster while adding more clusters to the algorithm can point towards a sensitivity on the initial centroid locations. This is most likely if cluster centroids are located near each other. The appearance of two peaks close to the main peak in the wind veer PDF of cluster 1 supports this statement.

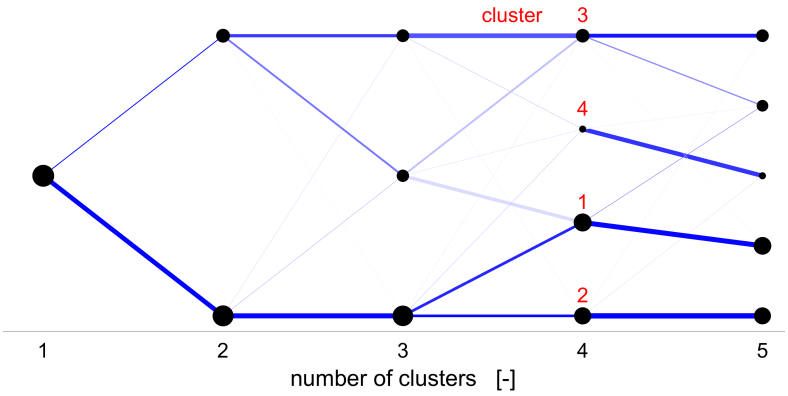

Figure 35: Digraph of ShaftTilt

The bar chart showing the contributions of the undisturbed wind sectors to the four clusters is shown in Figure 36. With an SD of 62.3%, the sector dependence is similar to the previous subsection and relatively high.

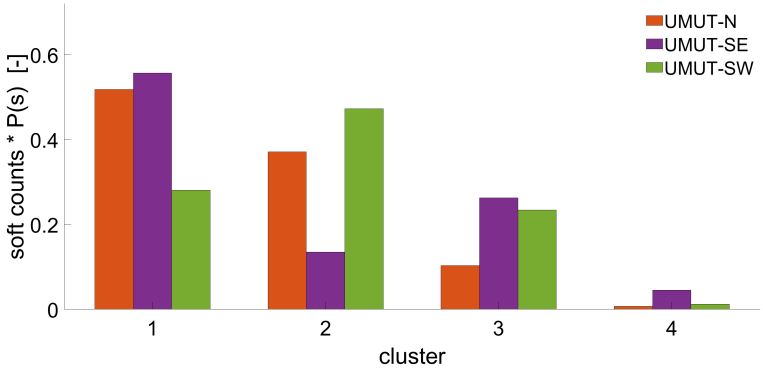

Figure 36: Wind sectors of clusters of ShaftTilt

5.3 Clustering with the disturbed wind sector

This section regards a comparison between the clustering results based on only undisturbed wind sectors and the clustering results based on all wind sectors.

The amount of data points in each cluster of each bending moment is stated in Table 6. Also in this case the cluster numbers are related to the size of the cluster such that cluster 1 is largest and cluster 4 is smallest. The cluster names of different bending moments are not related to each other. Moreover, they are not related to the cluster names of the clustering results with only undisturbed wind sectors.

Table 6: Number of data points in clusters of all wind sectors

bending moment	cluster 1	cluster 2	cluster 3	cluster 4	total
out-of-plane	8028	5680	1630	572	15909
flapwise	5684	5001	3189	2035	15909
in-plane	6749	4117	3189	1854	15909
edgewise	6259	4844	3105	1701	15909
side-to-side	8266	3962	2655	1920	16803
yaw	1927	1714	828	428	4897
tilt	2167	1815	497	417	4897

Depending on the occurrence of the different inflow conditions, the algorithm gives different results. If an inflow condition occurs relatively often (e.g. wake situation), other inflow conditions are less likely to be found.

The location and orientation of the clusters resulting from the out-of-plane bending moment are shown in Figure 37. The ellipses in this figure and in similar figures in this section represent contours with equal probability. The inside of the ellipses represent a total probability of 80%. I.e., on average 80% of the data points belonging in this cluster would fall inside the ellipses.

Most noticeable is a cluster with relatively low $wdci$ and $\Delta\alpha$ and relatively high α_2. It is found in the result based on all wind sectors. The low $wdci$ might be related to the relatively high turbulence intensity. For equal U and TI, no differences in $wdci$

were expected (Section 5.1). High α_2 and low $\Delta\alpha$, were expected from the analysis discussed in Section 5.1.

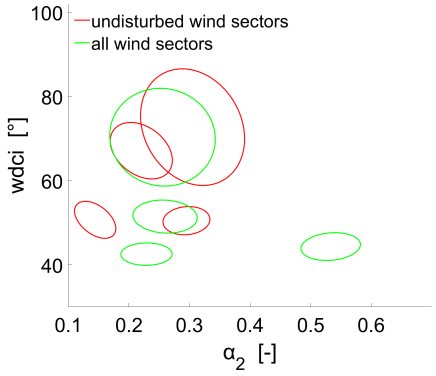

(a) Wind shear exponent and wind direction change intensity

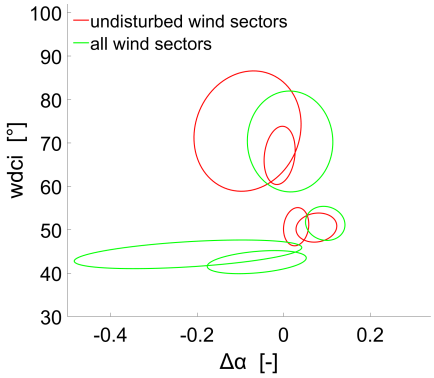

(b) Wind shear change and wind direction change intensity

Figure 37: Compare clusters of BladeOut

Clusters in the clustering space of the flapwise bending moment with U, TI and α are shown in Figure 38. Most noticeable is the removal of the cluster with low turbulence intensity if the disturbed sector is added. The Southern sector includes wake situations and therefore has a relatively high turbulence intensity (Section 5.1).

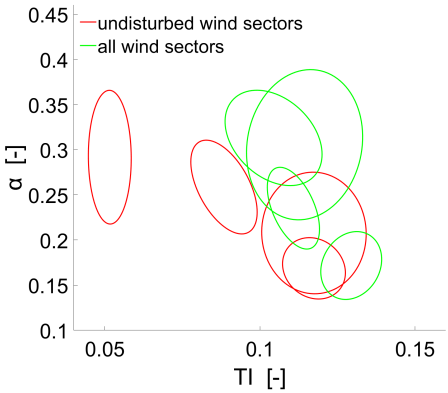

Figure 38: Compare clusters of BladeFlap

Figure 39 shows the clusters for the in-plane bending moment. The clusters based on all wind sectors are relatively close to each other. The two clusters which equal probability contours overlap each other, might be better represented as a single cluster. This is not investigated in detail.

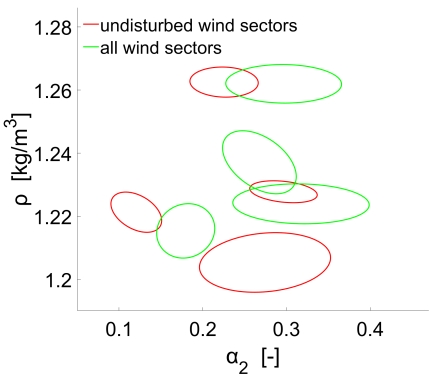

Figure 39: Compare clusters of BladeIn

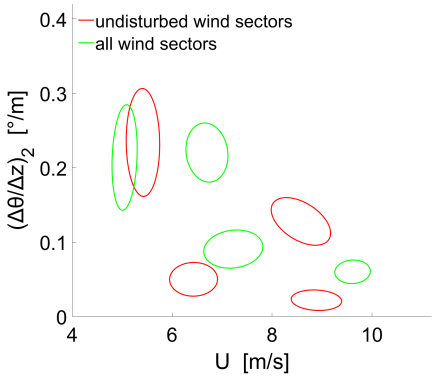

Figure 40: Compare clusters of Tower-Side

Figure 40 shows the clustering space of the side-to-side bending moment. The first cluster for the result of all wind sectors contains about half the data points. The second wind veer variable of the disturbed sector was found to be comparable with the Southeastern sector but higher than the other two (Section 5.1). As a result, the location of three of the four clusters are shifted upwards when the disturbed sector is added to the dataset.

Figure 41, regards the clustering space of the yaw bending moment. It is similar to that of the tilt bending moment (Fig. 42). Different from the flapwise bending moment, a cluster with low turbulence intensity is found when clustering all sectors. The cluster result based on all four wind sectors gives one cluster with low TI and three clusters with high TI. It points towards the existence of undisturbed situations within the Southern wind sector. A full or partial wake situation could not result in such low turbulence intensities. Most logical explanation for the difference with the flapwise moment, would be that the yaw and tilt bending moments regards different datasets. However, as shown in Table 3 the Southeastern sector giving mostly low turbulence is relatively small compared to the other datasets. One should therewith expect the reversed situation. Alternatively, the use of other variables in the clustering space should cause the differences.

Also relevant is the cluster based on all wind sectors having a relatively high wind veer and turbulence intensity. The existence of strong wind veer with a relatively high turbulence intensity is not expected. Mixing the atmospheric boundary layer, a high turbulence would result in low wind veer.

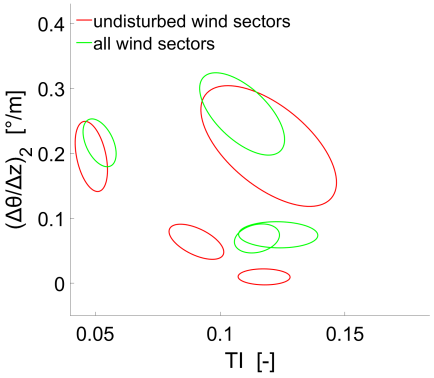

Figure 41: Compare clusters of ShaftYaw

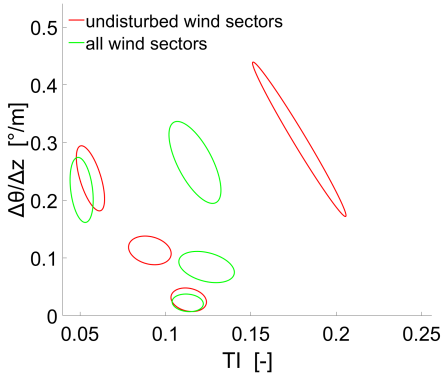

Figure 42: Compare clusters of ShaftTilt

The cluster of the tilt bending moment with high TI and high wind veer based on the

undisturbed sectors is the small cluster with 5 data points. It is therewith not very relevant in this project.

In general one can conclude that the clusters from the undisturbed sectors cannot be used to represent inflow conditions of the disturbed wind sector. The main differences are caused by the turbulence intensity. However, also the second wind shear exponent, the second wind veer variable and the wind direction change intensity are different.

6 Atypical fatigue loading

This chapter discusses the results regarding atypical fatigue loading. The eight bending moments are discussed one by one starting with the out-of-plane bending moment. With exception of the two blade root bending moments (edgewise and flapwise), each bending moment is given a separate section. The edgewise and flapwise bending moment are not discussed in detail because they are dependent on the out-of-plane and in-plane moments via the pitch angle.

The methodology used to obtain the results stated in this chapter is discussed in the first part of this report. This also regards information on how the figures are obtained.

The regression models and linear fits used to define the expected fatigue loading are shown in Appendix C. This appendix also includes the number of data points used to make the fatigue load expectation. The size of the dataset containing the yaw and tilt bending moments measured on the main shaft is limited (see Table 3 in Ch. 2). This resulted in considerable uncertainty on the results and conclusions.

For several bending moments, the variation in load residual of the disturbed sector is found to be higher compared to the other sectors. This was expected, because the sector includes different wakes of different turbines. The metmast and turbine can also be in full wake or in partial wake.

6.1 Out-of-plane bending moment

This section regards the out-of-plane bending moment. First, the expected fatigue loading is discussed together with differences between wind sectors. Afterwards, the results of the stepwise regression are stated. In the last subsection the clustering results are discussed.

6.1.1 Wind sectors and expected fatigue loading

The three regression models for the out-of-plane bending moment are shown in Figure 43. The model of the Southeastern sector (UMUT-SE) shows some unexpected behaviour (multiple curvatures). Cause of this behavior can be the limited number of data points. These data points might not all be independent of each other. Because the three models are not used in further analysis, the behaviour is not discussed in detail.

While the regression models of the two sectors with inflow from land are mostly parallel to each other, the Southeastern sector is not. In this case, the fatigue loading seems to be less affected by the mean wind speed. It is not necessarily a causal relationship, but only regards correlation. The model mainly deviates from the others in the higher wind speeds. As a result, the standard deviation based on all wind sectors is largest for the higher wind speeds.

Only the slope of the turbulence intensity fit is included in E(TI). One can therefore derive from the three regression models that the damage in the out-of-plane bending moment tends to zero for decreasing mean wind speed.

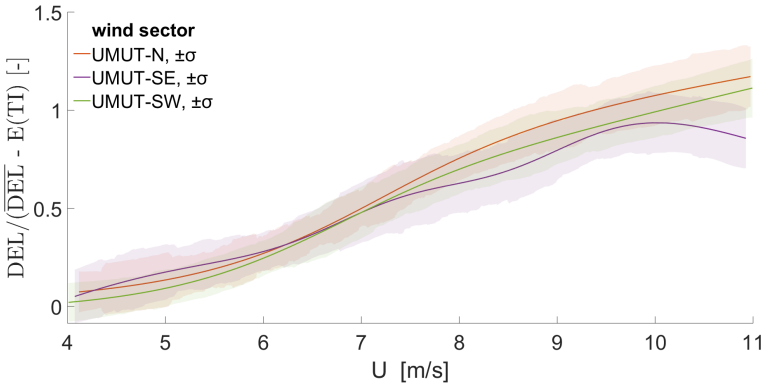

Figure 43: Wind speed regression models of BladeOut

The linear fits used to include the effect of the turbulence intensity are shown in Figure 44. Similar to the mean wind speed, the regression models of UMUT-N and UMUT-SW are, in approximation, parallel. The slope of the Southeastern sector is lower. I.e., the turbulence intensity correlates less with the out-of-plane bending moment.

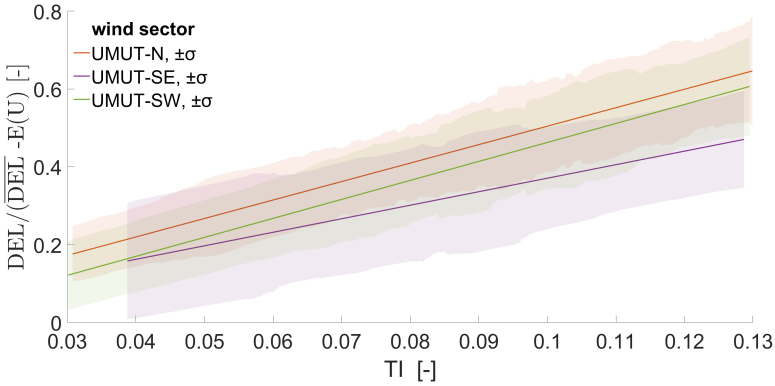

Figure 44: Turbulence intensity fits of BladeOut

From Figures 43 and 44 one can conclude that the turbulence intensity and the mean wind speed cannot explain all differences in the out-of-plane bending moment between the three undisturbed wind sectors. The moment of the Northern wind sector is higher than expected and the moment on the Southeastern sector gives lower loading. However, there is also a lot of overlap between the moving standard deviation bounds of the linear fits. The deviation within each sector is relatively large compared to the deviations between sectors.

As stated, the slopes of the linear fits with turbulence intensity are approximately equal for UMUT-N and UMUT-SW. Factors that cause the difference in fatigue loading, can therefore not be correlated to the turbulence intensity. However, multiple factors that are related to TI can have an affect on the fatigue loading if the effects cancel each other out.

Probability distributions of the residuals are shown in Figure 45. Data points in this figure are not restricted to a turbulence intensity range, and the distribution of the fourth sector with a disturbed metmast and turbine is also shown.

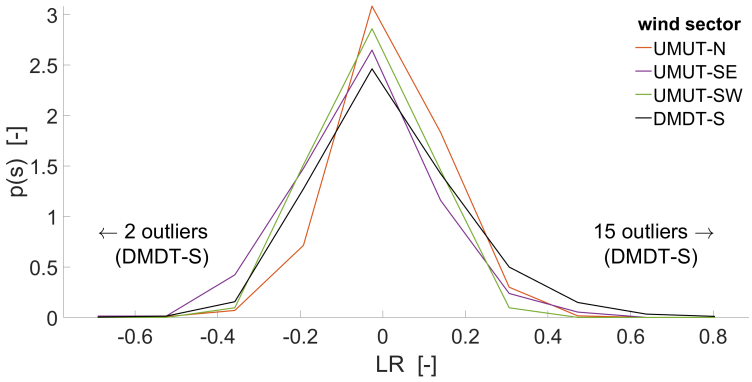

Figure 45: Residuals after turbulence intensity fit of BladeOut

Both the highest and the lowest load residual belong the the disturbed sector (outside of figure boundaries). Because this sector includes multiple wake situations and more data points, this is not unexpected. As previously stated, the Southeastern sector gives a little lower fatigue than expected and the Northern sector a little higher.

Given the mean load residuals of the wind sectors, a new load expectation can be made. In this case the decrease in relative error (DRE, see Section 4.6) is 2.2%. If different inflow conditions result in larger differences in fatigue, these inflow conditions cannot be strongly related to wind sectors.

Assuming that the distribution functions of the individual wind sectors are Gaussian and independent on the mean wind speed, the distribution containing all sectors is likely not. The distribution changes with wind speed because the regression model of UMUT-SE is not parallel to the others. Moreover, the final distribution is not Gaussian because the mean of the different wind sectors differ from each other (Figure 44 and 45).

The differences between the wind sectors with inflow from land and the sectors with inflow from the lake (UMUT-SE) support the need for multiple PDFs. Because of differences in regression models, the fatigue loading cannot be properly represented by a single Gaussian process.

6.1.2 Stepwise regression

The linear model resulting from the stepwise regression (Section 4.1) is shown in Equation 6.1. Sorted from most important to least important terms, the model proves that the turbulence intensity is most important after the wind speed is considered. Higher order terms of the turbulence intensity are not included in the model. I.e., the correlation between fatigue and TI is linear by approximation.

$$\begin{aligned} LR \approx -c_0 + c_1 TI - c_2\alpha + c_3\alpha^2 - c_4\left(\frac{\Delta\theta}{\Delta z}\right)_2 + c_5\left(\frac{\Delta\theta}{\Delta z}\right) \\ - c_6\left(\frac{\Delta\theta}{\Delta z}\right)_2^2 + c_7\left(\frac{\Delta\theta}{\Delta z}\right)_2^3 - c_8\left(\frac{\Delta\theta}{\Delta z}\right)_2^4 + c_9 wdci \end{aligned} \tag{6.1}$$

The second and third term includes the wind shear exponent (α). From the different signs in front of the coefficients, it is not directly clear if wind shear gives a positive or negative effect on fatigue. The squared term does imply that the correlation is not linear. The fact that these and other terms are included in the linear model does not necessarily mean that they are all important in a wider point of view. However, the relevance of wind shear was also found by Dimitrov et al. (2015).

The PDFs of the residuals are shown in Figure 46. The PDFs are different from those in Figure 45. The difference between the Northern sector and the other two undisturbed wind sectors is eliminated. The disturbed wind sector however, gives a higher load residual than the others. I.e., the increased precision in fatigue estimation of the undisturbed wind sectors uncovers the differences from the disturbed sector. The variables used in the regression model cannot explain these differences.

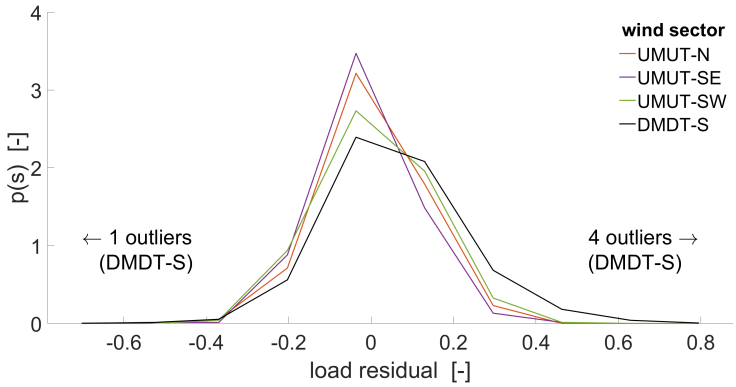

Figure 46: Residuals after stepwise regression of BladeOut

The decrease in relative estimation error caused by the linear model is 13.1%. Part of this increased precision can be explained by differences between the undisturbed wind sectors (DRE = 2.2%). By using an improved model (see Ch. 9), the relative estimation error can be decreased further. However, although the linear model does improve the fatigue estimation, it cannot be said with certainty that the wind shear and wind veer relate to the main source of error.

Figure 47 shows the extremes of the load residual in the most important space for stepwise regression (α and $(\Delta\theta/\Delta z)_2$). Data points with LR lower or higher than two times the standard deviation of the load residual are shown. On the background, the density of data points in the whole dataset is shown. A dark area represents a lot of data points (high density).

Two groups of data points with high LR can be determined. The first and largest group has low wind veer and high wind shear. The second group has high wind veer and low wind shear. In general, data points with high LR have either a strong wind veer or a strong wind shear. The data points with low LR are close to the area with highest density.

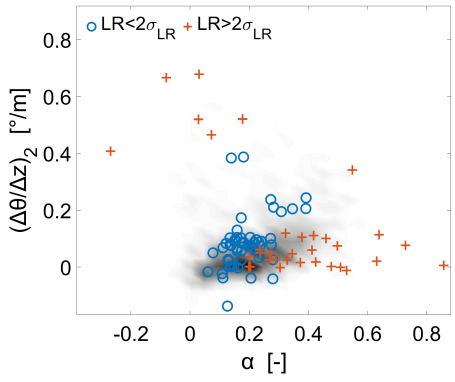

Figure 47: LR extremes of BladeOut in a part of the stepwise regression space

6.1.3 Clustering

As explained in Section 4.6, a variable selection has been done based on clustering different combinations of inflow variables. The best three combinations of three variables are shown in Table 7.

Clustering with three variables gives the best results. The used variables are the second wind shear exponent (α_2), the change in wind shear ($\Delta\alpha$) and the wind direction change intensity ($wdci$). The clustering result is able to decrease the relative error by 4.1% (DRE = 4.1%). The second best combination of variables includes the first wind shear exponent instead of the second. The third best includes the wind veer ($\Delta\theta/\Delta z$) instead of the wind shear change.

Comparing to the stepwise regression, the wind shear exponent is again important. The wind shear change on the other hand, was not included by the stepwise regression and $wdci$ only at the end. The groups of data points determined from Figure 47 are not found.

Table 7: Clustering with 3 variables for BladeOut

α_2	Δα	wdci	α	Δθ/Δz	DRE %	SD %	VD %
●	●	●			4.1	48.8	42.6
	●	●	●		4	48.9	41.6
		●	●	●	3.9	49.2	41.4

The best result with 3 variables can be compared with the results of two variables both also used in the best result (Table 8). All three combinations of two variables result in a considerably smaller decrease in error. The first two (α_2-$wdci$ and α_2-$\Delta\alpha$) are also the best two combinations considering only results based on two variables. From the table, one can conclude that the wind shear exponent is most essential to the clustering problem.

Given the use of $alpha$ in the linear model, a large part of the 4.1% is caused by differences in wind shear. The decrease in relative error is therewith mainly caused by a continuous effect of wind shear rather than discrete differences between inflow conditions. I.e., no significant discrete differences are found.

Table 8: Clustering with best variables for BladeOut

α_2	Δα	wdci	DRE %	SD %	VD %
●	●	●	4.1	48.8	42.6
●		●	3.4	47	31.6
●	●		3.1	48.5	29.4
	●	●	1.4	49.2	32.6

Adding a fourth variable in the clustering problem is not found to be useful. Adding for example the wind veer gives worse results in terms of decrease in relative error (DRE).

The PDFs of the load residual (LR) are shown in Figure 48. It regards the clustering result based on the undisturbed wind sectors. The first, third and fourth cluster show similar distributions.

The second cluster however, gives lower load residuals. In this cluster, the Northern wind sector is more important than the other undisturbed sectors (Fig. 24). However, the load residuals of the Northern sector in general, are higher than the other sectors. This fact points towards a situation with large differences in load residual within this sector. Containing more than a 1/3 of the data points, the differences in load residual between this and other clusters can be important for load expectation.

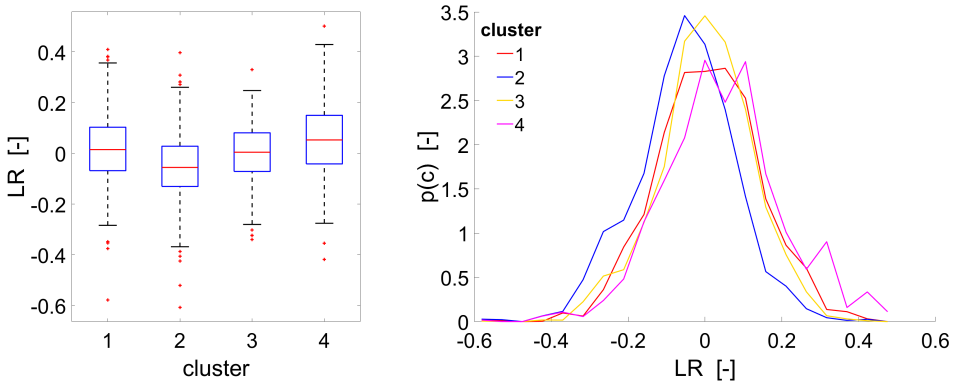

(a) Boxplots (b) Probability distributions

Figure 48: Residuals clustering of BladeOut

Data points with extremely low or high LR are shown in Figure 49 in the clustering space. The same data points as in Figure 47 are shown. Most data points away from the high density area are included in the cluster with largest variance. A cluster with small variance in a specific part of a low density area would not efficiently increase the total likelihood.

As expected, most data points with high LR have a high second wind shear exponent α_2 (just like α in Fig. 47). The subfigure with $wdci$ and $\Delta\alpha$, shows no separation between extremely low and extremely high LR in the high density area. Data points with low LR and out of the high density area are still relatively close to this area. Data points with high LR are generally further away given that they are not in this area.

With the very low load residuals occurring in between two groups of high load residuals, they might refer to neutral atmospheric conditions. More convincing proof on this regard is found by analysing the extremes of the flapwise bending moment (see Sec. 6.3).

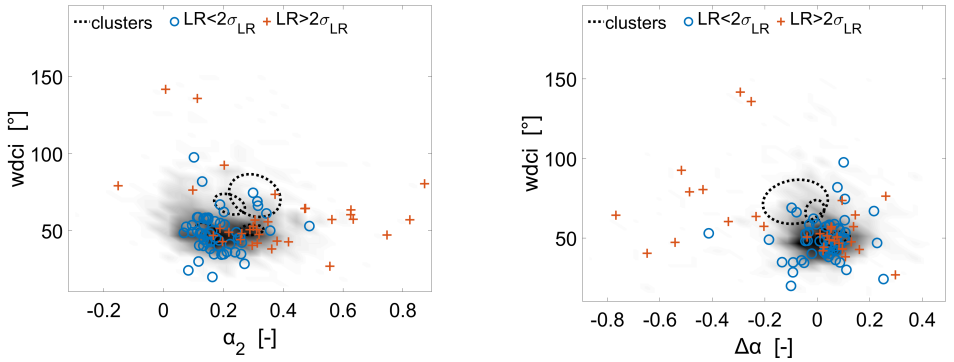

(a) Wind shear exponent and wind direction change intensity (b) Wind shear change and wind direction change intensity

Figure 49: LR extremes of BladeOut in clustering space

6.2 In-plane bending moment

In this section, the results for the in-plane bending moment are discussed. The first subsection regards the expected fatigue loading in relation with the wind sectors. Afterwards, results of the stepwise regression and clustering are discussed.

6.2.1 Wind sectors and expected fatigue loading

The regression models of the in-plane bending moment and the mean wind speed are shown in Figure 50. Before discussion, one should note that the y-axis does not start at zero. The in-plane bending is dominated by gravitational forces. The model of the Northern sector behaves poorly for higher wind speeds.

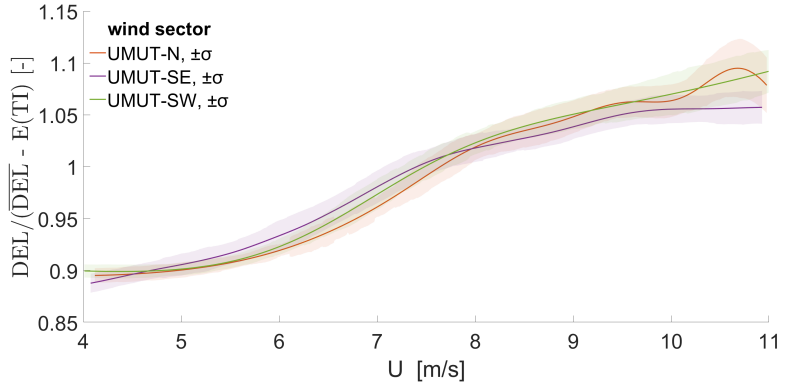

Figure 50: Wind speed regression models of BladeIn

Just like the out-of-plane bending moment, the Southeastern sector (coming from the lake) gives lower correlation between U and the fatigue loading, compared to the other undisturbed sectors. In this case however, the correlation between turbulence intensity and fatigue is stronger for this sector. The variation in fatigue within sectors is relatively large compared to the variation between sectors. This is caused by the limited amount of data points in this region.

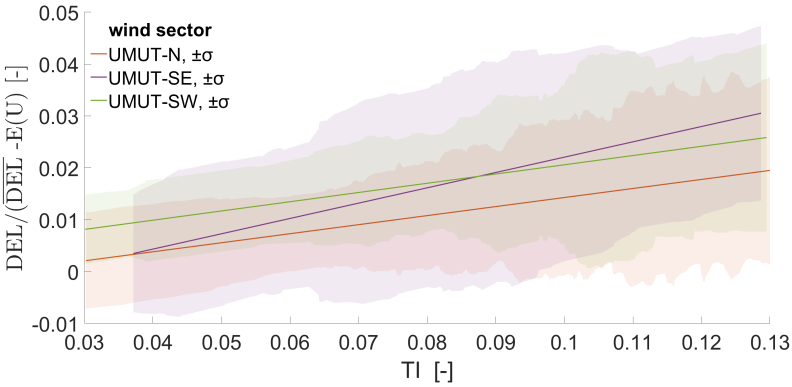

Figure 51: Turbulence intensity fits of BladeIn

The PDFs of the residuals are shown in Figure 52. Differences between the undisturbed wind sectors are small. Including the wind sector in the fatigue load estimation decreases the relative estimation error with 0.9%.

Also in this case, the disturbed sector gives the highest load residual. Different from the out-of-plane bending moment, the load residual is in general higher than in the other sectors.

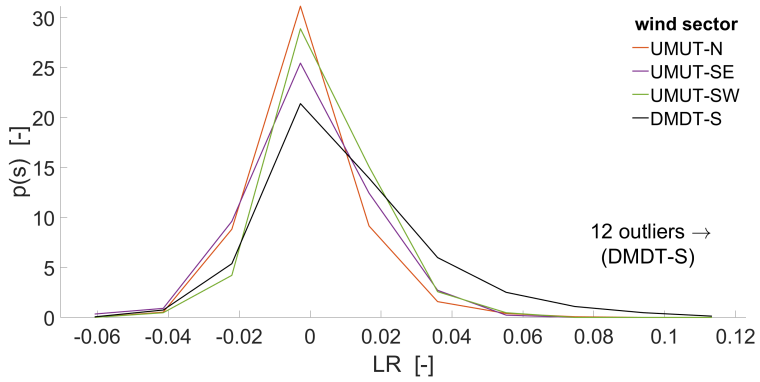

Figure 52: Residuals after turbulence intensity fit of BladeIn

6.2.2 Stepwise regression

The linear model for the fatigue by the in-plane bending moment is shown Equation 6.2.

$$LR \approx c_0 + c_1 TI - c_2 \rho - c_3 \lambda + c_4 U + c_5 \lambda^2 - c_6 \lambda^3 + c_7 \alpha \tag{6.2}$$

Again, the first term considers the turbulence intensity. The other less important terms however, are different. Although the wind shear exponent is included in the model, it has a minor role (last term). Instead of the wind shear exponent, TI is followed by the air density (ρ). The air density negatively correlates with the load residual. This is counter intuitive. However, it only regards correlation. Being related to other inflow variables that are not measured (e.g. atmospheric stability), a causal relationship is far from certain.

Also included in the model is the tip speed ratio (λ) and the mean wind speed. Because higher terms are included, it cannot be said that the tip speed ratio increases or decreases fatigue. However, based on the extremes, an increase in fatigue is most likely (Fig. 53). Being mainly dependent on gravitational forces, a small difference in λ can give a different in-plane bending moment.

Tip speed ratios can be high if the power output is larger than expected based on the mean wind speed. The in-plane bending moment is likely dominated by the rotational speed instead of the mean wind speed. The mean wind speed affects the power output and therewith the rotational speed. Most of the effect of rotational speed on the in-plane bending moment is therefore accounted for by the mean wind speed model. Because the effect of turbulence on the power output is relatively small, the effect of turbulence intensity on the in-plane bending moment is limited. This results in the low correlation with turbulence intensity.

Figure 53 shows a relatively equal spread of data points with very low and very high LR. A high tip ratio seems to give a higher probability for a very high LR. However, compared to the density of points in the whole dataset, this ”high” tip speed ratio is not exceptional.

Most notably is the group of data points with low air density and high tip speed ratio. This group largely consist of data points from the Southeastern wind sector and is mainly measured in the summer (see Section 5.1). It contains an unexpectedly high amount of data points with a load residual higher than $2\sigma_{LR}$. Moreover, the tip speed ratio is relatively high for these points. This is likely part of the source of the high fatigue loading. However, given the negative correlation between air density and the load residual, other factors are expected to play a role as well.

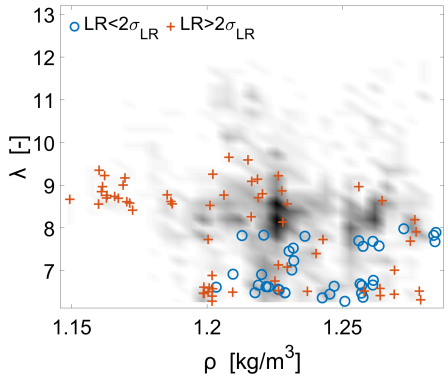

Figure 53: LR extremes of BladeIn in a part of the stepwise regression space

The total decrease in relative estimation error by the model is 14.2 %. The PDFs of the residuals of the linear model are shown in Figure 54. They are similar to those based on solely the turbulence intensity and mean wind speed. Differences between the disturbed and undisturbed sectors cannot be explained by the linear model.

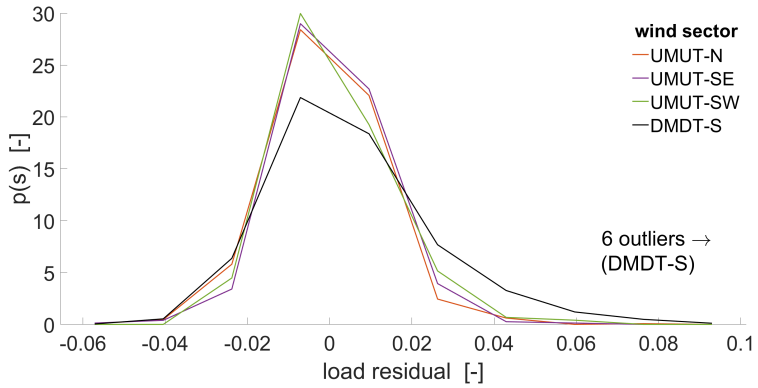

Figure 54: Residuals after stepwise regression of BladeIn

6.2.3 Clustering

The air density and the second wind shear exponent (α_2) give the best clustering results. The relative error is decreased by 4.3% (Table 9). Clustering with three results gives at best a decrease of 3.5% with the combination α, $(\Delta\theta/\Delta z)_2$ and ρ.

Compared to the relative error decrease of 14.2% by the stepwise regression, the clustering method performs poorly. The difference can be connected to the fact that the tip speed ratio is not considered for the clustering space. Because the tip speed ratio is not considered for clustering, the used combination of variables agrees well with the stepwise regression.

Table 9: Clustering with 2 variables for BladeIn

α_2	ρ	Δα	α	DRE %	SD %	VD %
●	●			4.3	47.9	40.5
	●	●		3.8	50.1	45.9
	●		●	3.8	46.6	39.8

The PDFs of the residuals of the four clusters are shown in Figure 55. The PDF of cluster 3 is almost an exact copy of that of cluster 2. Moreover, cluster 1 gives the lowest load residuals and cluster 4 the highest. This fact supports the assumption that at least four clusters are needed. This is relevant, because the Gaussianity of the clusters pointed towards a better result with three clusters.

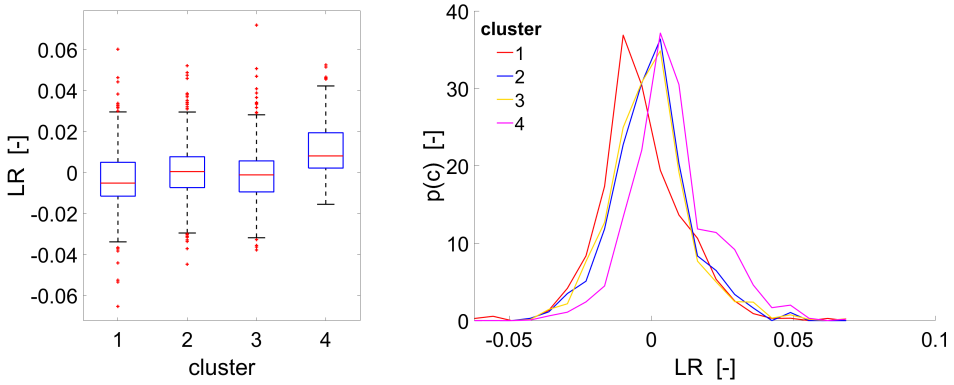

(a) Boxplots (b) Probability distributions

Figure 55: Residuals clustering of BladeIn

In Figure 56, the data points with very high and very low LR are shown in the clustering space. The clusters cannot properly differentiate between the two extremes. Moreover, multiple groups can be identified. Firstly, as already noted, a group of high LR was found for low air density. Secondly, the points with very high LR are located to the right (higher wind shear) and points with low LR are located to the left. In case of an about average air density, very low load residuals are also found at other wind shear values.

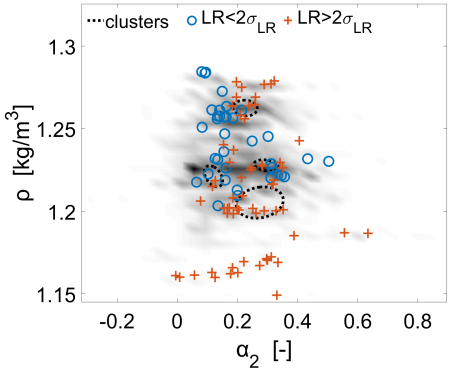

Figure 56: LR extremes of BladeIn in clustering space

6.3 Flapwise & edgewise bending moments

The flapwise and edgewise bending moments are related to the out-of-plane and in-plane bending moments. They are therefore not discussed in detail, but the results are compared with those of the rotor loading.

6.3.1 *Wind sectors and expected fatigue loading*

The importance of the mean wind speed is found to be lowest for the flapwise bending moment and the importance of turbulence intensity highest. The importance of U and TI for the edgewise moment is similar to that for the in-plane bending moment. The small differences can be explained by the influence of the out-of-plane component being part of the edgewise moment.

From the bending moments measured at the blade root, the load residual of the flapwise bending moment is most dependent on wind sectors. The relative error is decreased by 3.3%.

6.3.2 *Stepwise regression*

The linear model of the flapwise moment produced by stepwise regression (Eq. 6.3) differs from that of the out-of-plane bending moment. Two terms of the wind veer variables are included after the turbulence intensity. The model does not include the two terms of the wind shear exponent. However, this does not necessarily mean that it is not affected by wind shear at all. The main correlation can be included by the other terms (e.g. wind veer). It does points towards the fact that wind veer is more important than wind shear. The linear model decreases the relative error by 10.1%. This is lower than the 13.1% for the out-of-plane.

$$LR \approx c_0 + c_1 TI - c_2 \left(\frac{\Delta\theta}{\Delta z}\right)_2 + c_3 \left(\frac{\Delta\theta}{\Delta z}\right) + c_4 wdci - c_5 \left(\frac{\Delta\theta}{\Delta z}\right)_2^2 + c_6 \left(\frac{\Delta\theta}{\Delta z}\right)_2^3 - c_7 \left(\frac{\Delta\theta}{\Delta z}\right)_2^4 \tag{6.3}$$

A clear distinction between very high and very low load residuals is found in the two dimensional space with wind veer and wind direction change intensity (Fig. 57). Five outliers with very high LR have high $wdci$ and high wind veer. In a more general sense, the wind direction change intensity is relatively high for very high load residuals. The extremes are discussed in more detail when considering the clustering space.

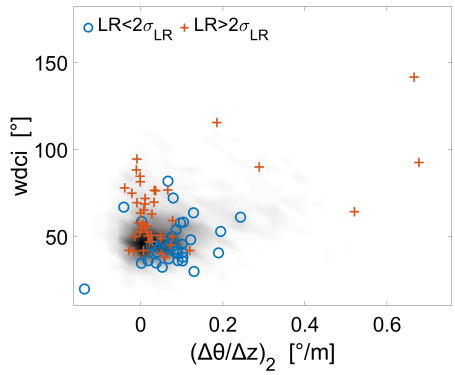

Figure 57: LR extremes of BladeFlap in a part of the stepwise regression space

As expected, the terms used for the edgewise bending moment (Eq. 6.4) are similar to those of the in-plane bending moment. In this case, the tip speed ratio and the mean wind speed are not included. The usefulness of stepwise regression for the edgewise bending moment is relatively low with a decrease of 6.1% in relative estimation error.

$$LR \approx c_0 + c_1 TI - c_2 \rho + c_3 \alpha \tag{6.4}$$

6.3.3 Clustering

A major difference between the flapwise bending moment and the out-of-plane bending moment are the variables used for clustering. The flapwise bending moment uses three different variables, namely U, TI and α (see Table 10). The values of DRE are comparable. This combination of variables only gives a slightly smaller DRE (3.8%) for the flapwise bending moment compared to the the out-of-plane bending moment. As stated in Appendix B, the GMM algorithm did not produce well defined clusters.

Table 10: Clustering with 3 variables for BladeFlap

U	TI	α	$(\Delta\theta/\Delta z)_2$	wdci	α_2	Δα	DRE %	SD %	VD %
●	●	●					3.8	47.4	40.5
●			●	●			3.3	49.7	44.9
			●		●	●	2.9	54	40.6

A smaller bound of wind shear exponents is found for the very low load residuals compared to the very high load residuals (Fig. 58). This corresponds to neutrally stable atmospheric conditions. Holtslag et al. (2014a, 2016) also found that blade root and rotor loading are lowest in neutral conditions. In Figure 57, the low load residuals correspond to medium wind veer. This fact also points towards neutrally stable atmospheric conditions.

Moreover, very high load residuals have either a medium turbulence intensity or a very low turbulence intensity. Neutrally stable conditions are therewith not included. These two groups can be related to the groups found in Figure 57. For very stable conditions, the wind veer is, as expected, relatively high. The very unstable conditions result in the low wind veer.

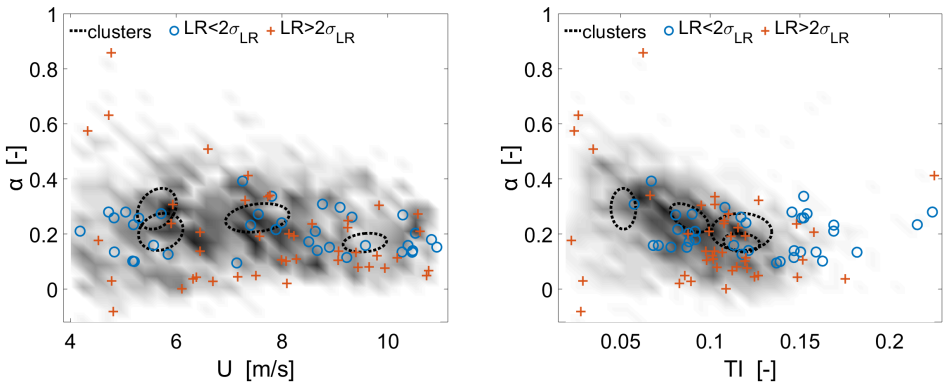

(a) Mean wind speed and wind shear exponent (b) Turbulence intensity and wind shear exponent

Figure 58: LR extremes of BladeFlap in clustering space

The best variables for the edgewise bending moment are found to be the same as the best variables for the in-plane bending moment (α_2 and ρ). The DRE for the edgewise-moment is a little lower with 3.9 % compared to 4.3% for the in-plane bending moment. The values of SD and VD are related to the used variables and are therefore also the same.

6.4 Fore-aft bending moment

This section regards the fore-aft bending moment measured at the tower bottom. Only the expected fatigue loading is discussed in relation with the undisturbed wind sectors. The linear model produced by stepwise regression included the wind direction change intensity after the turbulence intensity. Because the decrease in estimation error is as low as 1.2%, the results are not discussed further. The performance of the clustering result is with a DRE of 2% also poor. The best variable combination is found to be U, ρ and α. Also these results are not discussed in more detail.

6.4.1 Wind sectors and expected fatigue loading

The wind speed regression models of the undisturbed wind sectors are shown in Figure 59. A comparable increase in fatigue is found for all three wind sectors. Different from other bending moments, the variation in fatigue loading increases with mean wind speed within the three wind sectors. Being the most damaging conditions, high uncertainty for high wind speeds is undesired.

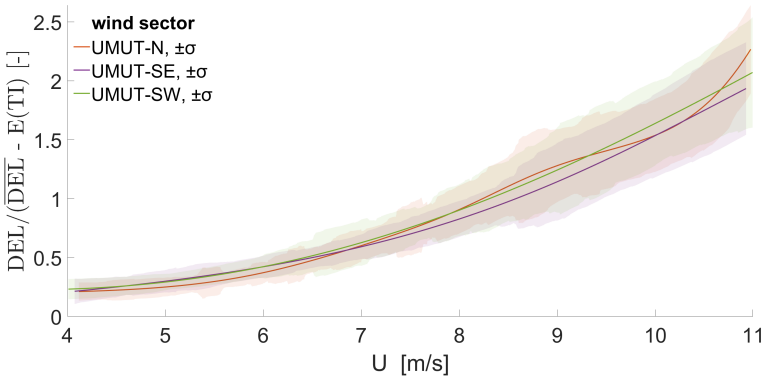

Figure 59: Wind speed regression models of TowerFore

Also the linear fits with turbulence intensity (not shown) showed only very small differences between the three sectors. Moreover, the variance is strong compared to the slopes of the fits.

The found increase in fatigue for turbulence intensity is consistent with research of Holtslag et al. (2016) and Sathe et al. (2013). Both found higher fore-aft bending moments for unstable conditions. However, with a DRE of 8.9%, this bending moment is, after the in-plane bending moment, the least correlated with turbulence intensity.

Sathe et al. (2013) states that the rotor filters small eddies. One could therefore expect that the disturbed sector, resulting in larger eddies, will give a higher load residual. This is not found in this research project. The PDFs of the load residuals for the four wind sectors are all equal by approximation. They are therefore not shown in this report.

6.5 Side-to-side bending moment

In this section, the results of the side-to-side bending moment are discussed. Similar to other bending moments, the expected fatigue loading is discussed first in relation with the wind sectors.

The side-to-side bending moment is known to have little damping (e.g. Bir and Jonkman (2007)). The effect of inflow conditions on fatigue loading can therefore differ from other bending moments.

6.5.1 *Wind sectors and expected fatigue loading*

The mean wind speed models for the three undisturbed wind sectors are shown in Figure 60. Similar to the out-of-plane and in-plane bending moment, the model of the Southeastern sector shows weaker correlation with fatigue.

Differences between the Northern and Southwestern sector are visible for wind speeds higher than 7 m/s. Just like the out-of-plane bending moment, the fatigue for the Northern sector is a bit higher than expected in this wind speed range.

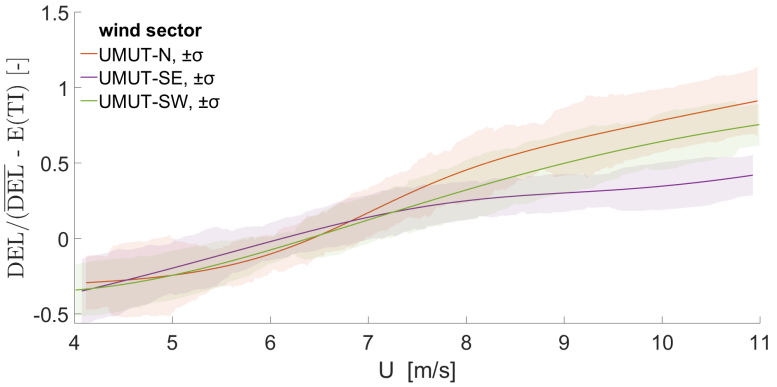

Figure 60: Wind speed regression models of TowerSide

With a DRE of 32.3%, the correlation with wind speed and fatigue loading is lowest for the side-to-side moment. The importance of the turbulence intensity is relatively large (DRE = 42.3%).

The linear fits with TI of the three different sectors are shown in Figure 61. The slope of the models are approximately equal. In other words, the correlation between TI and fatigue loading does not differ between the wind sectors. The slightly more gentle slope of the Southeastern sector does agree with the correlation of turbulence intensity with the out-of-plane bending moment.

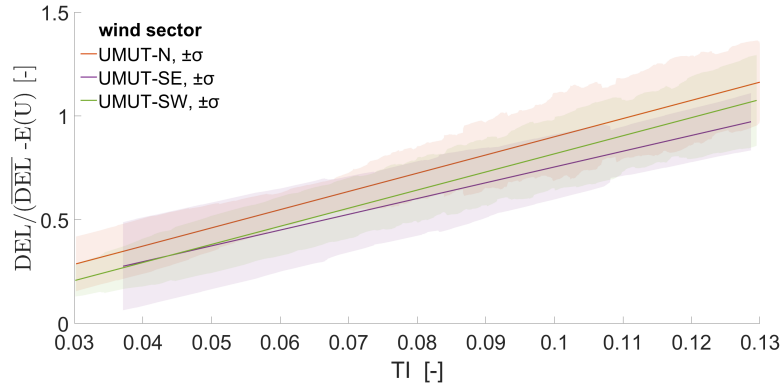

Figure 61: Turbulence intensity fits of TowerSide

The PDFs of load residuals are shown in Figure 62 for all four sectors. The regression models used for these residuals are based on all three undisturbed sectors and shown in Figure 90 in the appendix.

The disturbed Southern sector gives the lowest load residuals. As discussed above, the Southeastern sector also gives lower LR than the other sectors and the Norther sector gives the highest LR. The four PDFs seem to be the opposite of the PDFs of the second wind veer variable (Fig. 19). Below, more proof is shown that the two are related.

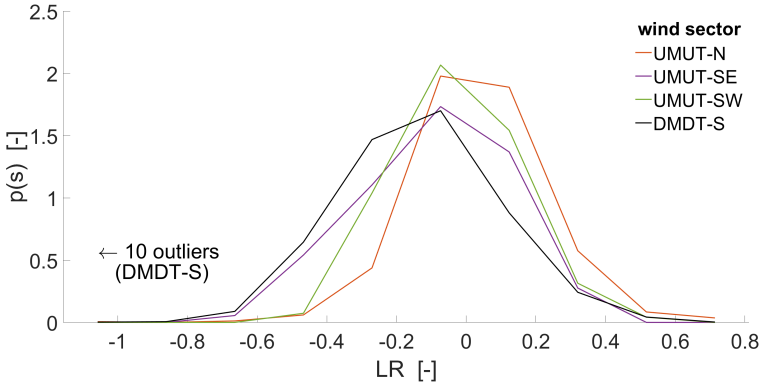

Figure 62: Residuals after turbulence intensity fit of TowerSide

6.5.2 *Stepwise regression*

The turbulence intensity is lastly removed from the linear model, after terms of the two wind veer variables (Eq. 6.5).

$$LR \approx c_0 + c_1 TI - c_2 \left(\frac{\Delta\theta}{\Delta z}\right)_2 + c_3 \frac{\Delta\theta}{\Delta z} - c_4 \alpha_2 \tag{6.5}$$

Being dependent on each other, the use of two wind veer variables is not expected. However, small differences between the two variables were found previously (Section 5.1).

The linear regression model is able to decrease the relative estimation error with 9.2%. The resulting residuals are shown in Figure 63. The differences between the PDFs of the different wind sectors are for a large part eliminated. This is caused by including the second wind veer variable, which PDFs are opposite to that of the load residual. It therewith also confirms the importance of wind veer for the side-to-side bending moment.

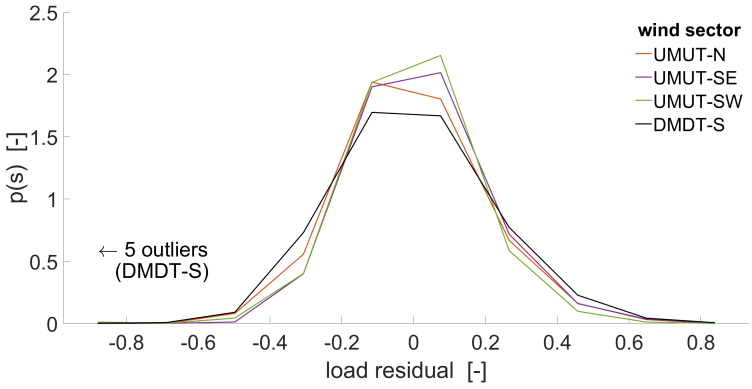

Figure 63: Residuals after stepwise regression of TowerSide

Despite being slightly different, the wind veer variables are dependent on each other. It is therefore decided not to plot the extremes on the space with wind veer variables but to include the wind shear (Fig. 64).

The figure clearly show that most data points with very high LR have both low wind veer and low wind shear. The opposite is the case for data points with very low LR. Considering atmospheric stability, the low load residuals likely relate to stable conditions and the high residuals to unstable conditions. Exceptions are the three data points with low LR and low wind veer.

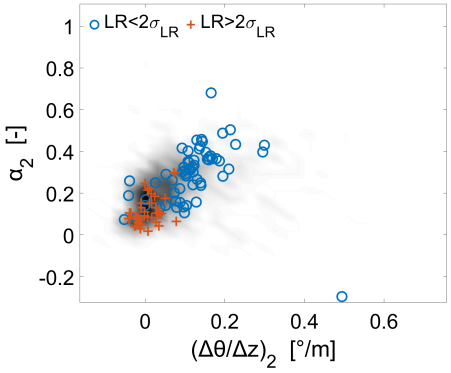

Figure 64: LR extremes of TowerSide in a part of the stepwise regression space

6.5.3 Clustering

The best combination with two variables (U and $(\Delta\theta/\Delta z)_2$) gives a DRE of 10.6% (see Table 11). The best three combinations with three variables do not include wind veer and result in a lower decrease in relative estimation error.

With 10.6% the DRE of the clustering result is slightly higher than that of the stepwise regression and more than twice as high as the clustering DRE of other bending moments. Moreover, it is three times higher than the DRE based on the undisturbed sectors. This is especially important because of the issues with the wind veer variables. Given that the differences across clusters are larger than the differences between clusters, issues with measurement cannot depend on wind sector.

Table 11: Clustering with 2 variables for TowerSide

U	$(\Delta\theta/\Delta z)_2$	TI	α_2	DRE %	SD %	VD %
●	●			10.6	57.6	39.9
	●	●		4.9	56.4	34
		●	●	4.4	50.4	32.4

PDFs of the load residual of the four clusters are shown in Figure 65. The PDFs of cluster 1, 2 and 3 are similar to each other. The third cluster, however, gives much lower loading than the other sectors. In this cluster, consisting of 334 of the 1793 data points, the Southeastern wind sector is most important (about half the data points) (see Subsection 5.2.3). Based on the large contribution of this sector, the lower load residual is expected. However, with a DRE of 10.6%, the fatigue estimation is better than if the wind sectors were used instead of clusters (3.6%). One can conclude that the inflow condition represented by this cluster lowers the average LR in the Southeastern sector instead of the other way around.

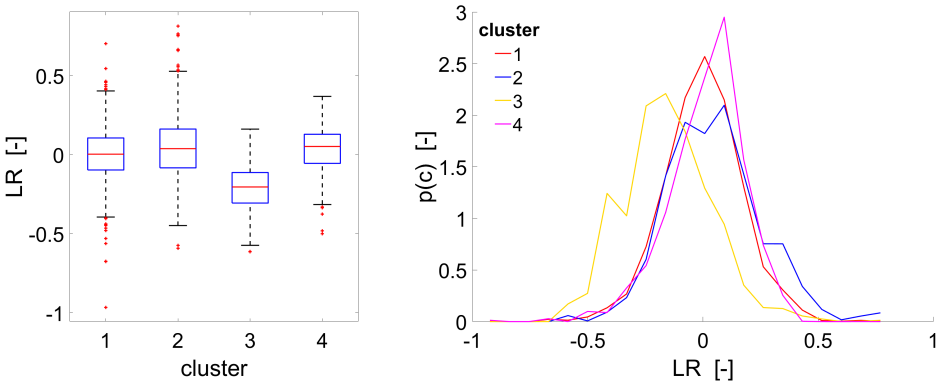

(a) Boxplots (b) Probability distributions

Figure 65: Residuals clustering of TowerSide

The data points with either extremely low or extremely high LR are shown in Figure 66. Three groups of extremes can be determined. The group with very high LR is found for higher wind speeds and low wind veer. As previously stated, these data points relate to unstable atmospheric conditions. The first group with very low LR has low wind speed and various values for wind veer.

The second group with low LR has the highest wind speeds in the wind range considered, and high wind veer. Given the little amount of data points in this area, the low load residuals can relatively easily been separated from other conditions. Moreover, given the low correlation with wind speed for the Southeastern sector, this group of very low load residuals likely correspond to this sector. More proof on this statement can be found in Section 5.1. The Southeastern sector has a relatively high second wind veer variable compared to the other undisturbed sectors.

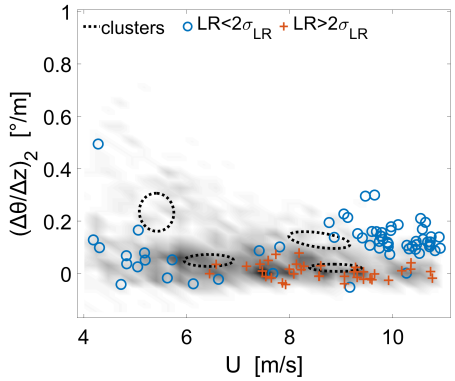

Figure 66: LR extremes of TowerSide in clustering space

6.6 Yaw bending moment

This section regards the yaw bending moment measured at the main shaft. First, the expected fatigue loading is discussed in relation with the different wind sectors.

6.6.1 Wind sectors and expected fatigue loading

As shown in Table 19, there are only 22 data points for sector UMUT-SE. This is not enough to make a proper fit. However, the data is used to evaluate the regression models. Based on the mean wind speed, regression models are made for two of

the three undisturbed wind sectors. The result can be seen in Fig. 67. No large differences between the two sectors are found.

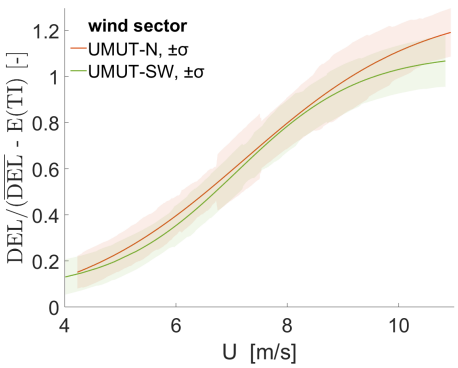

Figure 67: Wind speed regression models of ShaftYaw

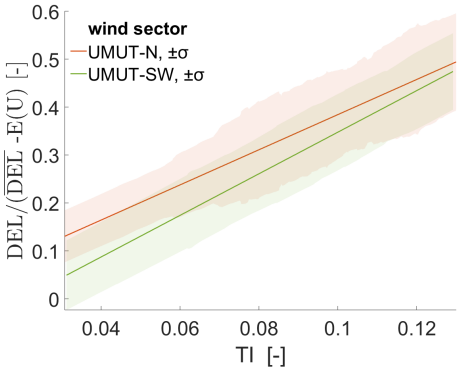

Figure 68: Turbulence intensity fits of ShaftYaw

In Figure 68, the two linear fits with turbulence intensity are shown. The slope of the Southwestern sector is steeper than that of the Northern sector. In case the models would be perfectly aligned, the difference in fatigue between the different sectors, can be fully explained by a difference in turbulence intensity. Because this is not the case, other parameters that differ from sector to sector, should also affect the fatigue loading. However, because the difference is fairly small, and the dataset size of especially the Southwestern sector is also limited, no solid conclusions can be drawn on this regard.

The PDFs of the residuals of all four sectors are shown in Figure 69. The load residual of the disturbed sector (UMUT-S) is found to be comparable with that of the Northern sector. The residuals of the Southeastern sector are highest and the Southwestern sector lowest. However, because of the limited data, the PDF of the Southeastern sector is not reliable.

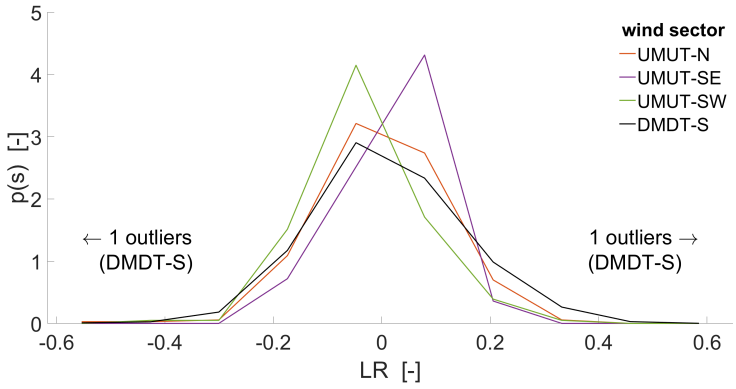

Figure 69: Residuals after turbulence intensity fit of ShaftYaw

6.6.2 *Stepwise regression*

The linear model resulting from stepwise regression only includes two terms of the turbulence intensity (Eq. 6.6). The model is able to decrease the estimation error with 4.7%. The main differences between the wind sectors are eliminated (PDFs not shown).

The squared term with turbulence intensity does not support widely accepted theory (see Section 3.2). Because the decrease in estimation error is not so large, and the dataset size is small, no solid conclusions can be drawn on this regard. More-

over, the not linear relation can be caused by the difference in dataset used for the expected loading and the stepwise regression. With a relatively high number of data points from the Northern sector used for the expected loading (see App. C), differences between sector contributions can affect the linear model. For future research, it is therefore advised to investigate this relationship in more detail, when the sector contributions are equal at all times.

$$LR \approx -c_0 + c_1 TI - c_2 TI^2 \tag{6.6}$$

Because of the limited dataset size, it is also difficult to analyse extremes for the yaw and tilt bending moments. Nevertheless, the extremes in LR of the yaw moment are shown in Figure 70. No clear pattern can be recognised. However, the data points with very high LR seem to be located in high density areas (area with a lot of other data points), whereas data points with very low LR are located away from these areas.

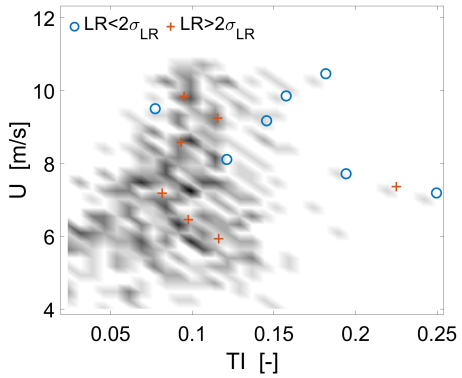

Figure 70: LR extremes of ShaftYaw in a part of the stepwise regression space

6.6.3 *Clustering*

Clustering with three variables gives the strongest decrease in error. The combination with TI, α and $(\Delta\theta/\Delta z)_2$ gives the best result with a DRE of 4.5%. From these three variables, the wind shear exponent is most important (Table 12). The combination of α and wind veer give the best results if only two variables are used.

Park et al. (2015) and Gutierrez et al. (2016) both found that the wind veer has an affect on the tower torsion/tower-top yawing moment. Because these moments directly relate to the yawing moment of the shaft, the same results should be expected. Although the second wind veer variable is included in the clustering space, it does not continuously affect the yaw bending moment (see linear model).

Table 12: Clustering with best variables for ShaftYaw

TI	α	$(\Delta\theta/\Delta z)_2$	DRE %	SD %	VD %
●	●	●	4.5	63.2	39.9
	●	●	3.6	66.2	26.6
●	●		3.4	62.3	38
●		●	2.1	64.2	32.3

The probability distributions of LR in the clusters are shown in Figure 71. Cluster 1 contains more than half the data points and gives the highest load residuals. The

wind sectors are all about equally important for this cluster. The average LR of the other clusters are more or less the same. The decrease in load residual is therefore mainly caused by the difference between cluster 1 and the other clusters. Variance within clusters is much larger than variance between clusters. The clustering result itself is therefore not useful for load prediction.

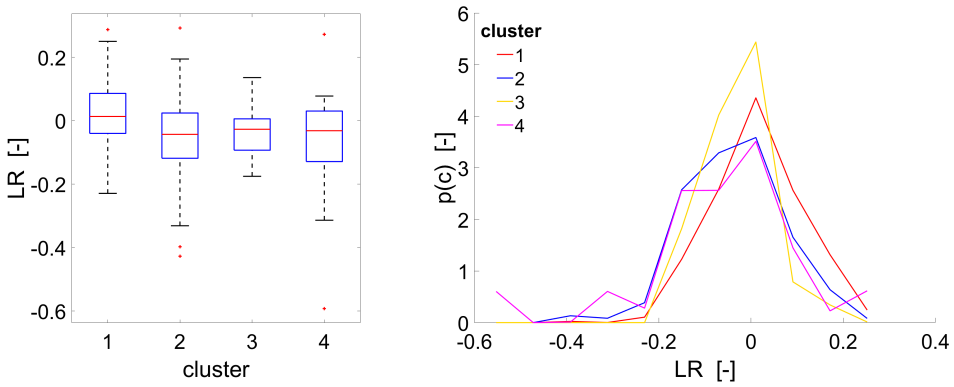

(a) Boxplots (b) Probability distributions

Figure 71: Residuals clustering of ShaftYaw

Data points with very low or high load residual are shown in Figure 72 in the clustering space. Two groups of extremes can be determined. Very low load residuals are found for low wind shear and wind veer (high atmospheric stability), and very high load residuals for higher wind shear and wind veer (low atmospheric stability). Similar to Figure 70 the very high LR are located in high density areas. However, because of the small amount of data points, no proper analysis can be done.

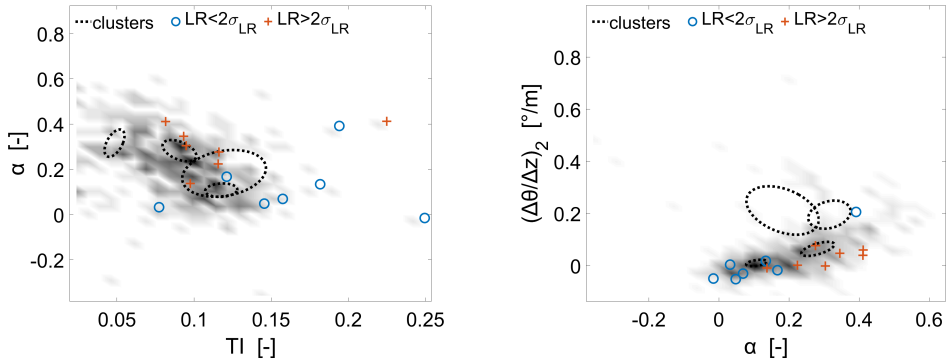

(a) Turbulence intensity and wind shear exponent (b) Wind shear exponent and wind veer

Figure 72: LR extremes of ShaftYaw in clustering space

6.7 Tilt bending moment

This section discusses the results of the tilt bending moment. Both the load expectation, stepwise regression and clustering results are discussed.

6.7.1 Wind sectors and expected fatigue loading

Similar to the shaft bending moment, no wind speed model of the Southeastern sector could be made. The wind speed models of the other two undisturbed sectors are

shown in Figure 73.

The fatigue loading at the higher wind speeds is a bit lower for the Southwestern sector than the Northern sector. Because the out-of-plane, side-to-side and the yaw bending moment also showed a small difference in higher wind speeds, the difference is not unexpected. However, because of the limited amount of data points, a more accurate model is preferred.

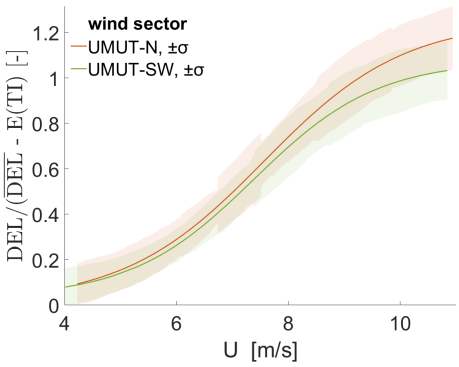

Figure 73: Wind speed regression models of ShaftTilt

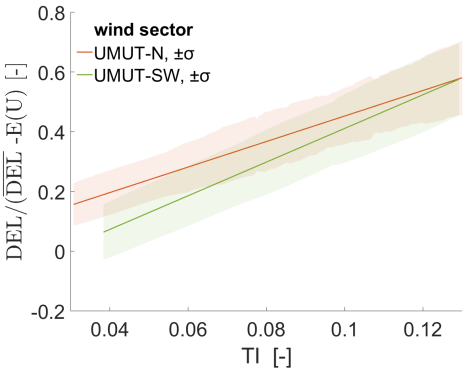

Figure 74: Turbulence intensity fits of ShaftTilt

The slope of the turbulence intensity model of the Southwestern sector is found to be steeper than the Northern sector (similar to yaw bending moment). Because the amount of data is limited one should be careful with drawing conclusions. Because the fits in the yaw bending moment are based on the same data, it cannot give a valid confirmation on the existence of different slopes.

The PDFs of the residuals based on the mean wind speed and turbulence intensity regression are shown in Figure 75. Small differences between the sectors are found. Based on the sectors, the estimation error can be decreased by 2%.

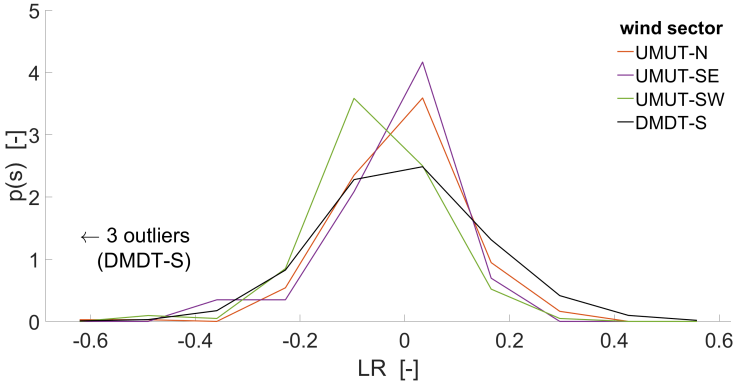

Figure 75: Residuals after turbulence intensity fit of ShaftTilt

6.7.2 Stepwise regression

After the turbulence intensity, the second term included in the linear model is the second wind veer variable. This term, is able to decrease the estimation error by 4.3%. Moreover, differences between the wind sectors are more clear compared to Figure 75. The disturbed wind sector DMDT-S gives slightly higher load residuals than the undisturbed wind sectors (Fig. 76). This relates to the higher second wind veer variable (Section 5.1) in this sector. The expected load is decreased with the wind veer term, and the load residuals are therefore higher. In future research, it is

worth investigating what happens if the stepwise regression is used in combination with the clustering results (see Ch. 9). This could clear the way for analysing the differences between the disturbed sector and the undisturbed sectors.

The distribution shape of the Southeastern wind sector is different from the others. However, because of the low amount of data points, this PDF is not reliable.

$$LR \approx c_0 + c_1 TI - c_2 \left(\frac{\Delta\theta}{\Delta z} \right)_2 \tag{6.7}$$

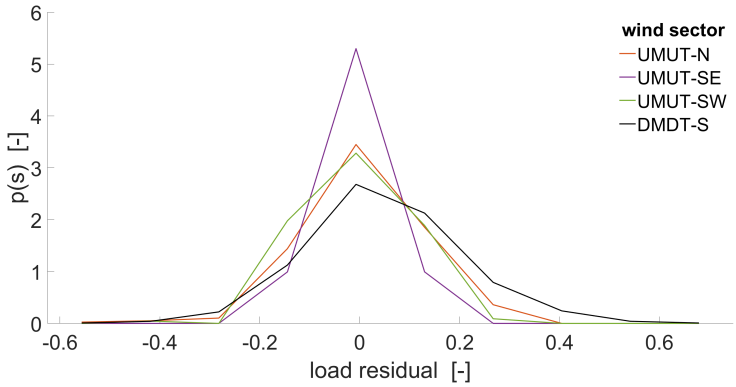

Figure 76: Residuals after stepwise regression of ShaftTilt

The data points with either very low or very high load residual are shown in Figure 77. Similar to the yaw moment, the extremes with high LR are located at high density areas and extremes with low LR away from these areas. Apart from this, no pattern can be recognised. A larger dataset might give more information on this regard.

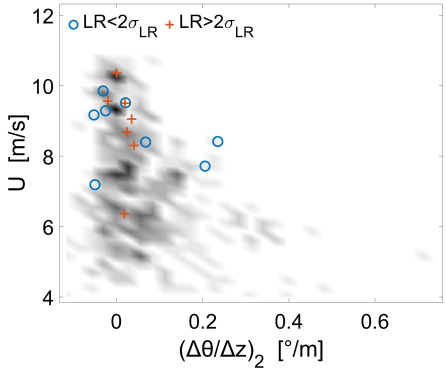

Figure 77: LR extremes of ShaftTilt in a part of the stepwise regression space

6.7.3 Clustering

The best clustering result for the tilt bending moment is found with the turbulence intensity, the first wind veer variable and the air density (Table 13). A decrease in estimation error of 5.1% is achieved. The performance of the stepwise regression and the clustering results are therewith comparable.

Table 13: Clustering with 2 variables for ShaftTilt

TI	α	U	ρ	DRE %	SD %	VD %
●	●			3.6	62.3	32.1
●		●		3.5	60.6	41.3
●			●	3.1	60.6	45

The PDFs of the residuals in the three largest clusters (cluster 1-3) showed small differences. Moreover, the PDF of the fourth cluster is not reliable as it is based on only 5 data points. This cluster does however include 2 data points with very low LR. In case more data is available, these data points are worth investigating in more detail.

The extremes in the clustering space (not shown) gave no new relevant information compared to Figure 77. Extremes with high LR are located at high density areas and extremes with low LR away from these areas. The result is therewith similar to that of the yaw bending moment.

7 Comparison between research methods and bending moments

In the previous chapter, the results of the eight bending moments were discussed one by one. However, it is also useful to compare the results with each other. The inflow conditions that result in atypical fatigue differ between bending moments and between research methods.

This chapter discusses two types of comparisons: Comparisons between bending moments and comparisons between fatigue load expectation methods (e.g. regression and clustering). Differences in variable selection between the bending moments are discussed in the first section. The second section concerns the variables and number of clusters selected by clustering. Also in this case, the different bending moments are compared with each other. The two methods for variable selection are compared in the third section. Section 7.4 discusses the accuracy of the different research methods. It compares the importance of different research methods for each bending moment and the importance across bending moments. The fifth and last section regards the data points with very low and very high load residuals. Their location in the clustering space and in the space defined by the regression models is discussed. In addition, it compares the extremes of the different bending moments.

7.1 Variables selected by stepwise regression

The selected variables by stepwise regression differ between the discussed bending moments. Table 14, presents a summary of the differences. The numbers refer to the importance in the regression model. A variable with a ”1” is the most important variable. Higher numbers refer to decreasing importance. In case for, for example the out-of-plane bending moment, the turbulence intensity is most important followed by the wind shear exponent, the second wind veer variable, the first wind veer variable and the wind direction change intensity. The higher order terms in the models are ignored.

Table 14: Inflow variables used for stepwise regression

bending moment	U	TI	α	α_2	λ	$\Delta\theta/\Delta z$	$(\Delta\theta/\Delta z)_2$	ρ	$wdci$
out-of-plane		1	2			4	3		5
flapwise		1				3	2		4
in-plane	4	1	5		3			2	
edgewise		1	3					2	
side-to-side		1		4		3	2		
yaw		1							
tilt		1					2		

In case of the stepwise regression, the predicted variable is a load residual based on solely the mean wind speed model. The fact that the turbulence intensity is the most important other variable, supports the assumptions made in Section 3.2. The use of the mean wind speed for the in-plane bending moment can be related to the tip speed

ratio also being in the model. It is therewith not of great concern.

The wind shear exponents are found relevant for four bending moments. However, considering the in-plane and side-to-side bending moment, the correlation with wind shear is weak.

Having a component in the out-of-plane direction, the edgewise bending moment is related to the out-of-plane bending moment. A small influence of wind shear could therefore be expected. However, in case wind shear is related to the out-of-plane component, the flapwise bending moment should have been affected more. Instead, the importance of the wind shear could have its peak between the out-of-plane and edgewise bending moment. This would explain why the flapwise bending moment does not include wind shear in the linear model but the edgewise bending moment does.

With exception of the in-plane and edgewise bending moment, at least the second wind veer variable is included. The use of wind veer could refer to a causal relationship. However, based on previous research (Robertson et al., 2018), no significant causal relationships were expected with the bending moments analysed in this project. Moreover, considering the second wind veer variable, it could also refer to differences between wind sectors in general. As shown in Section 5.1, the second wind veer variable is strongly sector dependent.

The air density is only found to be relevant for the related in-plane and edgewise bending moments. Included after the turbulence intensity the variable is most important to decrease the relative estimation error of both bending moments. However, having a low estimation error beforehand (see Section 7.4), it is not considered important in a wider point of view.

The wind direction change intensity ($wdci$) is used in the linear model of the related out-of-plane and flapwise bending moments. However, its importance in the linear models show that the correlation with fatigue loading is weak. It is therefore not considered to be a truly relevant variable.

7.2 Variables and number of clusters selected by clustering

In Chapter 5, the clustering results of five different combinations of variables are discussed. These can be compared to each other in terms of the appropriate number of clusters and the dependence on wind sectors.

An overview of the variables used for the clustering results of the different bending moments is shown in Table 15. For four bending moments, a combination of three variables are used. The other three bending moments use a combination of two variables. Because of the limited decrease in relative error, the fore-aft bending moment is not shown (see Section 6.4). The in-plane and edgewise bending moments produced the same clustering results, and are therefore discussed together.

Table 15: Inflow variables used for clustering

bending moment	U	TI	α	α_2	$\Delta\alpha$	$\Delta\theta/\Delta z$	$(\Delta\theta/\Delta z)_2$	ρ	$wdci$
out-of-plane				X	X				X
flapwise	X	X	X						
in-plane				X				X	
edgewise				X				X	
side-to-side	X						X		
yaw		X	X				X		
tilt		X				X		X	

The variable dissimilarity (VD, see Section 4.6) cannot be compared between combinations with a different number of variables. Moreover, it is found that no large differences exist when the same number of variables are used. The values are therefore not discussed in detail. In general it is found that the variable selection is independent on the variable dissimilarity. New information in the clustering space can result in a better decrease in relative error, but can also increase the noise.

The combination with the highest sector dependence (SD = 66.5%) is α_2, $(\Delta\theta/\Delta z)_2$ and ρ. This combination did not give the optimal decrease in estimation error for any of the discussed bending moments. This fact points towards a larger variation in fatigue within sectors than variation between sectors.

The clustering algorithm was not able to define proper clusters for the flapwise bending moment (see Appendix B). The results of the other five different combinations of variables can be divided into two groups. The first group pointed towards 3 inflow conditions and relatively low sector dependence. The second group pointed towards more than 4 inflow conditions and has a higher dependence on the wind sectors.

Use of the mean wind speed in the clustering space can, but does not necessarily point towards differences between wind sectors. The use of the mean wind speed models imply that the average load residual is constant with mean wind speed. However, this is not the case, because the mean wind speed model is based on a different and smaller dataset. The points that are removed were selected based on the wind sector. Dependencies between LR and U are caused by a difference in LR between wind sectors.

The same analysis does not hold for the turbulence intensity. Because it is forced in a linear fit, dependencies between LR and TI already exist in the smaller datasets. The use of turbulence intensity in the clustering space does therefore not point towards differences between sectors.

3 inflow conditions with low sector dependence

In two cases, the appropriate number of clusters is found to be three. It regards the combination for the out-of-plane bending moment with α_2, $\Delta\alpha$ and $wdci$ and the in-plane or edgewise bending moment with α_2 and ρ.

It is not investigated how similar the clustering results are. However, the number of points in the clusters do differ. I.e., in the second combination the points are better distributed over the clusters than in the first combination. Moreover, the contri-

butions of the different wind sectors largely differ between the two clustering results. One can therewith conclude that the results give different clusters. Inflow conditions that are important for the out-of-plane bending moment are not relevant for the in-plane/edgewise bending moment and vice versa.

4+ inflow conditions with high sector dependence

Discussion can exist for the appropriate number of clusters for the combination U and $(\Delta\theta/\Delta z)_2$ (used for side-to-side bending moment). Two peaks are found in the largest cluster. However, adding a fifth cluster divides a different cluster into two. Possibly, a sixth cluster is needed. The contributions of the different wind sectors to the clusters is clearly different from the two previously discussed combinations of variables. Moreover, it gives a higher sector dependence (57.6% compared to 48.8 and 47.9%).

The sector dependence is highest for the combinations used for the yaw bending moment (TI, α and $(\Delta\theta/\Delta z)_2$) and tilt bending moment (TI, ρ and $\Delta\theta/\Delta z$). Moreover, the bar charts containing the sector contributions for the clusters are both similar to the bar chart for the side-to-side bending moment combination. The use of a wind veer variable can explain the relatively large sector dependence for the three variable combinations. The analysis discussed in Section 5.1, resulted in an especially strong dependence on wind sector for the second wind veer variable $(\Delta\theta/\Delta z)_2$.

Because of the limited dataset size, no solid conclusions could be drawn on the appropriate amount of clusters. The Gaussianity of the first cluster of the tilt bending moment does point towards the existence of more than four inflow conditions.

7.3 Comparison between variable selection methods

Depending on the bending moment, the variables used in the clustering space are also used in the linear model resulting from stepwise regression. The use of the same variables can point towards the importance of continuous relations over discrete relations. In this case, the differences in the average value of the considered variable between clusters result in a decrease in estimation error.

In Chapter 9, recommendations for future work are discussed that combine the advantages of the two research methods. The potential of a combination of the two methods depends on the differences in variable selection. This section therefore also touches upon this recommendation.

Considering the out-of-plane bending moment, the second wind shear exponent used in the clustering space is represented by the first wind shear exponent in the linear model. Moreover, the two both use the wind direction change intensity. The wind veer variables are only used in the regression model. A combination of the two research methods is therewith expected to result in a better fatigue estimation.

The variables used in the clustering space of the flapwise bending moment are not included in the linear model (disregarding TI). This could point towards a proper clustering result with significant differences in load residual between clusters. However, as stated in Appendix B, this is not the case. Clustering also result in a lower DRE. The variables selected by stepwise regression are therefore considered more meaningful.

The variable selection of the in-plane and edgewise bending moments for the two research methods largely agree with each other. In both cases, the air density and a wind shear exponent is included. The importance of the tip speed ratio in the stepwise regression for the in-plane moment is not tested in the clustering space and can therefore not be compared. However, because this variable relates to a turbine state and not to an inflow condition, it is save to assume it would not initiate discrete differences between the clusters.

Also the two variable selections of the side-to-side bending moment partly agree with each other. In both cases the second wind veer variable is relevant.

Disregarding the turbulence intensity, the stepwise regression only includes the second wind veer variable for the tilt bending moment. In the clustering space, the first wind veer variable is included instead. In this case however, also the air density is used.

Stepwise regression for the yaw moment does not include other variables in addition to TI. However, it does include a second term $-c_2 TI^2$. Use of the turbulence intensity in the clustering space therewith agrees with the stepwise regression, that the linear approximation with turbulence intensity is relatively poor. One should however, keep in mind that the used datasets includes differences in the turbulence PDF of the wind sectors. The regression fits are therewith biased towards sectors with relatively low and high turbulence. The linear fit shown in Figure 91 in Appendix C, does not support a higher order relationship. Moreover, the size of the dataset is too limited to draw solid conclusions on this regard.

7.4 Accuracy of research methods

In this section the accuracy/usefulness of different research methods are discussed. Large differences exist between the bending moments.

The bar graph in Figure 78 gives an overview on the usefulness of the mean wind speed and the turbulence intensity. The top of each part of the bars represent the standard deviation of the load residual (relative estimate of error) before the regression step is used. The bottom of each part of the bars represent the standard deviation after the regression step. In this way, the accuracy of the fatigue load prediction is visualised from top to bottom by increasing the precision of the fatigue load expectation and therewith decreasing the error.

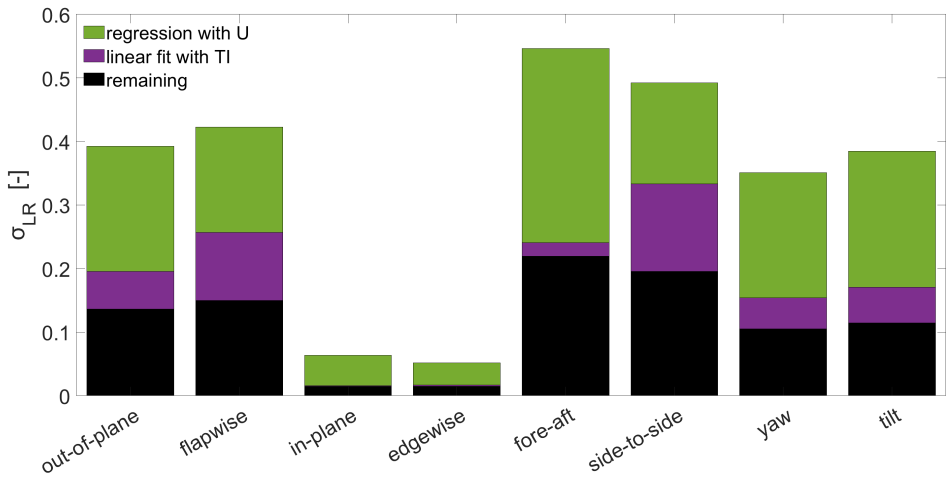

Figure 78: Relative estimation error

Table 16 also states the decrease in relative error by the other research methods. As given in the table, the reference estimation error differs between the research methods.

Table 16: Decrease in relative error by different research methods

	U	TI	stepwise regression	clustering	sectors
variables used for reference estimation error	-	U	U, TI	U, TI	U, TI
bending moment			DRE (%)		
out-of-plane	50.1	30.3	13.1	4.1	2.2
flapwise	39.3	41.6	10.1	3.8	3.3
in-plane	75	8.1	14.2	4.3	0.9
edgewise	67.2	11.3	6.1	3.9	1
fore-aft	55.9	8.9	1.2	2	0.4
side-to-side	32.2	41.3	9.2	10.6	3.6
yaw	56.1	31.7	4.7	4.5	1.4
tilt	55.6	32.8	4.3	5.1	2

7.4.1 Blade root & rotor loading

The most stand out information in the figure is the low estimation error for the in-plane and edgewise bending moments. As stated in Chapter 6, the in-plane and edgewise bending moments are dominated by gravitational forces. The relative error is therefore low before the mean wind speed is used to estimate the fatigue loading. In both cases, the mean wind speed decreases the error further. However, as discussed in Section 6.2, this only partly refers to a causal relationship. Being dominated by gravitational forces, the rotor speed is expected to be the main contribution.

The importance of turbulence largely differs between the four bending moments. For the in-plane and edgewise moments, the decrease in error after the turbulence intensity fit, is not large enough to be visible in the bar graph. The performance of stepwise regression of the edgewise bending moment is relatively poor with 6.1% with respect to other bending moments measured at the blade root (above 10.1%).

In case of the flapwise moment, the importance of the turbulence intensity is relatively large. Comparing the importance of turbulence for all four bending moments at the blade root, the maximum importance could be close to the flapwise bending moment.

In all cases, the stepwise regression is more effective than the clustering method and the clustering method is more effective than the differences between sectors. Compared to the turbulence intensity and the mean wind speed, all three methods are less useful considering the out-of-plane and flapwise bending moments.

7.4.2 Tower bottom loading

The fore-aft bending moment of the tower is largely dominated by the mean wind speed. The effect of the turbulence intensity is relatively small. However, the remaining error is still significant. It is highest compared to the other bending moments.

In case of the side-to-side bending moment, the importance of TI is comparable to that of the mean wind speed. Moreover, the decrease in relative error by the stepwise

regression is largest of all bending moments. Also the dependence on wind sector is highest. The result is therewith most comparable with the flapwise bending moment. Moreover, in both cases the mean wind speed is included in the clustering space.

The accuracy of the linear model resulting from stepwise regression and the clustering results are comparable for both the fore-aft and side-to-side moments. The results of the side-to-side moments are most promising. However, given that the second wind veer variable is used for both regression and clustering, a combination of the two methods (see Ch. 9) is not expected to significantly decrease the error further.

7.4.3 Main shaft loading

By analysing the clustering space, it was found that the yaw and tilt moment are partly related. Both pointed towards more than four inflow conditions and a strong relation with the wind sectors. In Figure 78 it is also shown, that the importance of mean wind speed and turbulence intensities are comparable. Being related to the same inflow conditions, the damage on the shaft as a whole and the damage of other nacelle components can be predicted at once.

In both cases, the results of stepwise regression and clustering barely decrease the relative error. Because the amount of clusters used might not be appropriate, significant improvements can be made for the clustering method. Because the stepwise regression did not include new variables with respect to the clustering spaces, a major improvement by combining the two methods is not expected.

7.5 Extreme load residuals of different bending moments

In the research discussed in Chapter 6, it is found that differences exist between the occurrence of extreme load residuals of different bending moments. In this regard, the bending moments can be divided into three groups. The first group has very low load residuals with rarely occurring inflow conditions. The second group has very high load residuals at these occasions. The third group of bending moments can also show a distinction between very low and very high load residuals. However, neither of the two are clearly related to areas with a high number of data points.

One should note that the variables investigated for extreme load residuals are related to the variables used in the linear model and the clustering result. The extremes of different bending moments are therefore investigated in different two-dimensional spaces.

Bending moments that belong to the first group are the side-to-side bending moment, the yaw bending moment and the tilt bending moment.

In case of the side-to-side bending moment, very low load residuals are found for a high second wind shear exponent,high second wind veer variable and a relatively high mean wind speed. Also with low wind speeds (uncertainty lower for low wind speeds).

Because of the limited number of data points with extreme low or high load residuals, no solid conclusions could be drawn for the yaw and tilt bending moments.

Given the wind shear exponent and the turbulence intensity, most data points with high LR for the yaw moment are in areas with a lot of data points. Points with very low LR are further away from these dense areas. A relatively low wind shear increases the probability of a very low LR.

The results for the tilt bending moment are similar. Points with high LR are also found in areas with a lot of other points. In this case other two dimensional spaces were investigated such as air density and wind veer/turbulence intensity. It is found that very low LR likely occur with low air density and high turbulence.

The out-of-plane and flapwise bending moment belong to the second group. In the first case, two groups of high load residuals are found. The best separation of these

groups is visible in the linear model space with α and $(\Delta\theta/\Delta z)_2$. Very low load residuals occur with low wind shear and low wind veer.

The result of the flapwise moment is similar. In this case the wind direction change intensity has the same role as the wind shear exponent for the out-of-plane bending moment. I.e., the separation is most clear with $wdci$ and $(\Delta\theta/\Delta z)_2$. Very low load residuals occur with low wind direction change intensity and low wind veer. Moreover, the low load residuals likely occur during neutrally stable conditions. Conditions with high LR have either a medium or a very low turbulence intensity.

The in-plane and edgewise bending moments belong to the third group. The area with a high amount of data points (medium air density) does not relate to very low or very high load residuals. The most distinctive group of points has a low air density, is measured in the summer and relates to an Southeastern wind. This group contains a relatively large amount of very high load residuals. In a more general sense, the high load residuals occur more often with a high tip speed ratio and very low load residuals with a lower λ.

The first group contains the same three bending moments that have a high sector dependence and high number of distinct inflow conditions. Despite that the importance of turbulence intensity is clearly higher for the side-to-side bending moment, the three bending moments are likely related. A part of the fatigue of the three bending moments could result from the same aeroelastic mode. Being dependent on the wind sectors, the relevant stiffness of the tower might not be fully radial symmetric.

8 Conclusions

The research question of this report regards the search for inflow conditions that result in atypical fatigue loading (Ch. 1). The fatigue resulting from eight different bending moments were investigated. The out-of-plane, flapwise, in-plane and edgewise bending moment were measured at the blade root. The fore-aft and side-to-side bending moment were measured at the tower bottom and the yaw and tilt moment at the main shaft. In Chapter 3, a quantitative measure for atypical fatigue was defined as the difference between measured fatigue and a combined regression model based on the mean wind speed and the turbulence intensity.

Two research methods (stepwise regression and Gaussian mixtures) were used to define relevant inflow conditions for atypical fatigue (Ch. 4). Depending on the considered bending moment and research method, different variables are found to be useful to define the inflow conditions. In all cases, however, the variance in atypical fatigue within the defined inflow conditions was large compared to the differences between inflow conditions.

In general, but especially for the yaw and tilt bending moments, the limited dataset size gave considerable uncertainty on the results and conclusions. Nevertheless, the most important and most solid conclusions following from the two used research methods are stated below. The in-plane and edgewise bending moments are dominated by gravitational forces and are therefore not of great interest.

- The estimation error for bending moments measured at the blade root or the tower bottom increases with mean wind speed.
- Differences in fatigue loading between wind directions are largest for the flapwise bending moment and side-to-side bending moment.
- The relation between fatigue and turbulence intensity is strongest for the flapwise and side-to-side bending moment. Correlation with fatigue by the in-plane, edgewise and fore-aft bending moment is limited.
- In general (with exception of the fore-aft bending moment), the correlation between mean wind speed and turbulence intensity with fatigue loading differs between wind from land and wind from a nearby lake. The differences between wind directions are largest for higher wind speeds.
- For the side-to-side bending moment, different atmospheric variables can be used to separate data points with highly overestimated fatigue loading from other data points. Likely, this is also the case for the yaw and tilt bending moment. However, more measurement data is needed for solid conclusions.
- For the out-of-plane and flapwise bending moments different atmospheric variables can be used to separate data points with highly underestimated fatigue loading from other data points. The most overestimated fatigue loading relate to neutral atmospheric conditions.

Multiple peaks in the frequency distribution of inflow variables are found. This could prove the need for multiple probability distributions in order to represent all inflow conditions. However, the used research methods did not allow for a strict distinction between continuous and discrete correlations. It is therefore not certain whether these separate probability distributions result in different fatigue loading.

Because of this issue, because of the limited amount of data and because of the relatively large variance in fatigue within the defined inflow conditions, the research question is only partly answered. In the next chapter, some recommendations are stated on finding a more accurate answer to the research question. This includes recommendations on separating continuous and discrete correlations.

9 Recommendations for future work

This chapter states and discusses recommendations for future work. The first section regards the test setup and the variables representing inflow conditions. The second section of this chapter discusses possible improvements on the used the research methods. Section 9.4 states a recommendation on how to use a new research method in order to improve the fatigue load expectation.

9.1 Test setup and variables representing inflow conditions

With the increasing size of wind turbines, different factors in inflow conditions can be of importance for fatigue loading. It is therefore desirable to have measurements available at higher altitudes. Use of a LiDAR could be considered. Given new and possibly more variables that could represent inflow conditions, the research project can be repeated for larger turbines.

Variables used in this report are measured at a meteorological mast. This has a major disadvantage for implementation. Metmasts are generally not available at wind farms, and can therefore not be used for control or end-of-life prediction. Instead, variables that can be measured at wind turbines should be used. E.g., mean wind speed, wind direction, power output, temperature, time of day and season.

The differences between the two wind veer variables could not all be explained. It is therefore necessary to investigate this factor in more detail and get a better view on the wind veer profile. Use of different measurement systems (wind vanes at two heights or wind vane at one height and sonic anemometer at other height) could potentially explain part of the differences.

Moreover, the differences in turbulence with height could not be measured because only one turbulence measurement is available. In a different test setup, a measure for differences in turbulence (intensity) profiles could also be used as a variable representing inflow conditions.

The estimation of the wind shear exponent can be improved by using measurements at more heights. In this case it would also be possible to define a better measure for the wind shear change. The used test setup did not allow for these improvements.

9.2 Expected fatigue loading

An equivalent wind speed could be used to estimate the fatigue loading. However, one should be careful by doing so, because the appropriate definition would most certainly differ between bending moments. For example, the importance of turbulence intensity is relatively large for the side-to-side bending moment but small for the fore-aft moment.

The accuracy of the regression models for fatigue load expectation is dependent on the dataset size. Parts of the datasets were not included in order to equalise the contributions of the three undisturbed sectors. By giving data points a weighting based on the sector contributions instead of randomly removing data points, more certainty on the models can be obtained.

At the considered test site, the used research methods could not be used for wind speeds above 11 m/s. One can consider a similar research method for wind speeds above 11 m/s (below 11 m/s excluded) and only include situations with an active pitch controller. In this case one would only include the Western wind sector when defining the expected fatigue loading. The availability of these situations in the Lawine

database is too limited for this purpose. However, in case a new test setup is being built, this option should be reconsidered.

9.3 Used research methods

Stepwise regression was used to select the most relevant variables. A limited order polynomial is used. It is therewith expected that the resulting model is underfit. In order to improve this method, higher order polynomials should be investigated. Limiting the computational effort, this can be done in two steps. The first step limits the used variables and is based on a low order polynomial. The second step allows for higher order terms, but does not allow for new variables in the linear model.

A number of more advanced clustering methods were considered for this project. These methods include different types of subspace clustering. They are expected to result in a larger computational effort. Moreover, the implementation of an advanced clustering method was considered out of the scope of this project. Kriegel et al. (2009) defined three types of subspace clustering. The methods are restricted to axis-parallel subspaces, have arbitrarily oriented subspaces or use a hybrid approach. In principle, an arbitrarily oriented approach has the highest potential. However, having a large overlap between the clusters, this method could result in significant problems. The use of a more advanced clustering method should only be reconsidered after other improvements are implemented.

As stated in Chapter 4, the number of clusters used is not necessarily optimal. There are several approaches possible to select a combination of inflow variables and the number of clusters. First of all one can test all combinations in search for a global optimum. Testing all possible combinations with different numbers of clusters, however, will come at a large computational cost.

Alternatively, one can find the most optimal combination of inflow variables for a fixed number of clusters first. Based on this combination, one can find the number of clusters. Afterwards one can check with this number of clusters if the optimal combination of inflow variables is still the same. This iterative approach does not guarantee to find to global optimum. Which local optimum is found, depends on the initial number of clusters.

The iterative approach also contains a major issue regarding computational costs. The computations for comparing two clustering results rapidly increases with the number of clusters (see subsection 4.4). For this reason, a high number of clusters limits the ability to find the optimal combination of variables.

Considering the new research method discussed below, the optimal number of clusters and clustering space might get independent on bending moment. The computational effort can therewith be limited by only using an iterative approach for one of the bending moments.

9.4 New research method

The clustering method is used by assuming no direct relationship between inflow variables and the fatigue loading exist. This direct relations are investigated by stepwise regression. However, if both direct and indirect relationships exist, both methods are relevant. The use of only one of the two methods would not result in an optimal fatigue estimation.

An iteration between the two clustering methods could solve this problem. This iteration is similar to the iteration used for the mean wind speed regression model and the linear fit with turbulence intensity (see Section 3.2). In an ideal situation, all four parts should be included in a single iteration. The variable estimated by each step is defined as the fatigue loading minus the contributions of the other steps. An example

for the turbulence intensity is shown in Equation 9.1.

$$E(TI) = DEL - E(U) - E(\alpha) - E(clusters) \tag{9.1}$$

with $E(\alpha)$ being the contribution of the wind shear exponent based on the stepwise regression. $E(clusters)$ includes the differences in fatigue loading between the defined clusters.

Each iteration would improve the values for $E(U)$, $E(TI)$, $E(\alpha)$ and $E(clusters)$. Because differences between inflow conditions are already included, it would no longer be necessary to equalise contributions of wind sectors when making the regression models. One should, however, stay careful with this approach because the method assumes a summation of the contributions. I.e., it does not include the possible dependence between $E(clusters)$ and U.

With this method, the direct relations with fatigue are removed before the clustering method is used. As a result, it is more likely that the clusters of the different bending moments are the same. I.e., the same clustering space is used. This would be a major advantage for future research, control strategies and lifetime prediction.

Bibliography

Beyer, K., Goldstein, J., Ramakrishnan, R., and Shaft, U. (1999). When is “nearest neighbor” meaningful? In Beeri, C and Buneman, P, editor, *Database Theory*, volume 1540 of *Lecture Notes in Computer Science*, pages 217–235.

Bir, G. and Jonkman, J. (2007). Aeroelastic instabilities of large offshore and onshore wind turbines. In *Journal of Physics: Conference Series*, volume 75, page 012069. IOP Publishing.

Blömer, J. and Bujna, K. (2013). Simple methods for initializing the em algorithm for gaussian mixture models. *CoRR*.

Bot, E. (2014). *Turbulence assessment with ground based LiDARs*. ECN.

Dimitrov, N., Natarajan, A., and Kelly, M. (2015). Model of wind shear conditional on turbulence and its impact on wind turbine loads. *Wind Energy*, 18(11):1917–1931.

Dimitrov, N., Natarajan, A., and Mann, J. (2017). Effects of normal and extreme turbulence spectral parameters on wind turbine loads. *Renewable Energy*, 101:1180–1193.

Dubnov, S., Tishby, N., and Cohen, D. (1996). Influence of frequency modulating jitter on higher order moments of sound residual with applications to synthesis and classification. In *PROCEEDINGS OF THE INTERNATIONAL COMPUTER MUSIC CONFERENCE*, pages 378–385.

Fraley, C. and Raftery, A. (2002). Model-based clustering, discriminant analysis, and density estimation. *Journal of the American Statistical Association*, 97(458):611–631.

Fraley, C. and Raftery, A. E. (1998). How many clusters? which clustering method? answers via model-based cluster analysis. *The computer journal*, 41:578–588.

Gutierrez, W., Araya, G., Kiliyanpilakkil, P., Ruiz-Columbie, A., Tutkun, M., and Castillo, L. (2016). Structural impact assessment of low level jets over wind turbines. *Journal of Renewable and Sustainable Energy*, 8(2).

Halkidi, M. and Vazirgiannis, M. (2001). Clustering validity assessment: Finding the optimal partitioning of a data set. In Cercone, N and Lin, TY and Wi, XD, editor, *2001 IEEE International Conference on Data Mining, Proceedings*, pages 187–194.

Højstrup, J. (1999). Spectral coherence in wind turbine wakes. *Journal of Wind Engineering and Industrial Aerodynamics*, 80(1-2):137–146.

Holtslag, M. C., Bierbooms, W., and van Bussel, G. J. W. (2016). Wind turbine fatigue loads as a function of atmospheric conditions offshore. *Wind Energy*, 19(10):1917–1932.

Holtslag, M. C., Bierbooms, W., van Bussel, G. J. W., and Iop (2014a). *Estimating atmospheric stability from observations and correcting wind shear models accordingly*, volume 555 of *Journal of Physics Conference Series*, page 012052. Iop Publishing Ltd, Bristol.

Holtslag, M. C., Bierbooms, W. A. A. M., and van Bussel, G. J. W. (2014b). Definition of the equivalent atmospheric stability for wind turbine fatigue load assessment. In *Science of Making Torque from Wind 2014 (Torque 2014)*, volume 524 of *Journal of Physics Conference Series*. European Acad Wing Energy.

IEC (2009). Iec 61400-3: Wind turbines part 3: Design requirements for offshore wind turbines. *International Electrotechnical Commission*.

Jimenez, A., Crespo, A., Migoya, E., and García, J. (2008). Large-eddy simulation of spectral coherence in a wind turbine wake. *Environmental Research Letters*, 3(1).

Kriegel, H.-P., Kroeger, P., and Zimek, A. (2009). Clustering High-Dimensional Data: A Survey on Subspace Clustering, Pattern-Based Clustering, and Correlation Clustering. *ACM Transactions on Knowledge Discovery from Data*, 3(1).

Moors, J. (1988). A quantile alternative for kurtosis. *The statistician*, pages 25–32.

Nelson, L. D., Manuel, L., Sutherland, H. J., and Veers, P. S. (2003). Statistical analysis of wind turbine inflow and structural response data from the list program. *Journal of solar energy engineering*, 125(4):541–550.

Park, J., Manuel, L., and Basu, S. (2015). Toward Isolation of Salient Features in Stable Boundary Layer Wind Fields that Influence Loads on Wind Turbines. *Energies*, 8(4):2977–3012.

Poodt, M. and Wouters, D. (2017). LAWINE Task A analysis report: on the added benefits of ground-based lidar for turbine load measurements. Technical report, ECN Wind Energy.

Rinker, J. M. (2016). Calculating the sensitivity of wind turbine loads to wind inputs using response surfaces. In *Journal of Physics: Conference Series*, volume 753. IOP Publishing.

Robertson, A. N., Sethuraman, L., Jonkman, J., and Quick, J. (2018). Assessment of wind parameter sensitivity on ultimate and fatigue wind turbine loads: Preprint. Technical report, National Renewable Energy Lab.(NREL), Golden, CO (United States).

Sathe, A., Mann, J., Barlas, T., Bierbooms, W. A. A. M., and van Bussel, G. J. W. (2013). Influence of atmospheric stability on wind turbine loads. *Wind Energy*, 16(7):1013–1032.

Sheskin, D. J. (2003). *Handbook of parametric and nonparametric statistical procedures*. crc Press.

Veldkamp, H. F. (2006). *Changes in Wind Energy; A probablistic approach to wind turbine fatigue design*. doctoral thesis, Delft University of Technology.

Wang, F., Franco-Penya, H.-H., Kelleher, J. D., Pugh, J., and Ross, R. (2017). An analysis of the application of simplified silhouette to the evaluation of k-means clustering validity. In *International Conference on Machine Learning and Data Mining in Pattern Recognition*, pages 291–305. Springer.

Wang, X.-F. and Huang, D.-S. (2009). A Novel Density-Based Clustering Framework by Using Level Set Method. *IEEE Transactions on Knowledge and Data Engineering*, 21(11):1515–1531.

Whittingham, M. J., Stephens, P. A., Bradbury, R. B., and Freckleton, R. P. (2006). Why do we still use stepwise modelling in ecology and behaviour? *Journal of animal ecology*, 75(5):1182–1189.

Zar, J. H. et al. (1999). *Biostatistical analysis*. Pearson Education India.

A Test site layout

Figure 79: Layout ECN Wind Turbine Test Site Wieringermeer

B Clustering result for the flapwise bending moment

This appendix regards the clustering results of the flapwise bending moment. In the figure captions, the bending moment is abbreviated as ”BladeFlap”.

Variables used in the clustering space of the flapwise bending moment are the turbulence intensity, the wind shear exponent and the mean wind speed. The data points based on the undisturbed wind sectors are not equally divided amongst the four clusters (Table 5). The largest cluster contains more than half the data points.

The first and by far largest cluster has a low kurtosis for both the turbulence intensity and the wind shear exponent (Fig. 80). Heavy tails usually refer to the existence of multiple inflow conditions within a cluster. In this case however, no clear additional peaks are visible in the PDFs.

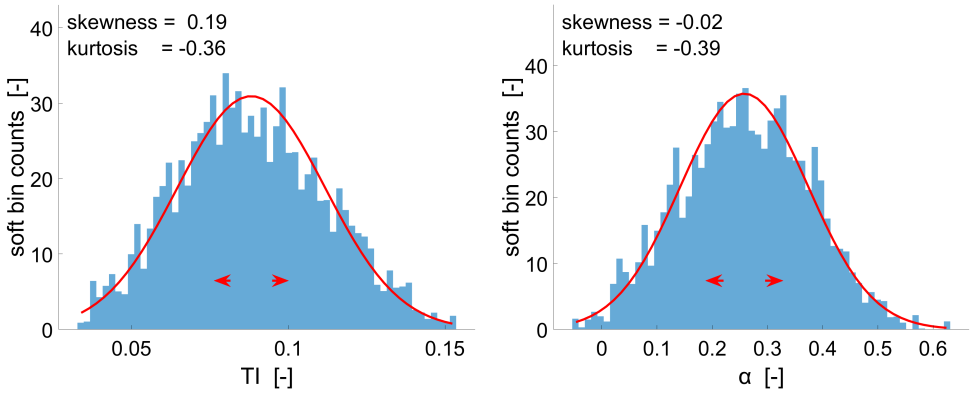

(a) Turbulence intensity (b) Wind shear exponent

Figure 80: Gaussianity cluster 1 of BladeFlap

The PDF of α of cluster 2 has a low kurtosis, high skewness and multiple peaks. It is therefore likely that it contains multiple inflow conditions. On the other hand, the kurtosis of the wind shear exponent of cluster 4 is exceptionally high (1.12). Combining the two clusters would give a more average kurtosis and combine two of the peaks of cluster 2. Moreover, the clusters mainly differ in mean wind speed (Fig. 38). Because no true clustering is expected in this variable, this division in clusters is not desired.

The digraph shown in Figure 84, show that the two clusters can be related. Moreover, there is a lot of weak connections in general between clustering results with 3-5 clusters. In this clustering space, the algorithm is likely sensitive to the initial conditions, and therewith finds ”weak” clusters. I.e., clusters that are difficult to differentiate from each other.

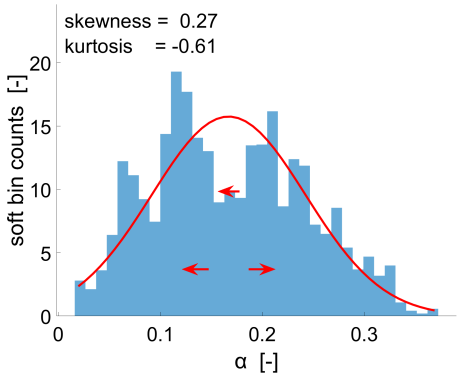

Figure 81: Gaussianity cluster 2 of Blade-Flap

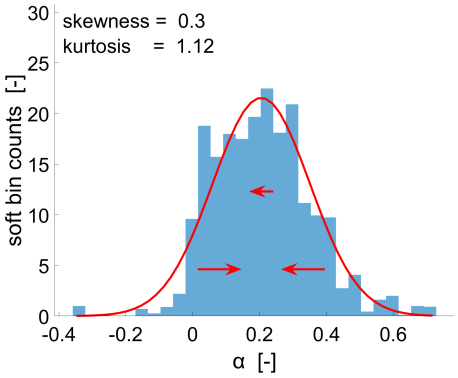

Figure 82: Gaussianity cluster 4 of Blade-Flap

The turbulence intensity PDF of the third cluster, show a low kurtosis and multiple peaks. Combining all the above stated aspects, one can conclude that the clustering algorithm is not able to produce well defined clusters in this clustering space.

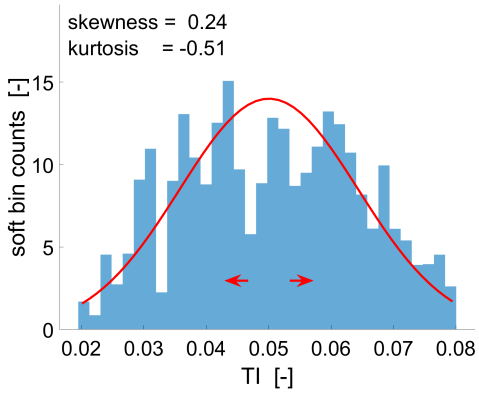

Figure 83: Gaussianity cluster 3 of Blade-Flap

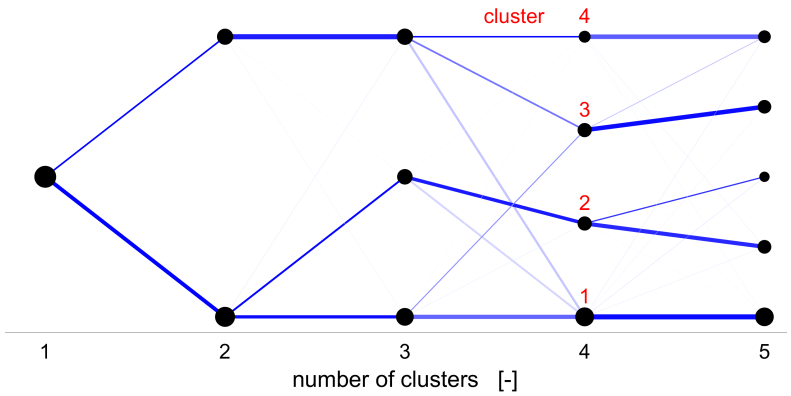

Figure 84: Digraph of BladeFlap

The dependence of clusters on the different wind sectors is not discussed in detail. The contribution of the Southeastern sector to the second cluster is small. If the contributions of clusters 2 and 4 are added to each other, the resulting cluster would still depend on wind sectors.

C Regression models

This appendix contains figures with the mean wind speed (U) regression models and the linear fits with turbulence intensity (TI) for each bending moment. On the y-axis of the first subfigures (a), the difference between the turbulence contribution (E(TI)) and the normalised design equivalent load (DEL) is plotted. In addition, it is stated whether an artificial neural network (ANN) is used or a Gaussian process regression model (GPR). On the second subfigures (b), the difference between the mean wind speed contribution (E(U)) and the normalised DEL is plotted on the y-axis.

C.1 Blade root & rotor loading

The number of points used to make the load expectation for the out-of-plane bending moment is stated in Table 17. Compared to the overall dataset (other cases), the contribution of sector UMUT-SE is relatively small. Mostly data points with low turbulence intensity are removed in this sector. Because it regards the same dataset, the table is similar to that of the in-plane bending moment, the edgewise bending moment and the flapwise bending moment.

Table 17: Number of data points for the out-of-plane bending moment

	UMUT-N	UMUT-SE	UMUT-SW	total	DMDT-S
expected loading	513	120	312	945	0
other cases	785	458	442	1685	14224

The four figures for the bending moments measured at the blade root are shown below. Correlation with the mean wind speed is strongest for the in-plane and edgewise moments. Correlation with turbulence intensity is relatively large for the out-of-plane and flapwise bending moments.

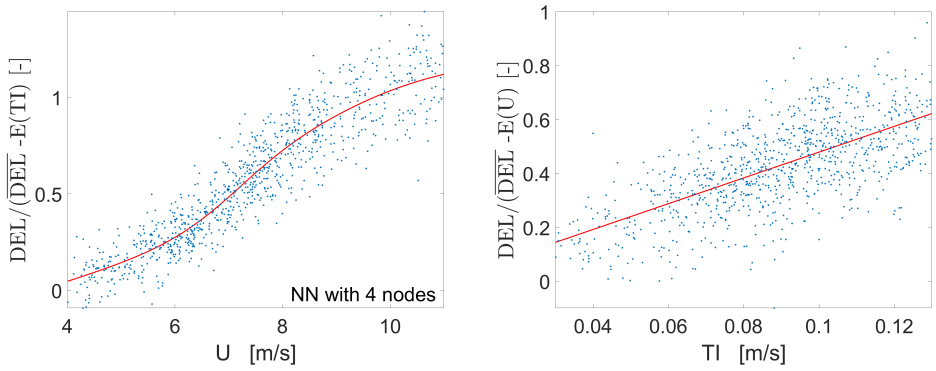

(a) Regression model with U

(b) Linear fit with TI

Figure 85: Regression models for the out-of-plane bending moment

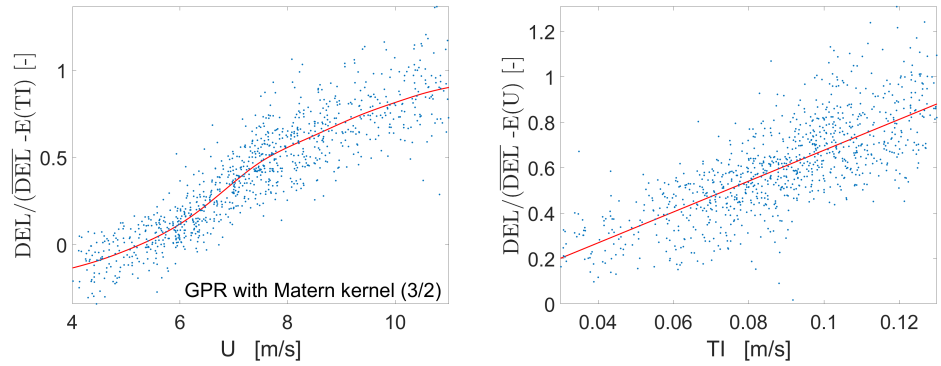

(a) Regression model with U (b) Linear fit with TI

Figure 86: Regression models for the flapwise bending moment

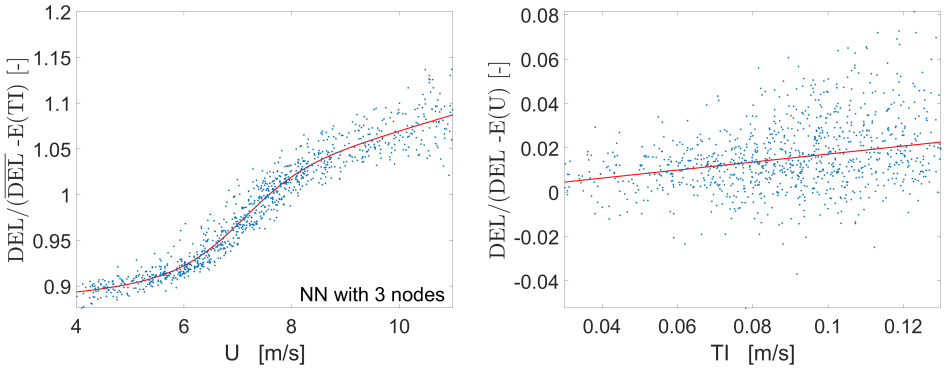

(a) Regression model with U (b) Linear fit with TI

Figure 87: Regression models for the in-plane bending moment

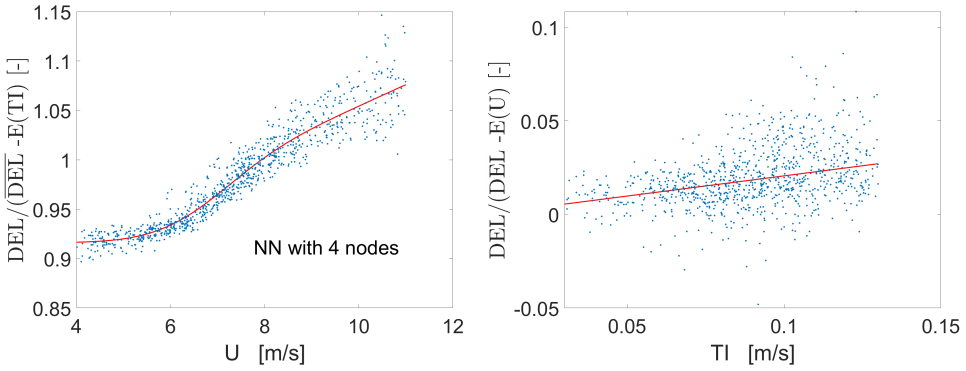

(a) Regression model with U (b) Linear fit with TI

Figure 88: Regression models for the edgewise bending moment

C.2 Tower bottom loading

The number of points used for the side-to-side moment are stated in Table 18. It is almost exactly the same for the fore-aft moment (one data point more from UMUT-SW and one less for UMUT-SE used for expected loading). Below the table, the regression models of the two bending moments are shown.

Table 18: Number of data points for the side-to-side bending moment

	UMUT-N	UMUT-SE	UMUT-SW	total	DMDT-S
expected loading	528	106	361	995	0
other cases	848	461	484	1793	15010

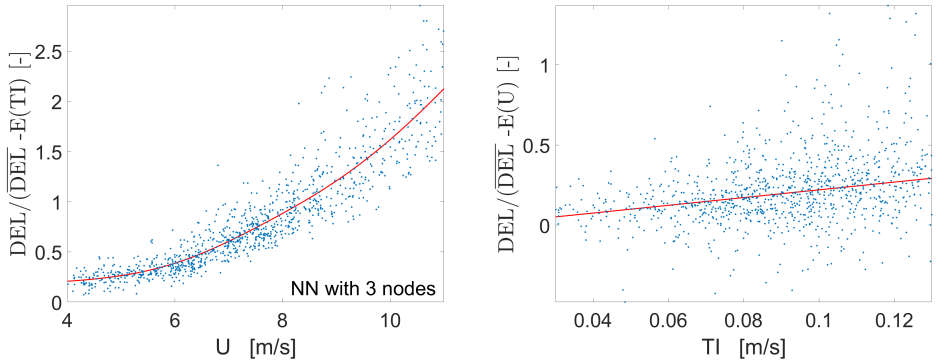

(a) Regression model with U (b) Linear fit with TI

Figure 89: Regression models for the fore-aft bending moment

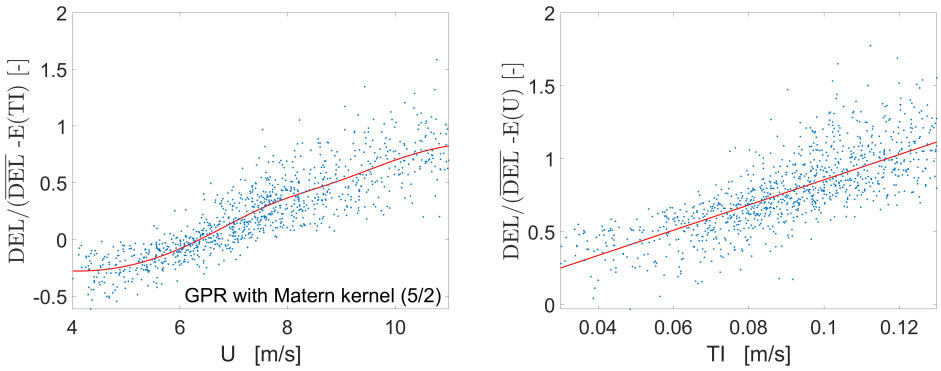

(a) Regression model with U (b) Linear fit with TI

Figure 90: Regression models for the side-to-side bending moment

C.3 Main shaft loading

As stated in Section 2.4, the size of the datasets for the main shaft loading is limited. The issue of limited data availability is largest for the Southeastern wind sector UMUT-SE. For both the yaw and the tilt bending moment, the algorithm equalising the distributions removed all data points of this sector. The expected loading is therefore based on two undisturbed sectors instead of three. The corresponding table for the yaw bending moment is shown in Table 19. The table for the tilt bending moment is similar, because they are based on the same dataset.

Table 19: Number of data points for the yaw bending moment

	UMUT-N	UMUT-SE	UMUT-SW	total	DMDT-S
expected loading	237	0	57	294	0
other cases	283	22	162	467	4430

Figures 91 and 92 show the regression models for the yaw and tilt bending moments respectively.

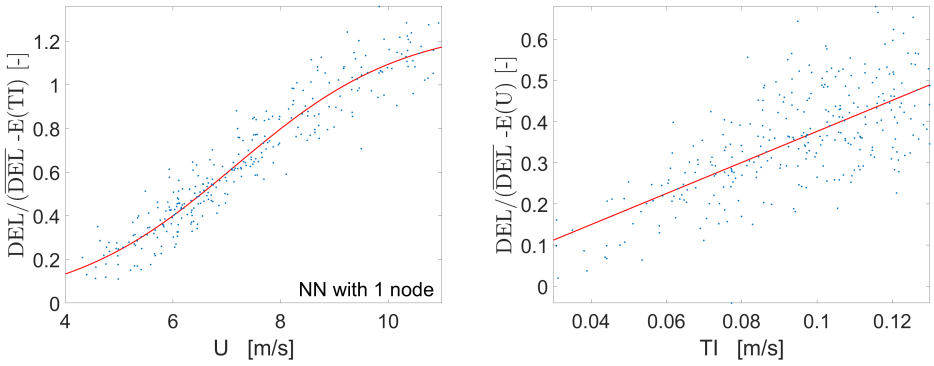

(a) Regression model with U (b) Linear fit with TI

Figure 91: Regression models for the yaw bending moment

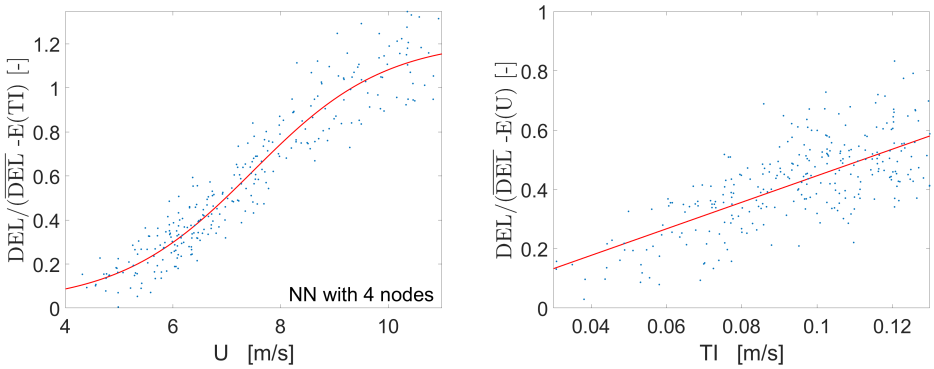

(a) Regression model with U (b) Linear fit with TI

Figure 92: Regression models for the tilt bending moment